

Petrology and tectonic evolution of seamounts
AC .H3 no.J83 15364



Johnson, Kevin T.
SOEST Library

Thesis - UH

070
Joh
Pet
ms

HAWAII INSTITUTE OF GEOPHYSICS
LIBRARY

THE PETROLOGY AND TECTONIC EVOLUTION
OF SEAMOUNTS AND BANKS OF THE
NORTHERN MELANESIAN BORDERLAND, SOUTHWEST PACIFIC

A THESIS SUBMITTED TO THE GRADUATE DIVISION OF THE
UNIVERSITY OF HAWAII IN PARTIAL FULFILLMENT
OF THE REQUIREMENTS FOR THE DEGREE OF

MASTER OF SCIENCE

IN GEOLOGY AND GEOPHYSICS

DECEMBER 1983

By


Kevin Todd Michael Johnson

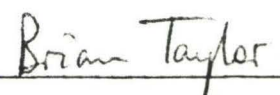
Thesis Committee:

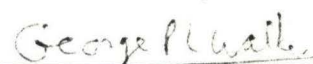
John M. Sinton, Chairman
George P. L. Walker
Brian Taylor

We certify that we have read this thesis and that, in our opinion, it is satisfactory in scope and quality as a thesis for the degree of Master of Science in Geology and Geophysics.

THESIS COMMITTEE


Chairman





ACKNOWLEDGEMENTS

As with all work, a thesis is really the product of efforts by a collection of individuals who, sometimes unknowingly, provide inspiration or material assistance in its preparation. I would like to acknowledge those who were important to me through this effort. Special thanks to my friend and advisor, John Sinton, whose energy, knowledge, and zeal got me interested in the project and kept me moving in the right direction, and who still had time after everything to pursue his manifold interests in Hawaiiana. Very special thanks also go to Tom Brocher whose contributions to the concepts in this thesis and to their coherent written expression cannot be given enough tribute. Tom's contributions extended far beyond those required and his active, imaginative approach to the project provided me with immeasurable inspiration. Many of the maps used in this thesis are either his work or are slightly modified versions of his originals.

Thanks also to my committee, Professors George Walker and Brian Taylor who provided useful comments and discussions during the final stages of thesis preparation. I would also like to thank Dr. Dick Price of LaTrobe University, Australia, for making his XRF and wet laboratories open to me and for giving his time to the project. Thanks are also due his charming family who put up with a guest whose appetite doubled the household food consumption for three weeks.

Without the technical support of several people at U.H., the work would not have been possible. Joann Sinton prepared thin sections, polished sections, and microprobe discs, often on short notice. Jean

Michel aided in my use of the microprobe. Thanks also to the captain and crew of the R/V KANA KEOKI for their patience and skilled seamanship.

I am also grateful to Dr. Charles Johnson, head of the Raw Materials Program of the East-West Center for providing me with a two year graduate scholarship and internship for support during my stay in Hawai'i. Dr. Harold T. Stearns also provided monetary support in the form of the Stearns Fellowship for the final stages of research in this project.

I wish to thank my friends and colleagues Dave Christie, Annabelle Lee, Cheney and Phil Milholland, Malcolm Pringle, Sugiarta Wirasantosa, and Elizabeth Zbinden for enlightening conversations on many subjects.

Very special thanks are given to my dear friend, Kumiko Makihara, who typed the first draft of this thesis and without whose understanding, support, and timely skepticism throughout our two years in Hawai'i, my experiences here would have been merely three dimensional.

Finally, I would like to thank my parents for constant, unconditional support and encouragement.

ABSTRACT

Petrologic study of volcanic rocks dredged from seamounts, banks, and islands of the Northern Melanesian Borderland (NMB) reveals several distinct provinces. Taviuni-Field, Lalla Rookh, and Combe Banks lie on an azimuth approximately parallel to Pacific Plate motion and to the Samoan Island chain, from which they extend to the west-northwest. They are geochemically and petrologically similar to Samoan lavas: Taviuni-Field and Lalla Rookh Bank lavas resemble Samoan post-erosional lavas in mineralogy and degree of silica undersaturation; Combe Bank lavas resemble Samoan shield basalts in their alkalic to transitional character, TiO_2 abundances, and K/Rb values. K/Ar ages of Lalla Rookh and Combe banks are consistent with their formation at a hot-spot located 80-200 km east of Rose Atoll. Sampled Taviuni-Field lavas were apparently formed near Tutuila in a hot-spot frame of reference. A fourth bank in the Samoan seamount lineament (SSL), Alexa, is composed of oceanic island tholeiite lavas distinctly lower in TiO_2 , P_2O_5 , and MgO than lavas from Samoa or other SSL lavas. Its age is inconsistent with its formation at the same sites as the other dated banks. It is inferred to be a product of mid-plate volcanism, but is probably not related to Samoan volcanism.

Horne (Futuna) Islands and Manatu seamount are situated on the North Fiji Basin (NFB) south of the Vityaz Trench lineament. They are arc tholeiitic in character with similarities to back-arc basin basalts. Two types of basalts were recovered from Horne: 1. high SiO_2 (52-53%), high MgO (8-11%) arc tholeiitic basalts, and 2. lower SiO_2 (49-50%),

lower MgO (6.5-7.5%) altered basalts similar to back-arc basin basalts. Both are very low in TiO_2 (0.9-1.2%) and K_2O (0.05-0.13%). Manatu seamount lavas are low TiO_2 (0.98-1.17%) tholeiitic basalts and medium-grained dolerites with modal quartz and hypersthene. The modal quartz appears as discrete grains and is apparently primary, but is anomalous in rocks of these compositions. Both edifices are inferred to be products of volcanism related to subduction at the Vityaz-Tonga Trench and spreading in the NFB.

Alkalic lavas dredged from the flanks of the Wallis Islands are fresh, glassy, quenched olivine basalts. Their low relative abundances of TiO_2 (2.2%) distinguish them from Samoan lavas. They may be products of volcanism related to extension along the Vityaz Trench induced by back-arc spreading in the Lau and North Fiji Basins.

TABLE OF CONTENTS

ACKNOWLEDGEMENTS	iii
ABSTRACT	v
LIST OF TABLES	ix
LIST OF ILLUSTRATIONS	x
INTRODUCTION	1
GENERAL GEOLOGIC SETTING OF STUDY AREA	5
CHAPTER 1. SAMOAN SEAMOUNT LINEAMENT	
1.1 Geologic Setting of Samoan Volcanism	8
1.2 Geochemistry and Petrology of Dredged Samples	
1.2.1 Taviuni-Field Bank - RD 1	11
1.2.2 Lalla Rookh Bank - RD 3	15
1.2.3 Combe Bank - RD 7	24
1.2.4 Alexa Bank - RD 14	32
1.3 Discussion	37
CHAPTER 2. VITYAZ TRENCH LINEAMENT	
2.1 Geologic Setting of Vityaz Arc-Trench	45
2.2 Geochemistry and Petrology of Dredged Samples	
2.2.1 Alofi, Horne Islands - RD 6	51
2.2.2 Manatu Seamount - RD 10	59
2.2.3 Wallis Islands - RD 4	61
2.3 Discussion	
2.3.1 Arc Volcanism: Horne and Manatu	64

2.3.2 Wallis Islands	69
CHAPTER 3. SUMMARY AND CONCLUSIONS	
3.1 Samoan Seamount Lineament	72
3.2 Vityaz Trench Lineament	75
APPENDIX A. WHOLE ROCK AND GLASS ANALYSES	77
APPENDIX B. PYROXENE ANALYSES	83
APPENDIX C. DREDGE LOCATIONS	91
APPENDIX D. PETROGRAPHIC DESCRIPTIONS	98
APPENDIX E. ANALYTICAL METHODS	105
REFERENCES	111

LIST OF TABLES

<u>Table</u>		<u>Page</u>
1	Chemical Analyses of Volcanic Rocks from the Samoa Seamount Lineament	41
2	Chemical Analyses of Volcanic Rocks from the Vityaz Trench Lineament	65
C-1	ANZUS/SOPAC Leg 2 Rock Dredges: locations and lithologies	91

LIST OF ILLUSTRATIONS

<u>Figure</u>		<u>Page</u>
1	Tectonic elements of Northern Melanesian Borderland . .	2
2	Bathymetry and ship track of study area	4
3	Pyroxene quadrilateral, Taviuni-Field Bank	12
4	Photomicrograph of olivine melilitite, Taviuni-Field .	14
5	Pyroxene quadrilateral, Lalla Rookh Bank	16
6	Wt% SiO ₂ vs. Al ₂ O ₃ , Lalla Rookh pyroxenes	18
7	Al ₂ vs. wt% TiO ₂ , Lalla Rookh pyroxenes	19
8	Photomicrograph of inclusion, Lalla Rookh sample 3-36 .	20
9	Normative Di-Ne-Ol, Lalla Rookh and Samoan lavas . . .	21
10	Alkali-silica diagram, Samoan seamount lineament lavas	23
11	TiO ₂ -MnO-P ₂ O ₅ discriminant diagram, all samples	25
12	Corrected alkali-silica diagram, Combe Bank lavas . . .	27
13	Pyroxene quadrilateral, sample 7-9 Combe Bank pyroxenes	29
14a	Wt% Al ₂ O ₃ /SiO ₂ vs. SiO ₂ , sample 7-9 cpx	30
14b	Wt% Al ₂ O ₃ /SiO ₂ vs. TiO ₂ , sample 7-9 cpx	31
15	Wt% K ₂ O vs. TiO ₂ , Alexa Bank lavas	34
16	Wt% TiO ₂ vs. P ₂ O ₅ , Alexa Bank and Samoan lavas	35
17	Pyroxene quadrilateral, Alexa Bank pyroxenes	36
18	K/Ar age vs. distance along Samoan lineament	39
19	Seismicity of the Northern Melanesian Borderland . . .	49
20	Location and bathymetry map, Horne Islands and Manatu seamount	52
21	Wt% FeO*/MgO vs. TiO ₂ for Horne and Manatu	53

22	Wt% K_2O vs. SiO_2 classification diagram, Horne Islands	54
23	Alkali-silica diagram, Vityaz Trench lineament lavas .	56
24	Wt% SiO_2 vs. Mg#, Horne Islands lavas	57
25	Photomicrograph, euhedral quartz grain, Manatu seamount	60
26	SiO_2 vs. TiO_2 , Wallis Island and Samoan lavas	63
27	Tectonic reconstruction of the N.M.B.	68
Bathymetry and location maps:		
C-1	Taviuni-Field Bank	92
C-2	Lalla Rookh Bank	93
C-3	Wallis Island	94
C-4	Horne Islands	95
C-5	Combe Bank	96
C-6	Alexa Bank	97

INTRODUCTION

This study describes the petrology of rocks dredged from five seamounts along the Northern Melanesian Borderland (NMB) (Figure 1) and from the submerged portions of Wallis and Aofu (Horne) Islands. One of the aims of the study is to compare the chemical characteristics of the seamounts forming the NMB with those of the Samoan Islands to constrain current hypotheses for the formation and tectonic setting of Samoa. Another aim is to assign the tectonic environment of formation of the seamounts based on previous studies of experimental and field relationships of these terranes. These geochemical and petrographical data, coupled with ages from some of the seamounts and with plate motion vectors, are used to constrain hypotheses for seamount consanguinity and the tectonic evolution of the NMB.

The thesis is divided into two sections. The first section describes and discusses the seamount lineament west-northwest of Samoa. Volcanism producing Samoa and the seamounts has been ascribed to plate tearing at the northern end of the Tonga Trench (Hawkins and Natland, 1975; Natland, 1980). Rocks collected from seamounts along the lineament are compared to previous geochemical and petrological studies of Samoan rocks. Radiometric ages (Duncan, in preparation) are used to further constrain hypotheses of formation of the Samoan seamount lineament.

The second section of this thesis examines seamounts along the NMB not belonging to the Samoan seamount lineament. Geochemical and

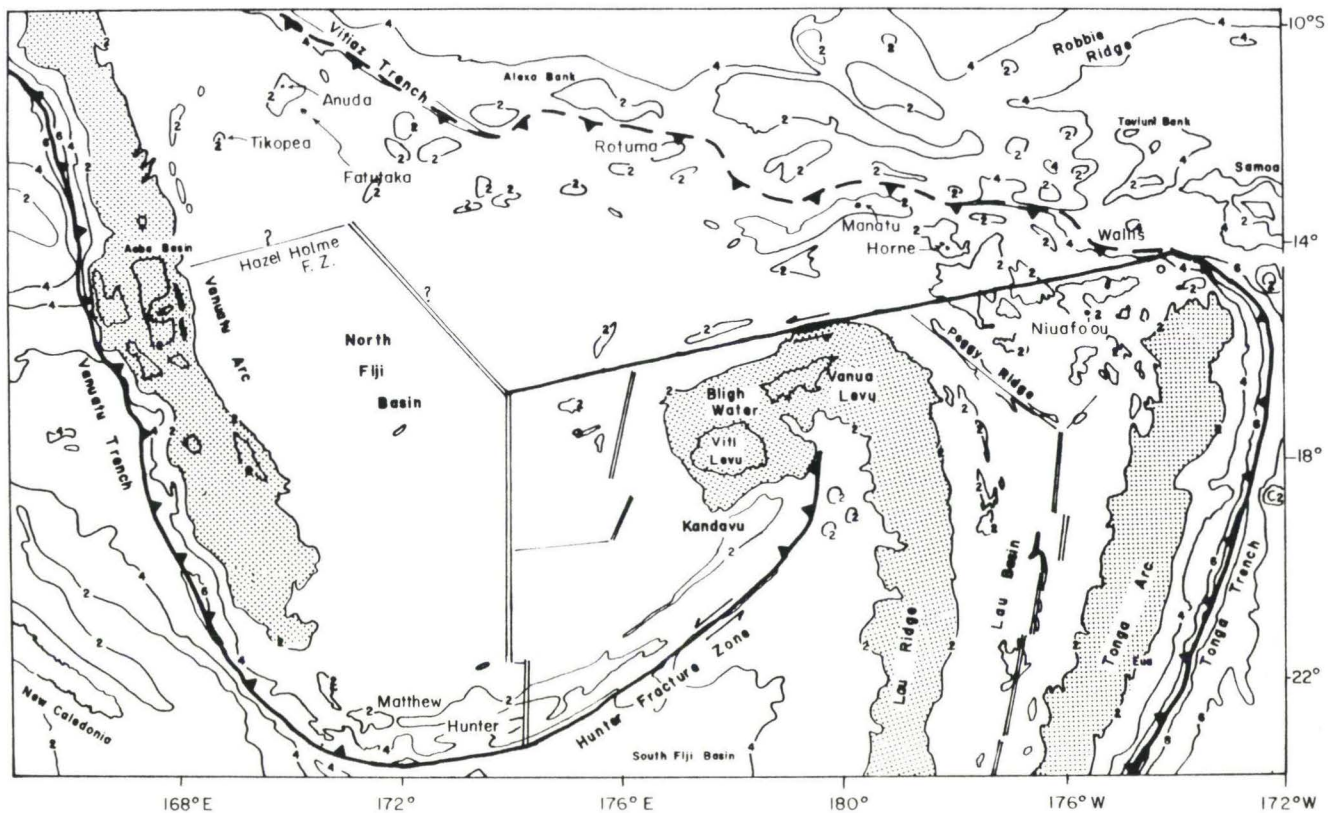


Figure 1. Tectonic elements of the Northern Melanesian Borderland (after Brocher, in preparation). Double lines = spreading centers; barbed lines = subduction zones, dashed where no longer active; solid lines = fracture zones/transform faults. Contours are in kilometers. Shaded areas emphasize the once continuous Vityaz Arc (see text for discussion).

petrological data from three of the seamounts possibly associated with Vityaz Trench subduction and arc fragmentation are used to test the hypothesis that subduction occurred along the Vityaz Trench (Figure 1) (Chase, 1971; Coleman and Packham, 1976; Gill et al., 1983). K/Ar ages (Duncan, in preparation) augment these data and help to revise current ideas about the evolution of the North Fiji Basin and the subduction history of the Vityaz Trench. The Wallis Islands (Figure 1) do not fit the pattern of volcanism of the Samoan lineament or the Vityaz Arc. However, they are discussed along with edifices of the Vityaz Trench lineament because of their inferred relationship to fragmentation of the Vityaz Arc.

In March and April, 1982, the R/V KANA KEOKI embarked on a scientific cruise (KK820316-2) to the NMB to survey the region and to sample its seamounts and basins (Figure 2). The cruise was organized by the Committee for Coordination of Offshore Prospecting in the South Pacific (CCOP/SOPAC) and funded by a tripartite consortium of government agencies from Australia, New Zealand, and the United States (ANZUS). The objectives of the cruises were to investigate the economic resource potential of the seafloor and sediments in the Southwestern Pacific and to carry out geological and geophysical surveys of the seamounts and basins of the NMB.

The NMB has not been extensively studied. Other investigations of the Borderland (Chase, 1971; Falvey, 1975, 1979; Hawkins and Natland, 1975; Coleman and Packham, 1976) have not concentrated on the seamounts

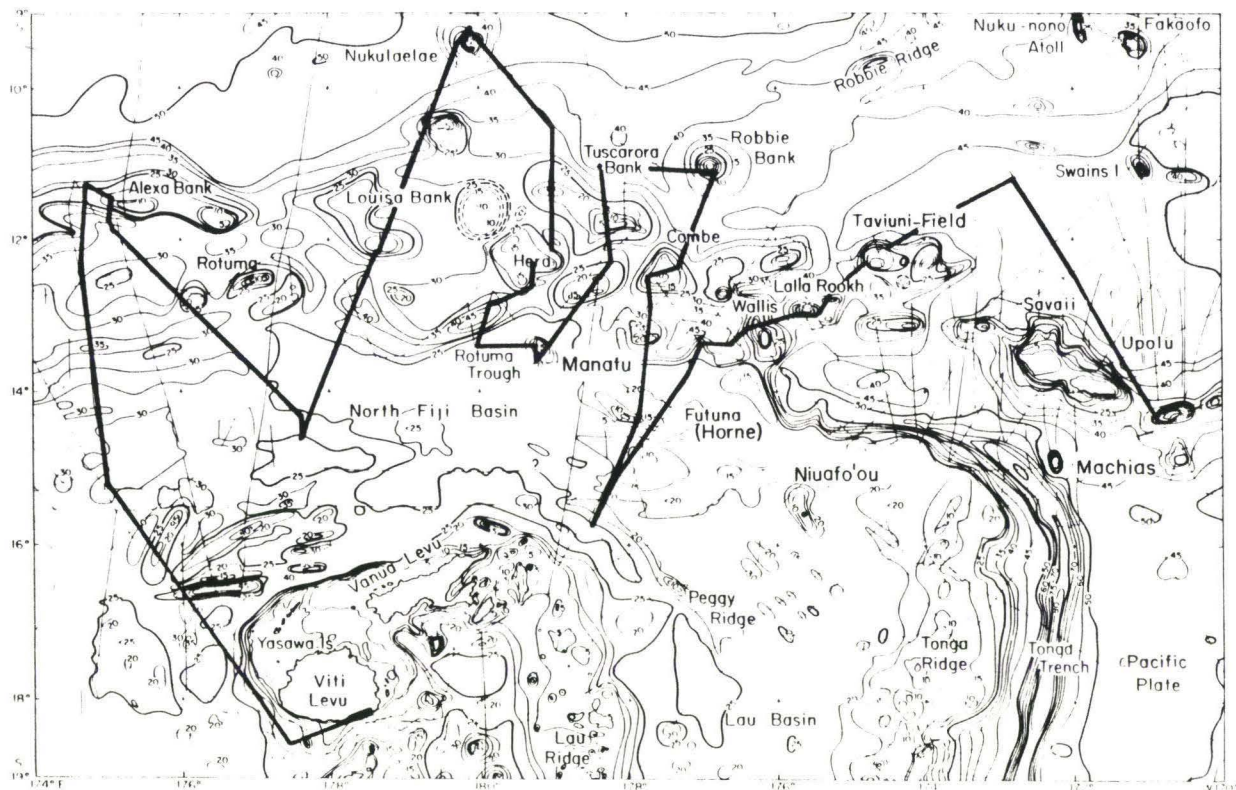


Figure 2. Bathymetric map of the study area (after Brocher, in preparation). Heavy line is the ship track of R/V KANA KEOKI, leg 2 of the ANZUS/SOPAC 1982 cruises. Contours are in hundreds of meters. Light lines are ship tracks from other cruises used to compile the map.

of the Borderland. The present study represents the first detailed look at the petrology and geochemistry of the NMB seamounts and the geotectonic interpretation arising from this information. Thirty new whole-rock XRF major and trace element analyses, 54 new microprobe glass analyses of lavas (Appendix A), and 99 new pyroxene analyses (Appendix B) from seamounts, islands, and marginal basins are presented. The evolution of the Samoan seamount lineament and the Vityaz Trench is discussed in the light of these new data.

General Geologic Setting of the Study Area

The NMB, in this and other studies, is defined as the region separating the Pacific Plate from the India-Australia Plate (Chase, 1971; Coleman and Packham, 1976; Gill et al., 1983)(Figure 1). The NMB is comprised of a linear array of seamounts and elongate basins extending approximately 1700 km to the west-northwest from the Samoan Islands (Figure 1). The Borderland forms the geological boundary between the Pacific plate to the north and the North Fiji Basin to the south, and separates crust of Cretaceous age (Pacific) from crust of late Miocene to Recent age (North Fiji Basin). Several major tectonic elements--the Tonga Trench, the Samoan Islands, the Northern Melanesian seamounts, the paleo-Vityaz trench, and the North Fiji Basin (Figure 1)--have interacted in combinations of convergence, spreading, and transform motion to produce the NMB since the late Miocene.

The NMB is bounded to the north by the Vityaz Trench, the western portion of which is a continuous basin, the eastern part a series of

discontinuous, elongate basins that trend to the southeast. These remnant basins have depths ranging from 4 to nearly 5 km, are filled with sediment to thicknesses of 1-3 km, and are asymmetrical in cross section; the dip of the northeastern flank is shallower than the dip of the southwestern flank (Brocher, in preparation). The basins join the Tonga Trench where it curves west-northwestward south of the Samoan Islands. The Tonga Trench forms the eastern boundary of the NMB and has been separated from the Fiji platform and the Lau Ridge by the Lau back-arc basin (Karig, 1970). The southwestern boundary of the NMB is marked by the Vanuatu Trench and the Hunter Fracture Zone, which merges with the Fiji platform at the Fiji-Lau elbow (Figure 1). Active subduction along the Vanuatu and Tonga Trenches is accompanied by back-arc spreading in the North Fiji and Lau Basins (Karig, 1970; Chase, 1971).

The Samoan Islands lie at the eastern end of the series of seamounts north of the Tonga Trench. Current hypotheses suggest that Samoan volcanism extends westward along the chain. The shield forming mechanism is not well constrained because of the lack of data from Samoan shield lavas, including their ages. Nonetheless, consanguinity of the lavas from the seamounts and from Samoa can be tested using geochemical discriminants and paleo-reconstructions. This is the aim of the first section of this thesis.

The Vityaz Trench may represent a failed subduction zone that was once actively subducting to the south-southwest (Chase, 1971; Gill and Gorton, 1973; Coleman and Packham, 1976). Contemporaneous volcanism producing island arc lavas took place in Lau, Fiji, and Vanuatu during

Eocene to early Miocene (Gill and Gorton, 1973) forming the then-continuous Vityaz Arc. If the discontinuous, elongate troughs of the Vityaz Trench lineament represent segments of a failed subduction zone, then volcanoes to the south of these troughs could be relicts of this volcanic arc. This hypothesis is tested in the section on the Vityaz Trench.

CHAPTER 1

SAMOAN SEAMOUNT LINEAMENT1.1 GEOLOGIC SETTING OF SAMOAN VOLCANISM

Natland (1975, 1980) and Hawkins and Natland (1975) studied the petrology and geochemistry of the Samoan Islands and some of the nearby seamounts (Machias seamount south of Savai'i at 15°S , $172^{\circ}11'\text{W}$, and Pasco Bank west of Savai'i). They argued that their Recent eruptive histories are related to interactions between the Pacific plate and the Tonga Trench as the former was sheared at the trench's northern bend, and that, as a result of its subduction at the Tonga trench and shearing north of the trench, the lithosphere of the Pacific plate is ruptured forming a rift. As in Hawai'i, the bulk of the Samoan Islands were presumably built by a voluminous shield-building stage. In Samoa, however, the subaerially exposed shield-stage consists mainly of alkalic basalts and small amounts of critically undersaturated lavas. It is not clear whether or not the hot spot model thought to be responsible for formation of linear island chains such as Hawai'i (Wilson, 1963; Morgan, 1972) controls the formation of the Samoan shield volcanoes. The shield-building stage of Hawaiian and Samoan volcanism is marked by caldera formation and filling when alkalic lavas generally erupt. After a period of quiescence (0.5-2.4 m.y. in Hawai'i), a rejuvenation (post-erosional) stage of volcanism often occurs marked by eruption of

nephelinitic and basanitic lavas (Honolulu series of O'ahu and Koloa series of Kauai; A'opo and Pu'apu'a series of Savai'i and Upolu, Western Samoa, Leone series of Tutuila, American Samoa; Macdonald, 1968; Natland, 1980; Macdonald, Abbott, and Peterson, 1983). The mechanism responsible for the production of these post-erosional, rejuvenation stage lavas is not well known, but in Samoa the plate-buckling induced by the oblique subduction at the northern end of the Tonga Trench may cause a rift zone or "tear-spot" thought to provide a series of eruptive conduits for undersaturated lavas to escape to the surface (Natland, 1980). By analogy with experimental melt compositions (Bultitude and Green, 1971) these lavas are believed to form at depths from approximately 100 km (post-erosional) up to unknown shallower levels (Upolu shield lavas) (Natland, 1980; Hawkins and Natland, 1975). If this model is correct, the undersaturated lavas that characterize the Samoan Islands post-erosional stage of volcanism should extend to the west-northwest along a linear trend parallel to the motion of the Pacific Plate for as long as the subducting Pacific Plate has existed in this configuration. Samoan shield volcanoes should also follow a trend of increasing age to the west-northwest if they are generated by a hot-spot or a tear-spot. The position of the hot-spot is currently unknown, but if present, presumably lies beneath the easternmost Samoan Islands.

Voluminous volcanic eruptions occurred in Savai'i, Western Samoa from 1902 to 1911 virtually blanketing the island in undersaturated alkalic, basanitic, and nephelinitic lavas (Stearns, 1944; Kear and Wood, 1959; Natland, 1980). Historical eruptions also occurred at the other

end of the Samoan chain on the submarine rift zone southeast of Olosega island (Stearns, 1944) and on Ta'u Island, Manu'a, American Samoa (Stice, 1968).

The difficulty with comparing radiometric ages from the various edifices is that these ages lack stratigraphic control. It is unknown what part of the volcano or what stage of volcanism is being dated. The age of post-erosional volcanism can be several million years younger than the age of shield-building volcanism in Hawaii and this relation is probably similar in the Samoan chain. It is possible, however, to make educated inferences on the relationships between lavas based on geochemical, mineralogical, and petrologic parameters. The use of elemental abundances and ratios in rocks and minerals enables us to judge whether genetic similarity exists between lavas. Comparing observed with experimentally and theoretically derived compositions helps to constrain conditions of formation of lavas based on pressure and compositional controls of mineral stability.

The following section contains descriptions of geochemistry and petrography of the dredged lavas from the Samoan lineament and a discussion of a possible model for their formation. Data referred to in the text is tabulated in Appendices C (dredge locations and seamount bathymetry) and D (sample descriptions). The four seamounts examined in this section are Taviuni-Field, Lalla Rookh, Combe, and Alexa Banks and will be discussed in this order, i.e. from east to west away from Samoa.

1.2 GEOCHEMISTRY AND PETROLOGY OF DREDGED SAMPLES

1.2.1 Taviuni-Field Bank - RD 1

Rock dredge 1 (sample 1-2) from Taviuni-Field Bank recovered an altered basanitoid lava made up of Ti-salite and a mineral resembling melilite. Undersaturated lavas such as this are characteristic of Samoan volcanism (Natland, 1980) and provide strong evidence of Samoan volcanism extending this far west.

The minerals of interest in this dredge are the Ti-salites which comprise a large percentage of the groundmass of the studied rocks. Analyses of this mineral are reported in Appendix B and a pyroxene quadrilateral plot comparing these minerals and Samoan pyroxenes is shown in Figure 3. The extremely high TiO_2 and Al_2O_3 and low SiO_2 contents of these pyroxenes are similar to the abundances of these elements in kaersutitic amphiboles, but the calcium and alkali abundances of the Ti-salites are twice those of kaersutites. The abundances of Ca-Tschermaks molecule (up to 32%) and Ti-Tschermaks molecule (up to 23%) in the pyroxenes probably reflects the abundances of Ca and Ti in the liquid as well as low pressures and perhaps high temperatures of crystallization (Onuma and Yagi, 1971; Thompson, 1974). The crystals are present only in the groundmass and nucleate on magnetite grains, providing further evidence of late-stage crystallization.

The rock was not analyzed because of its highly altered state. Therefore the minerals were used as indicators of magmatic composition.

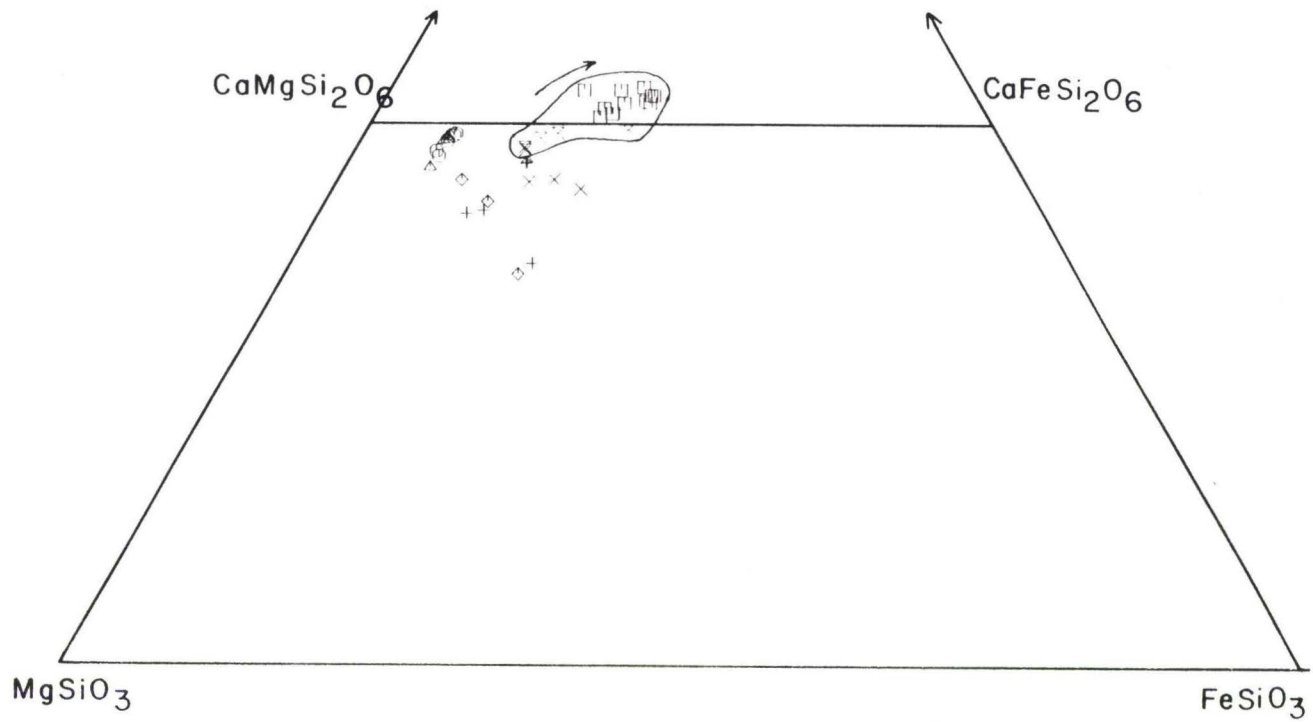


Figure 3. Plot of Taviuni-Field Bank pyroxenes on a standard pyroxene quadrilateral. Arrow shows crystallization trend of pyroxenes from nephelinic lavas from Hawai'i (Fodor et al., 1975). Field encloses Ti-salites from Taviuni-Field Bank along with pyroxenes from Samoan post-erosional lavas (Natland, 1975). Squares = Ti-salites, dredge 1; circles and triangles = cpx cores and rims, respectively, dredge 1; pluses and diamonds = cpx from Samoan tholeiites; X's and trees = cpx from Samoan alkalalic lavas; tables = cpx from Samoan post-erosional lavas (Natland, 1975).

Ti-rich pyroxenes are only found in strongly undersaturated lavas. Sinton (1979) described Ti-salites in the groundmass of a submarine basanitoid erupted near St. Paul's Rocks in the Atlantic Ocean. Studies of pyroxenes from Hawaiian lavas (Fodor and Bunch, 1972; Fodor et al., 1975) show rocks of the nephelinitic suite to contain salites characterized by high proportions of the wollastonite end member (>50%), Al_2O_3 , and TiO_2 as in the pyroxenes in dredge 1. Tracy and Robinson (1977) described Ti-augites from ankaramites in Tahiti that are nearly identical in composition to the Ti-pyroxenes found in Taviuni-Field Bank lavas. Wilkinson (1975) described similar Ti-salites in the groundmass of nephelinites in a sill in New South Wales. Therefore, it is concluded that the Ti-salites recovered from Taviuni-Field Bank crystallized from a highly undersaturated magma.

The only clinopyroxene phenocryst found in the studied thin sections is a chromian augite which is only slightly zoned, increasing in SiO_2 and decreasing in TiO_2 and Al_2O_3 from core to rim. The high chrome content is typical of many clinopyroxenes crystallized from alkalic magmas and inclusions in high pressure xenolith nodules. Its isolated occurrence and very different composition may indicate a residual origin from a deeper seated magma chamber or conduit wall, or from an earlier crystallization phase.

The abundant lath shaped mineral in the rocks from this dredge are severely altered (Figure 4). Their compositions are highly variable and oxide totals are always less than 91%. The mineral is now presumably smectite, pseudomorphous after melilite. This determination is made

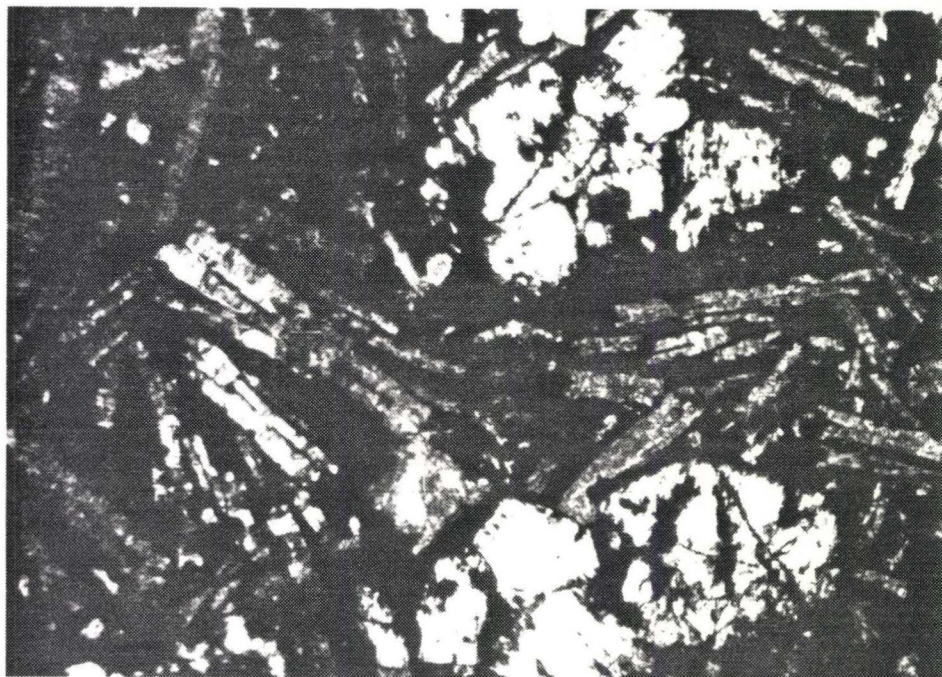


Figure 4. Photomicrograph of the abundant lath-shaped minerals in dredge 1 lavas. The minerals are interpreted to be smectite pseudomorphous after melilite. Determination of the minerals as melilite is based on tetragonal habit, peg structure, and associated undersaturated minerals (Ti-salites; Yang, 1975,1976). Plane-polarized light, 50x.

based on several considerations. The laths are tetragonal in habit and possess noticeable "peg" structure suggestive of melilite whose presence is expected with the Ti-salites (Yang, 1975, 1976). Smectite is a common alteration product of basic, alkaline igneous rocks whereas illite might be expected if the original igneous phase was feldspar. However, calcium is very low in the minerals and seawater alteration could account for this (Ito and Anderson, 1983). The two most likely original minerals represented by the laths are plagioclase and melilite. The less likely alternative, because of their crystal habit and composition, is that the laths represent altered plagioclase. It is therefore inferred, based on similarities with pyroxenes from suites of nephelinitic and basanitoid lavas and on the inferred presence of melilite, that the rock represented in RD 1 is a critically undersaturated melilitite or basanitoid.

1.2.2 Lalla Rookh Bank - RD 3

Chemically and petrographically, the undersaturated lavas of Lalla Rookh resemble the basanites, nephelinites, and ankaramites erupted in Tutuila, Upolu, and Savai'i, Samoan Islands. Shield lavas from Upolu and Manu'a Islands resemble Lalla Rookh ankaramites in their strongly bimodal assemblage of olivine and Ti-augite (Natland, 1980; Stice, 1968). Analyses of clinopyroxenes from ankaramites and a fine grained basanitoid recovered in RD 3 are listed in appendix B, and their positions in the pyroxene quadrilateral are shown along with Samoan pyroxenes in Figure 5. Plots of SiO_2 vs. Al_2O_3 and Ti vs. Al_z (Figures

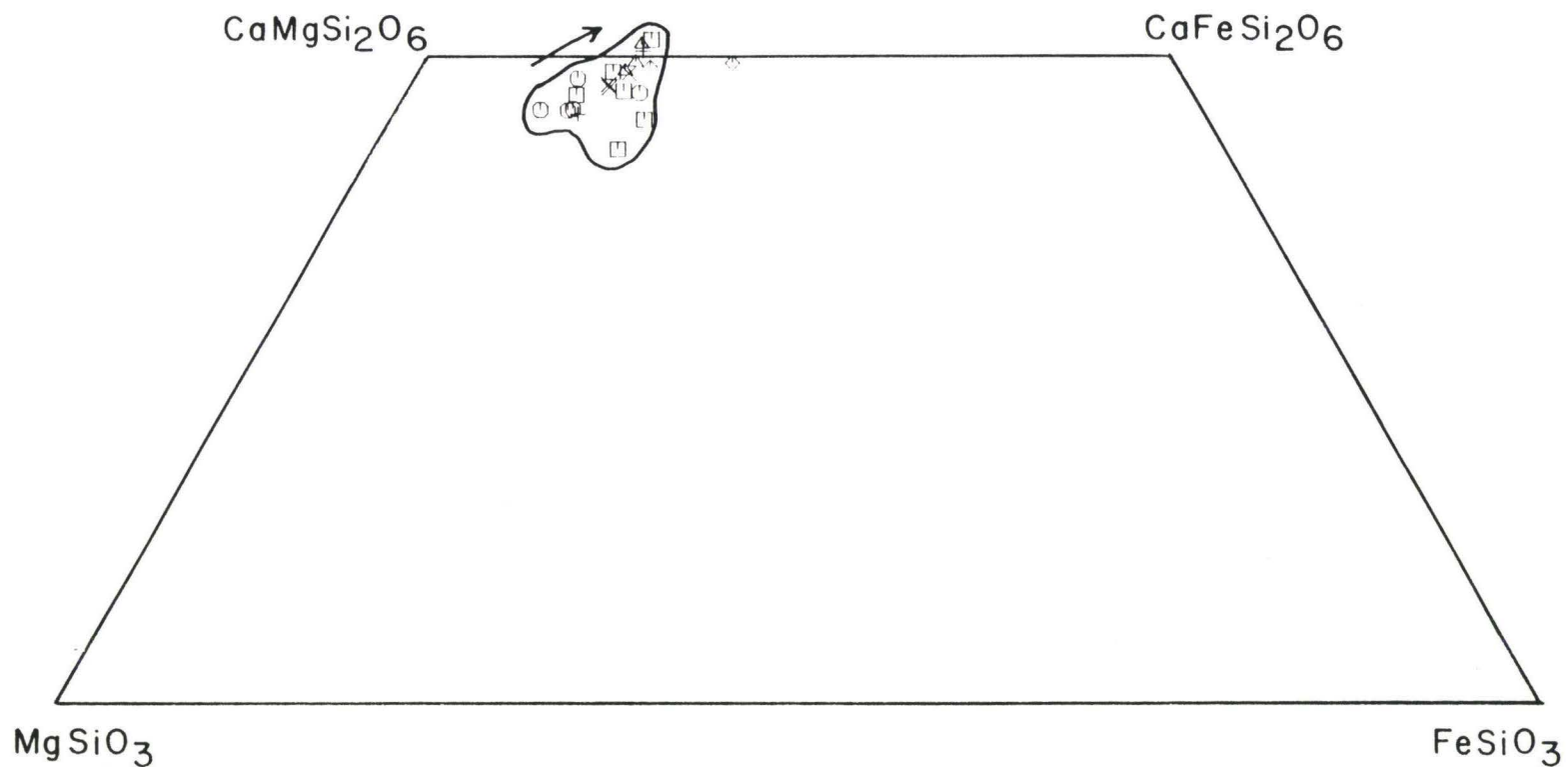


Figure 5. Lalla Rookh Bank pyroxenes plotted on the pyroxene quadrilateral. Arrow indicates crystallization trend of pyroxenes from Hawaiian nephelinitic lavas (Fodor et al., 1975). Field encloses Lalla Rookh pyroxenes: squares = sample 3-16 cpx; circles = sample 3-36 cores; triangles = 3-36 rims; pluses = 3-36 groundmass; X's and diamonds = cpx cores and rims respectively from Samoan post-erosional lavas (Natland, 1975).

6 and 7) show that all of the groundmass grains fall in the peralkaline field of Le Bas (1962). Furthermore, compositional trends of phenocrysts and groundmass phases coincide with crystallization trends of pyroxenes from posterosional lavas from Samoa and nephelinic lavas from Hawaii (Figure 5).

Sample 3-36 also contains a presumably high pressure inclusion made up of aluminous and calcic phases. It consists of extremely fine-grained (5 to 10 microns) green pyroxenes and a colorless aluminous phase, possibly plagioclase. The pyroxene crystals are generally euhedral and appear to be recrystallized (Figure 8). The inclusion resembles Ti-augite rimmed lherzolite inclusions in similar ankaramitic lavas described by Tracy and Robinson (1977). An inclusion of this kind supports the deep origin for the Lalla Rookh lavas.

The preceding analysis provides evidence for similarities between Lalla Rookh and Samoan post-erosional volcanism based on pyroxene compositions. Whole rock analyses for samples from Lalla Rookh are listed in Appendix A. The four analyzed samples vary widely in CaO, MgO, K₂O, and Al₂O₃ which is predicated on the variable quantities of clinopyroxene and olivine phenocrysts in the samples (see petrographic descriptions -- Appendix D). However, the normative compositions of the four analyzed rocks fall within the undersaturated nephelinic to basanitic field on a simplified basalt tetrahedron (Yoder and Tilley, 1962) characteristic of undersaturated lavas from Samoa (Figure 9). The lavas from Lalla Rookh, occupy the same field as the undersaturated basanites and nephelinites of Samoan post-erosional volcanism (Natland,

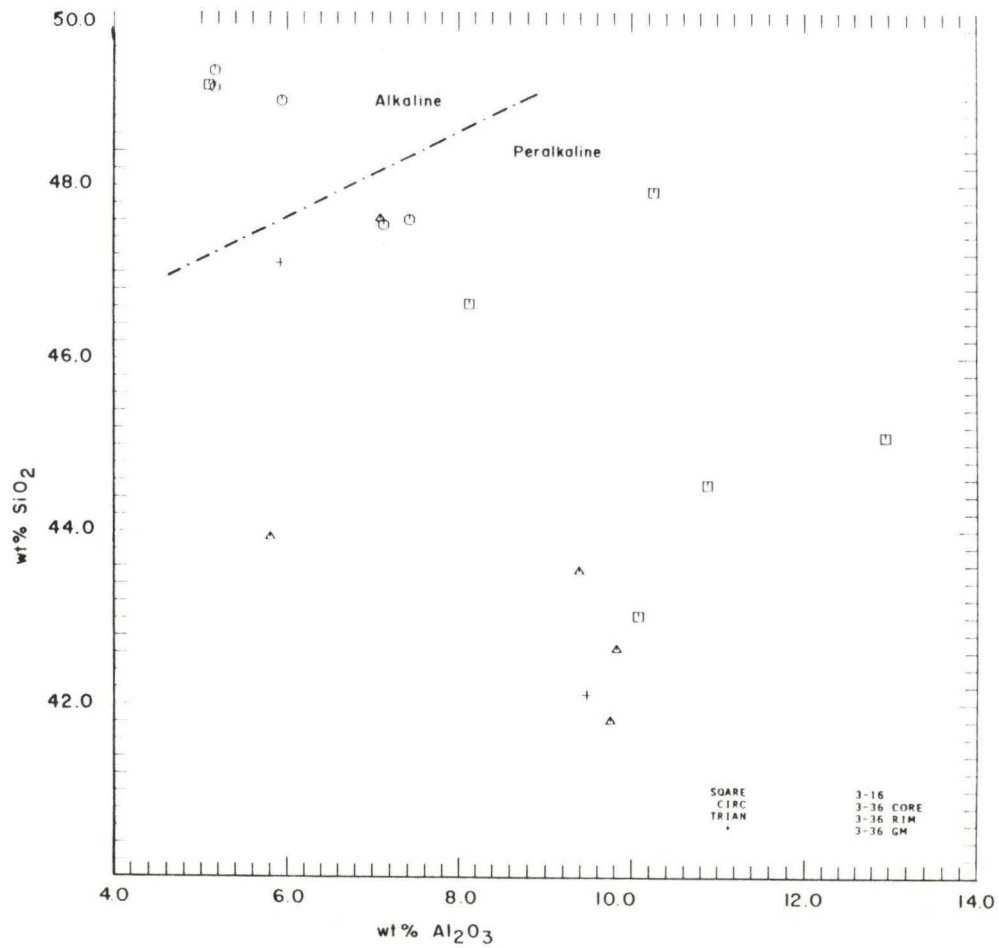


Figure 6. Wt% SiO₂ vs. Al₂O₃ for Lalla Rookh pyroxenes. Dot-dash dividing line is after LeBas (1962). Most of the phenocryst cores and all of the rims and groundmass phases plot within the peralkaline field. Symbols as noted.

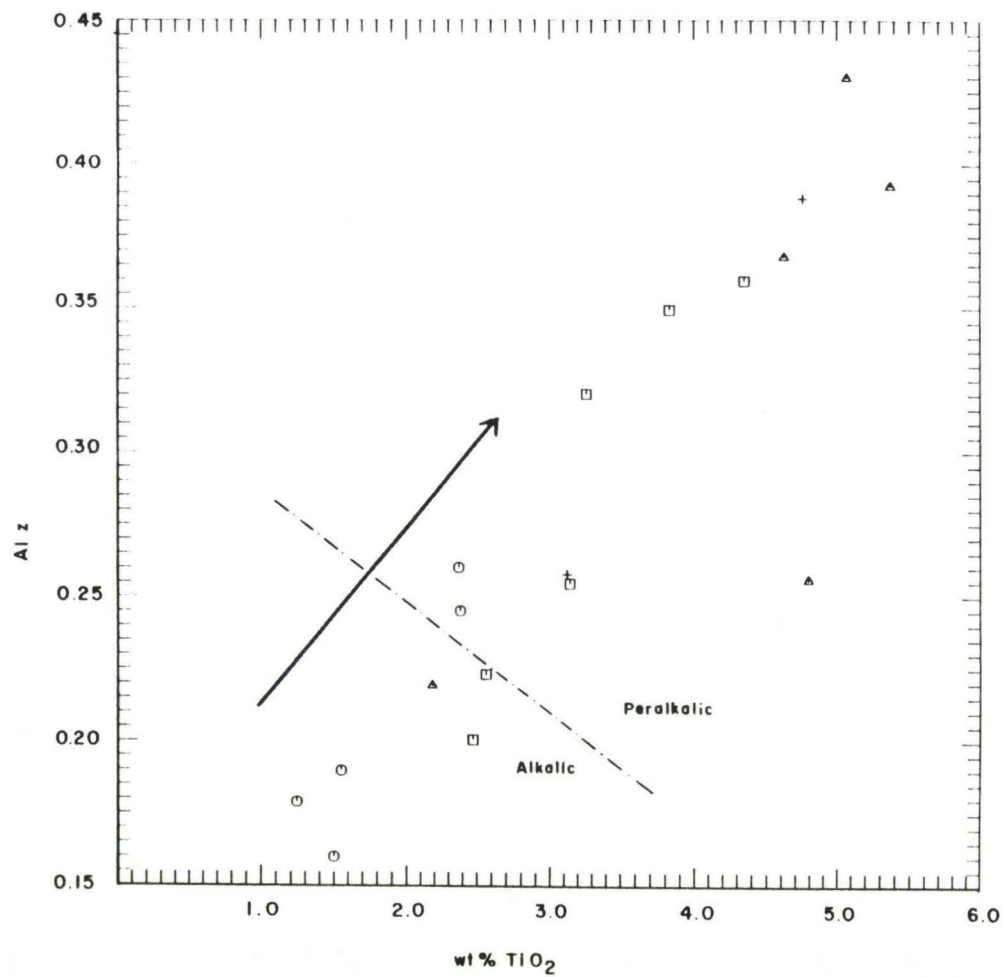


Figure 7. Tetrahedral aluminum (Alz) vs. wt% TiO₂ for Lalla Rookh pyroxenes. Dividing line is after LeBas (1962) and shows that most of the phases fall in the peralkalic field. Symbols as in Figure 6.

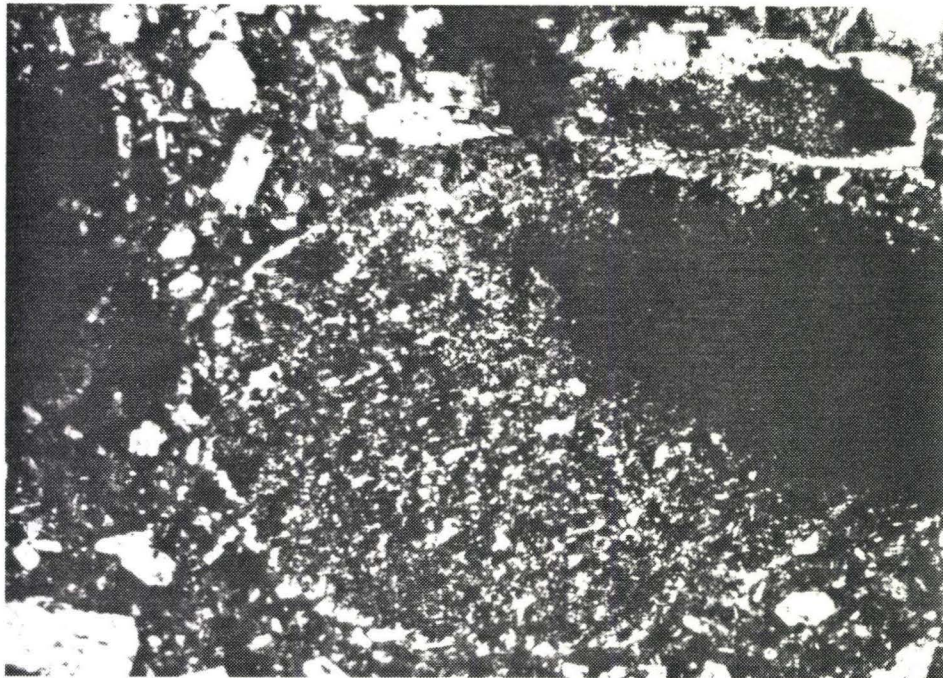


Figure 8. Photomicrograph of fine-grained inclusion in sample 3-36. The inclusion is composed of euhedral green pyroxenes 5-10 μ in size and a colorless aluminous phase, possibly plagioclase. Spinel may also be present. The inclusion resembles those described by Tracy and Robinson (1977) from Tahiti and supports a deep origin for these lavas. Plane-polarized light, 50x.

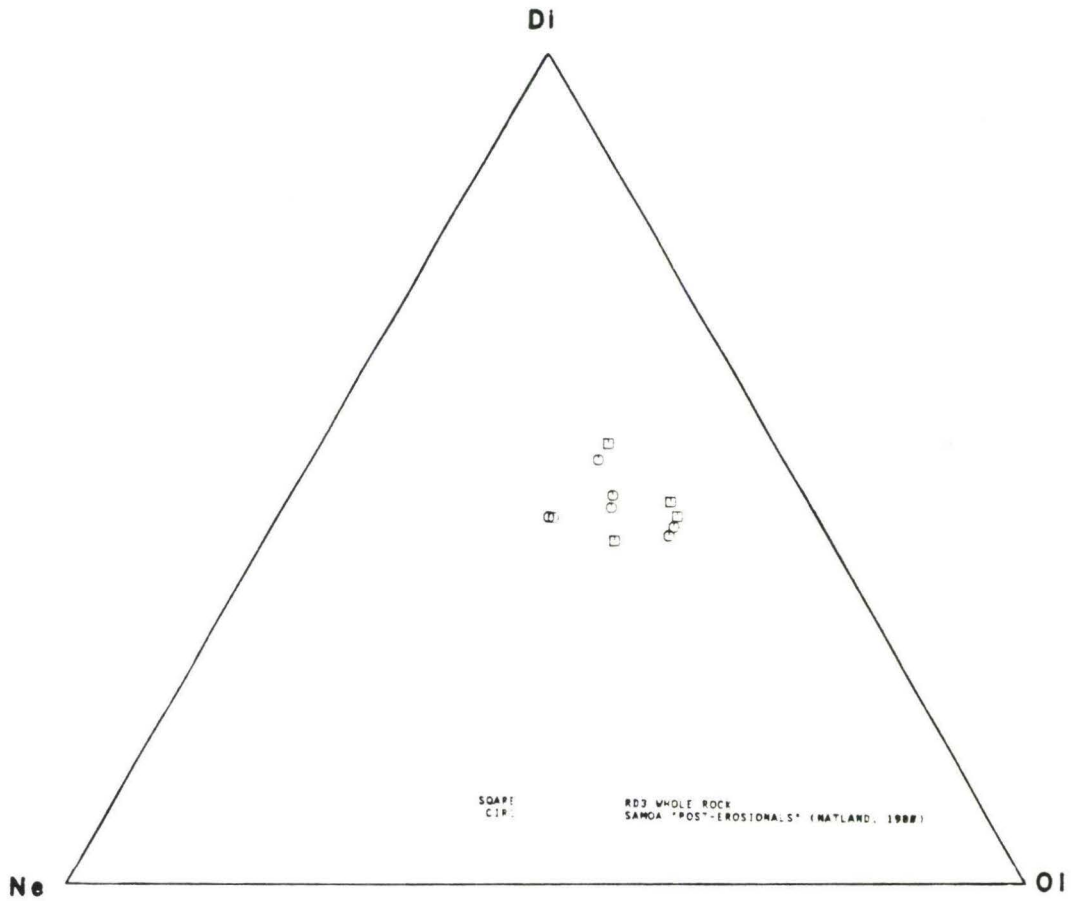


Figure 9. Normative Di-Ne-O1 ternary projection from the simplified basalt tetrahedron (Yoder and Tilley, 1962) comparing Lalla Rookh and Samoan post-erosional lavas (from Natland, 1980). The two sample suites occupy the same normative field reflecting their similar bulk-rock compositions.

1975) on an alkalis-silica diagram (Macdonald and Katsura, 1964) (Figure 10). However, these highly undersaturated lavas are not confined to post-erosional volcanism and Natland (1980) also reported an analysis of a highly nepheline normative basanite from the Fagaloa shield volcano on Upolu. Nonetheless, the lavas from post-erosional and shield stages of volcanism in Samoa are generally well separated on an alkali-silica diagram (Natland, 1980) and Lalla Rookh samples fall within the post-erosional field.

If basanites and olivine melilitites are generated by small degrees of partial melting of a garnet or spinel peridotite (Bultitude and Green, 1971), then partial melts will be Al-poor. The moderately low abundances of yttrium (25 ppm) found in dredge 3 lavas may indicate that garnet was a residual phase during the melting event that produced these lavas.

The levels of Rb and Sr in the Lalla Rookh samples are as high or higher than the Samoan post-erosional lavas. Incompatible trace element compositions of magmas produced by a small degree of partial melting should be high if the source is undepleted by previous melting. The $\text{Sr}^{87}/\text{Sr}^{86}$ ratios of Samoan lavas are among the highest sampled from oceanic islands (Hedge et al., 1972) implying an undepleted source. High Rb contents will produce high Sr^{87} contents. This trend of increasing Rb and Sr west from Samoa is consistent with the observed trend of increasing $\text{Sr}^{87}/\text{Sr}^{86}$ proceeding west along the Samoan chain (see discussion below) (Hedge et al., 1972; Natland, personal communication, 1983).

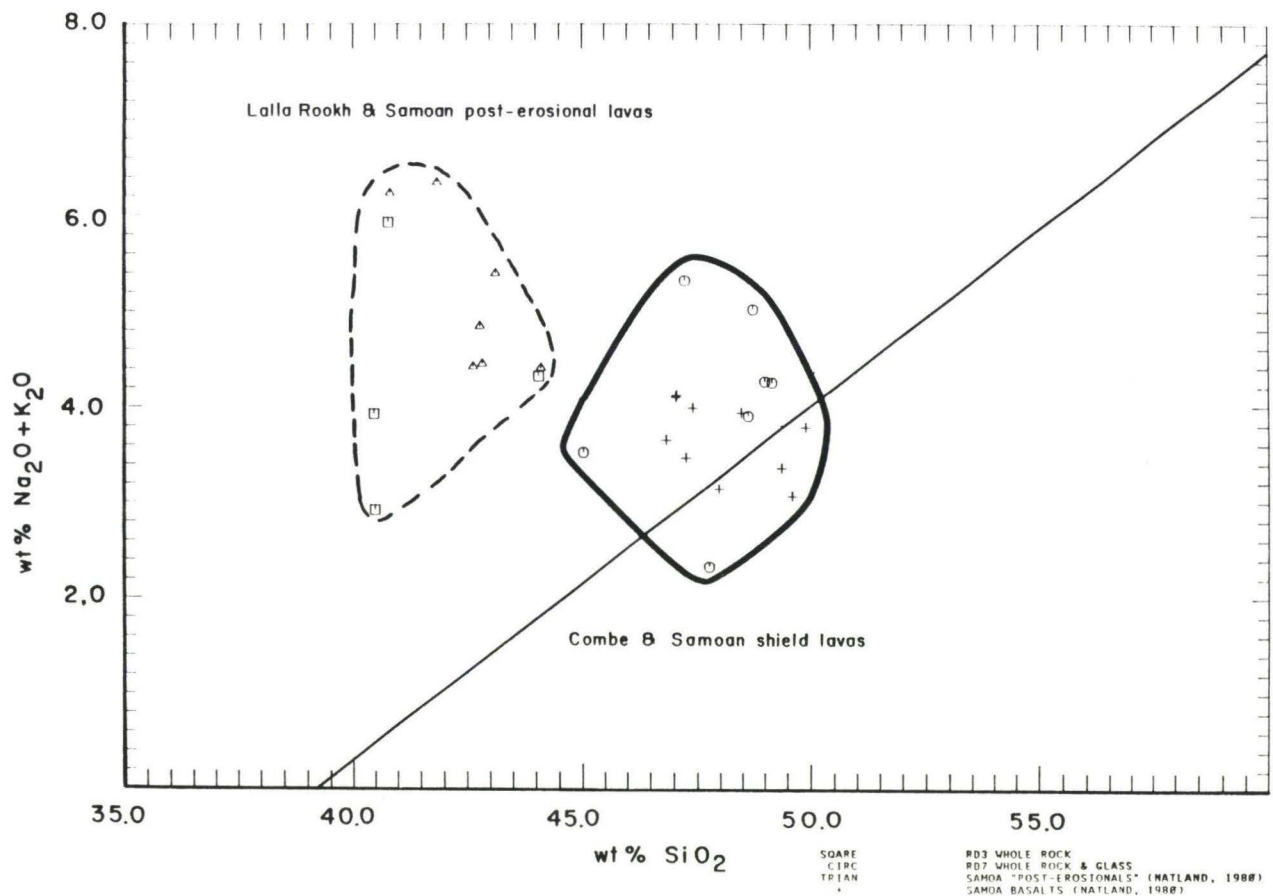


Figure 10. Alkali-silica diagram of rock analyses from Samoan seamount lineament lavas of this study and Samoan lavas (Natland, 1980). Two main groupings are defined: Samoan post-erosional lavas and Samoan shield-type lavas. See text for discussion of these two types. Diagonal line is the empirical tholeiitic-alkalic discriminant defined by Macdonald and Katsura (1964).

Rb/Sr ratios are generally less than 0.04 for shield lavas and between 0.05 and 0.11 for post-erosional lavas in Samoa. K/Rb ratios are between 1500 and 300 for shield lavas and between 350 and 270 for post-erosional Samoan lavas (Natland, 1980). Lavas of dredge 3 contain Rb/Sr ratios of 0.02 to 0.12 and K/Rb ratios of 370 to 260 typical of Samoan post-erosional lavas.

1.2.3 Combe Bank - RD 7

Rocks from dredge 7 are variable in chemistry and mineralogy, but generally exhibit alkalic to transitional affinities (TiO_2 - 2.5% to 4.5%, $\text{Na}_2\text{O} + \text{K}_2\text{O}$ - 2.5% to 5.0%). They plot in the appropriate alkalic to transitional field on an alkali-silica diagram (Figure 10), but seawater alteration may have produced anomalously high alkali abundances. Figure 10 illustrates the variability in compositions ranging from fairly strongly alkalic (more altered samples) to tholeiitic (freshest sample). On Mullen's (1983) discriminant diagram (Figure 11), the samples span the oceanic island fields from tholeiitic to alkalic. P_2O_5 may be added during alteration, however (Staudigel and Hart, 1983), so that this interpretation is somewhat uncertain.

Alteration of basalt can push tholeiites into the alkalic field of alkali - silica space due to the release of silica and the absorption of alkalis (Hart et al., 1970). Seawater alteration preferentially leaches some elements, mainly calcium and magnesium and enriches sodium, potassium and water (Ito and Anderson, 1983). Care must be applied in correcting for seawater alteration so as not to create false

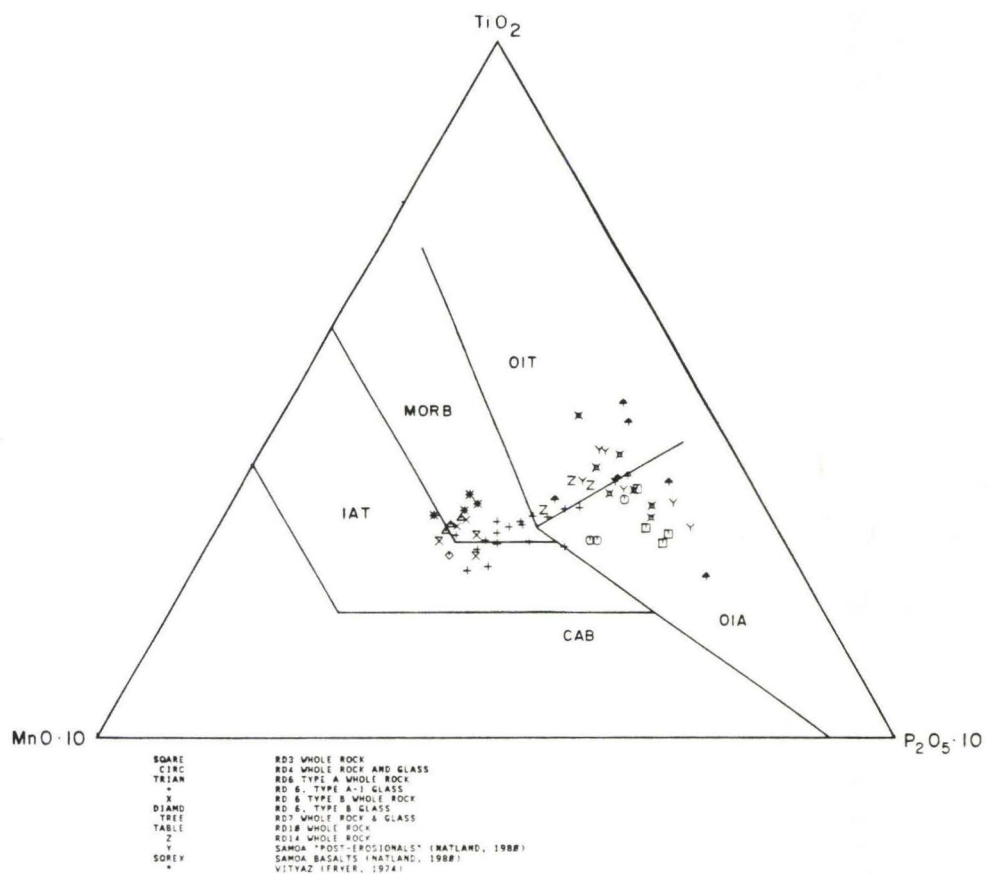


Figure 11. TiO₂-MnO-P₂O₅ discriminant diagram of Mullen (1983) used to separate basalts from various tectonic environments.

compositions. In recalculating the potassium contents of the more altered samples, I studied the petrography to make sure I was not trying to equalize vastly different phenocryst assemblages with true chemical differences. The amount of seawater alteration in the rocks was interpreted by relative amounts of Fe^{3+} vs. Fe^{2+} and H_2O^- . When Fe^{3+} exceeded Fe^{2+} and H_2O^- exceeded 1%, I corrected K_2O for probable seawater alteration. This correction factor was calculated using the $\text{Na}_2\text{O}/\text{K}_2\text{O}$ ratio of the least altered sample (sample 7-9, $\text{Na}_2\text{O}/\text{K}_2\text{O} = 3.2$). The factor was then applied to the altered samples and the adjusted alkali abundances plotted on the alkali - silica diagram. Figure 12 shows that none of the alkalic rocks from Combe Bank were shifted into the tholeiitic field by this correction, but they were obviously pushed toward more transitional compositions. If possible I would have employed many more analyses of altered and unaltered pairs for a more rigorous correction.

Sample 7-11 is noticeably different from the other samples from Combe Bank in its mineralogy as well as its freshness. Olivine is the only phenocryst in the rock and the chemical analysis reflects this ($\text{MgO} = 16 \text{ wt.}\%$). No olivine is present in the groundmass, however, and the olivine phenocrysts seem to be in reaction relation with the melt as evidenced by the embayed crystal boundaries on formerly euhedral grains. This feature resembles basalts from Tutuila shield volcanoes which also characteristically contain only olivine as a phenocryst phase (Natland, 1980).

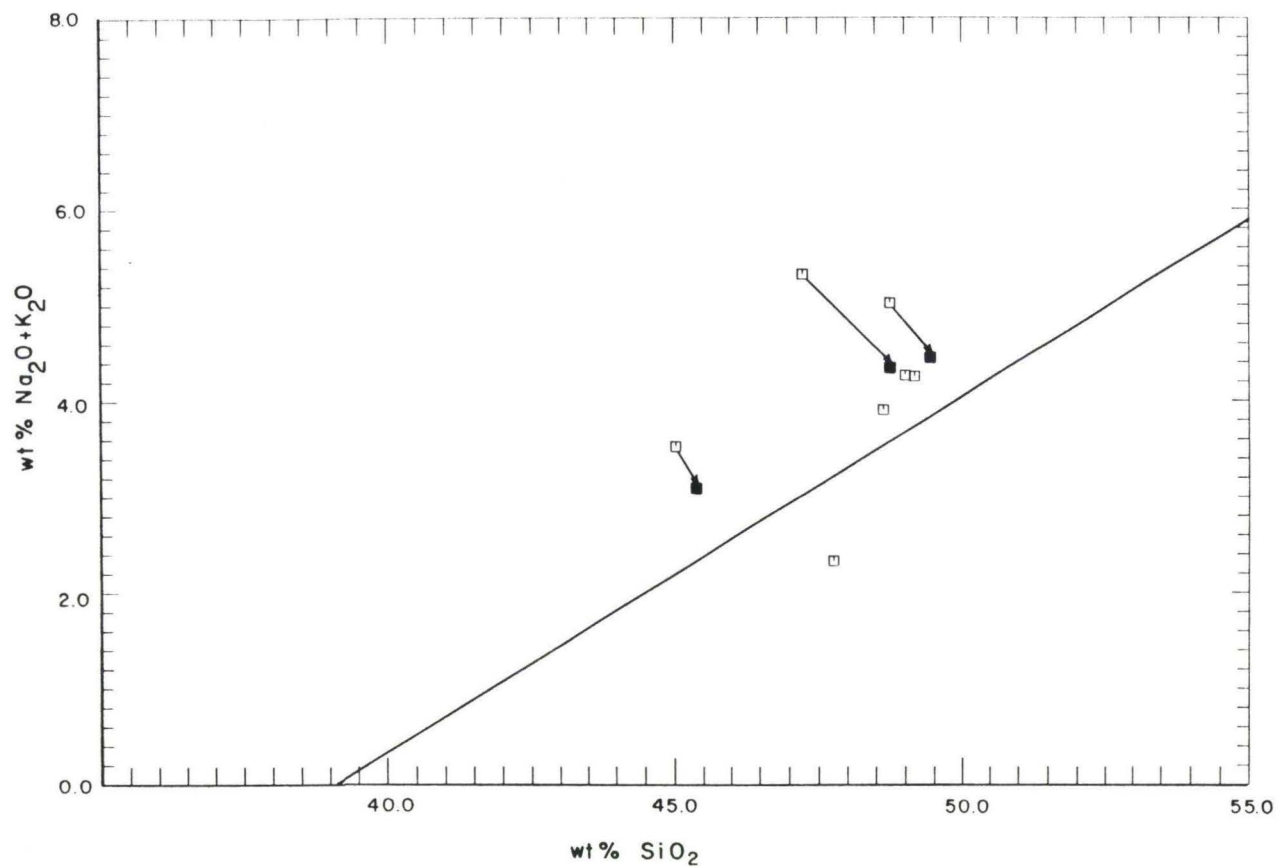


Figure 12. Alkali-silica diagram of Combe (dredge 7) lavas corrected for alteration effects. Solid squares mark the compositions of samples corrected for alkali enrichment due to seawater alteration (Staudigel et al., 1981; Ito and Anderson, 1983). Open squares are uncorrected values. See text for explanation of correction procedure.

Trace element ratios of the suite from Combe Bank are in the ranges exhibited by Samoan shield lavas, i.e.: Rb/Sr - 0.01 to 0.06; K/Rb - 975 to 250. In addition, the high nickel content in sample 7-11 reflects the high proportion of olivine in the bulk rock. This sample is therefore identified as an olivine tholeiite to picritic tholeiite based on the modal mineralogy, the abundant normative hypersthene, and the trace element composition.

Pyroxenes from sample 7-9 were analyzed and they cluster, for the most part, in the alkalic field of the pyroxene quadrilateral, but groundmass grains show a tholeiitic-type crystallization trend (Figure 13). Compositional variations of glomerocrysts typically show an increase in Ti and Al₂ and a decrease in Si and Mg from core to rim. The phenocrysts, however, show a systematic decrease in Ti and Al₂ and an increase in Si from core to rim (Figures 14a, 14b). This shift from alkalic crystallization trends at depth to a transitional tholeiitic crystallization trend toward the surface probably results from a decrease in pressure as the magma migrated from depth toward the surface (Le Bas, 1962; Thompson, 1974). The zonation of the different phases is outlined below:

<u>Average Al₂O₃/SiO₂ x 100</u>	
Phenocryst core	7.7
" rim	5.7
Glomerocryst core	5.8
" rim	8.4
Groundmass	10.0

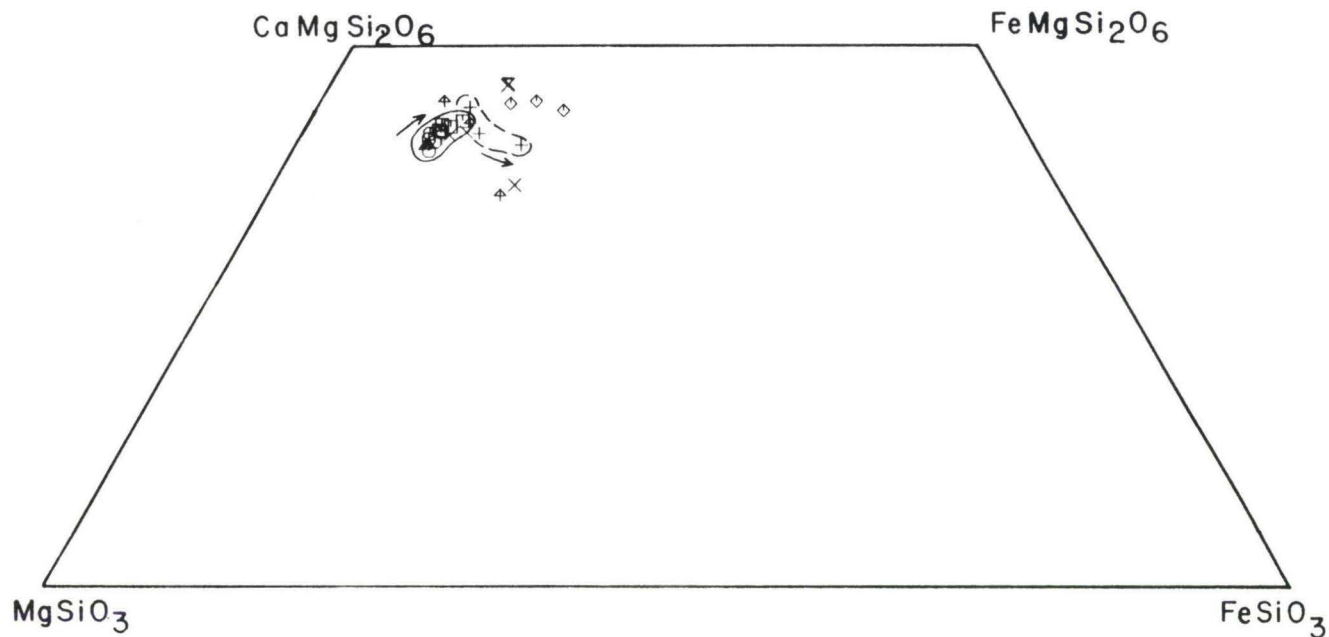


Figure 13. Plot of Combe pyroxenes from sample 7-9 on the pyroxene quadrilateral. Two groupings are evident: 1. alkalic trend (field enclosed by solid line), and 2. tholeiitic trend (field enclosed by dashed line). Arrows indicate crystallization trends of Hawaiian pyroxenes from Fodor et al. (1975). Squares = glomerocrysts; circles = phenocrysts; triangles = megacrysts; pluses = groundmass; X's and trees = Samoan tholeiitic cpx; diamonds and tables = Samoan alkalic cpx (Natland, 1975).

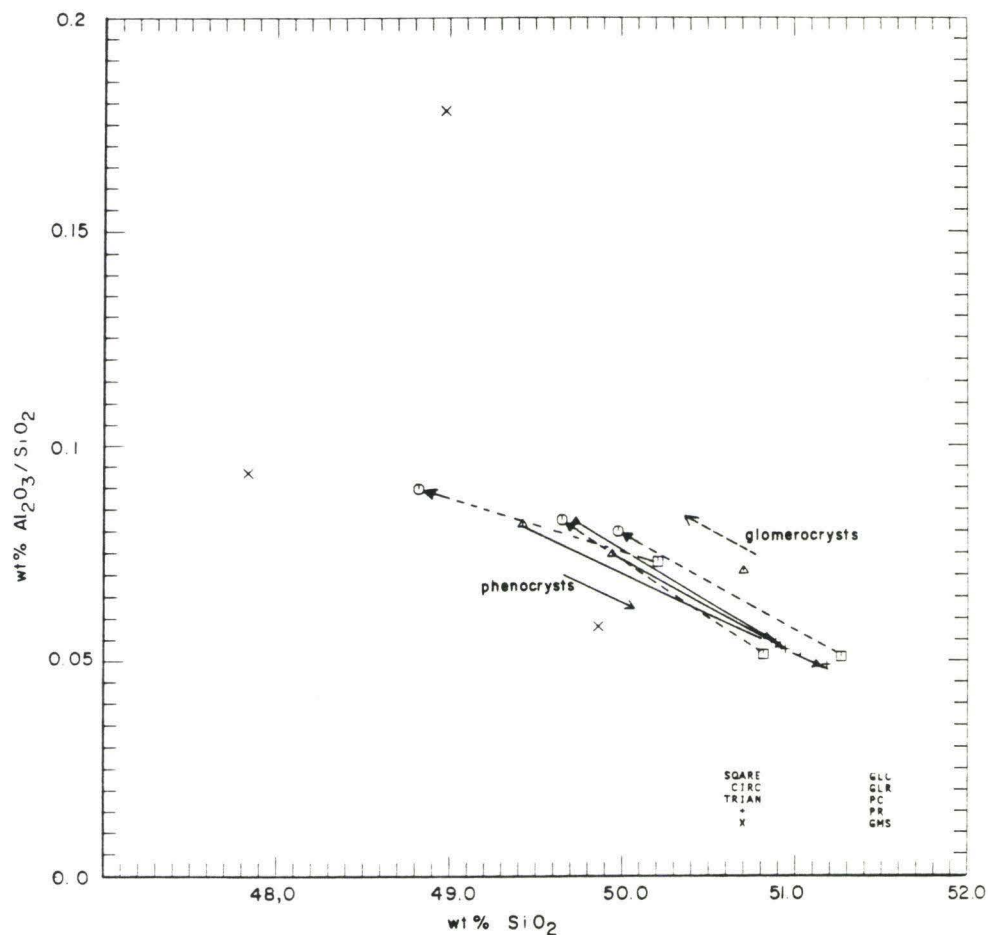


Figure 14a. Wt% Al₂O₃/SiO₂ vs. SiO₂ for cpx from sample 7-9. The ratio reflects alumina and silica activity and generally increases with crystallization in alkalic pyroxenes and decreases in tholeiitic pyroxenes. It may also be affected by pressure and temperature changes (Thompson, 1974). Note the increase in the ratio from core to rim of glomerocrysts and the general decrease from core to rim of phenocrysts, possibly reflecting decreasing pressure and temperature in a rising body of magma.

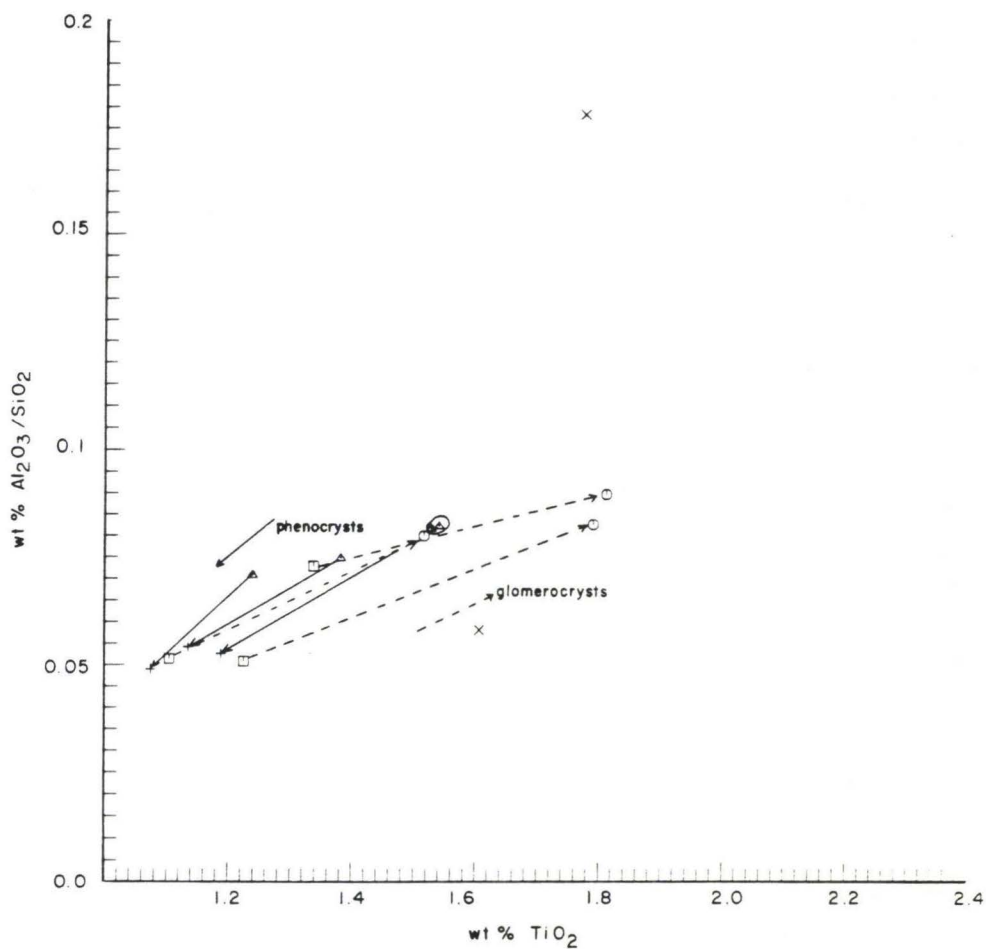


Figure 14b. Wt% $\text{Al}_2\text{O}_3/\text{SiO}_2$ vs. TiO_2 for cpx from sample 7-9. TiO_2 and $\text{Al}_2\text{O}_3/\text{SiO}_2$ are expected to increase with crystallization of cpx in an undersaturated liquid. Higher pressures may also promote higher values for these parameters (Thompson, 1974). The data indicate a change from silica undersaturated to saturated conditions from glomerocryst to phenocryst phases. Symbols as in Figure 14a.

Some of the glomerocrysts in 7-9 possess recrystallization textures, i.e. 120 degree grain boundaries. This reaction may record a change in the stability of the higher pressure glomerocrysts as they migrated upward into a lower pressure magma chamber where the more subalkalic pyroxenes crystallized.

Trace element abundances in sample 7-9 also reflect a tholeiitic to transitional affinity. Rb content is low as are high-field-strength cation abundances. Yttrium is relatively enriched, reflecting the abundance of clinopyroxene.

Figure 13 compares Combe pyroxene analyses to Samoan pyroxenes from alkalic and tholeiitic rocks (Natland, 1975). The Combe pyroxenes plot precisely on the Upolu and Tutuila tholeiitic pyroxenes for both phenocryst and groundmass phases. Hence, it appears that Combe Bank is related to Samoan shield lavas rather than to post-erosional lavas.

1.2.4 Alexa Bank - RD 14

Dredge 14 recovered a variety of sedimentary and volcanic rocks from the southern flank of Alexa Bank (Figure C-6). The sedimentary rocks consist of black, indurated, laminated shales, green argillites, and siltstones with generally undisturbed bedding planes. They appear to be deep-water sediments that experienced virtually no disruption prior to lithification.

The volcanic rocks are quite altered and only three were analyzed for major elements. Because these rocks were altered, their classification is tentative. The rocks, however, are not greatly

enriched in potassium although they do contain high proportions of oxidized iron (Appendix A).

The three samples plot in the tholeiitic to transitional region of the alkali - silica diagram (Figure 23). Normative compositions of the rocks range from slightly nepheline normative to strongly hypersthene normative and may be significantly affected by secondary alteration. On a TiO_2 - MnO - P_2O_5 discriminant plot of Mullen (1983) they lie within the oceanic island tholeiite field (Figure 11).

Their petrographic character is tholeiitic. The groundmass lacks olivine and contains abundant glass and phenocryst phases of mainly plagioclase and clinopyroxene with lesser olivine. They are lower in MgO and Al_2O_3 and higher in TiO_2 and incompatible trace elements than MORB (Appendix A). Judging from the diversity of samples in the dredge haul, the rocks may represent several different eruptive events if not different eruptive regimes. The rocks from Alexa Bank are distinctly higher in TiO_2 than rocks from the Vityaz Trench lineament (Fryer, 1974; this study) (Figure 15) and are probably not related to them. They are significantly more tholeiitic than basalts from Samoa, with lower concentrations of K, Rb, Sr, (Appendix A), TiO_2 and P_2O_5 (Figure 16).

Pyroxenes from the three samples (Appendix B), define both tholeiitic and alkalic trends on a pyroxene quadrilateral (Figure 17). Two samples, 14-15 and 14-19, follow a tholeiitic fractionation pattern, whose early stages are marked by a decrease in Ca and an increase in Fe. For these samples systematic decreases in SiO_2 , CaO, and MgO, and an

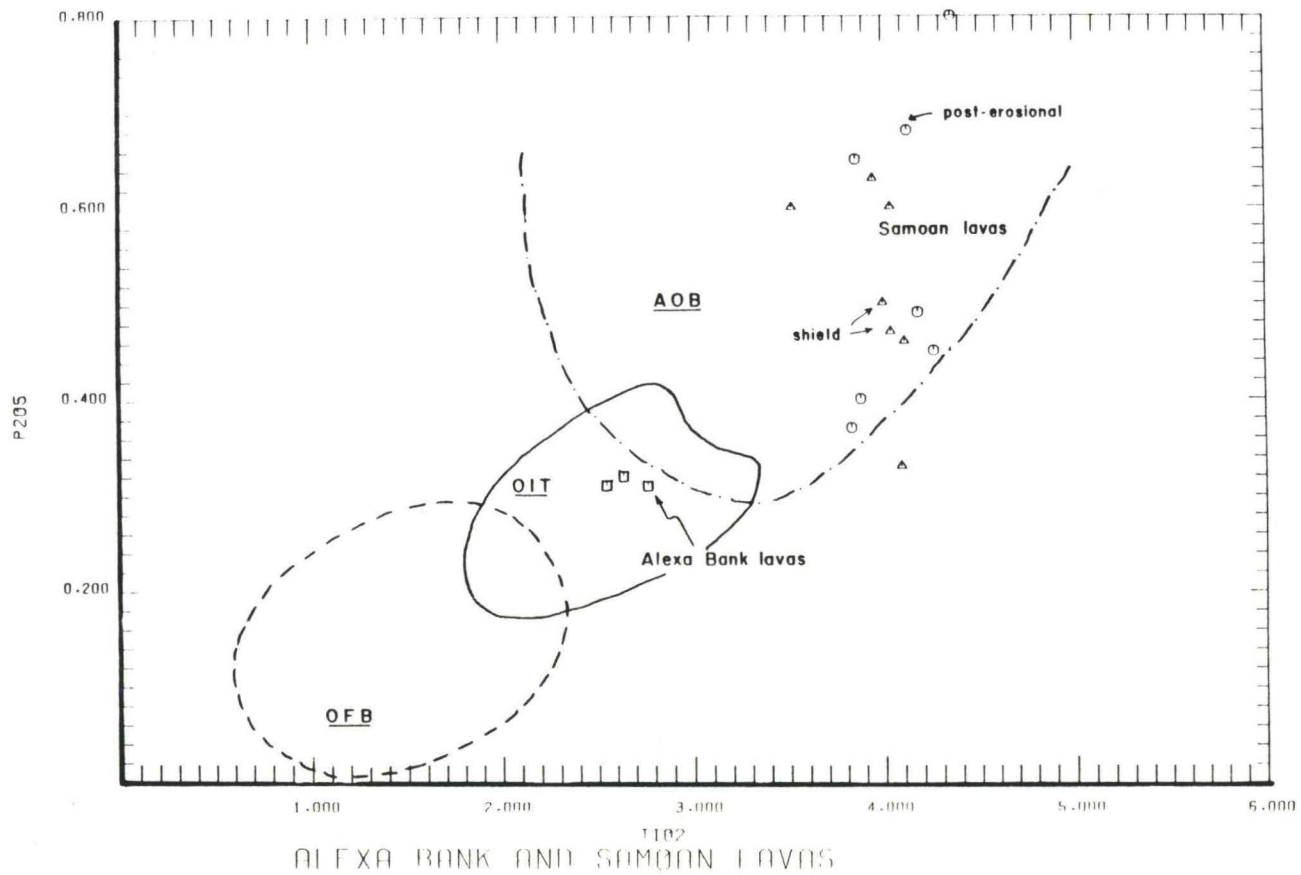


Figure 16. Wt% P_2O_5 vs. TiO_2 for Alexa Bank lavas and Samoan lavas to point out the distinct fields occupied by both. Samoan data from Natland (1980).

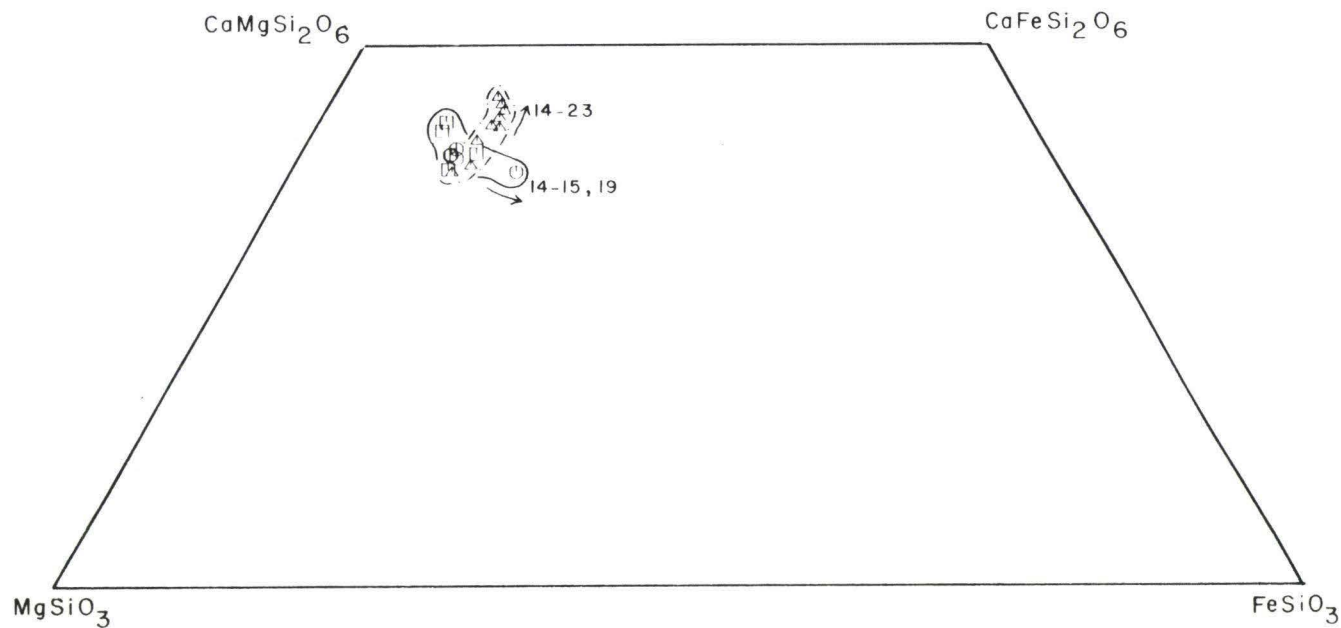


Figure 17. Pyroxene plot for Alexa Bank (dredge 14) samples. Pyroxenes from three samples, 14-15, 14-19, and 14-23 are shown. Samples 14-15 and 14-19 follow tholeiitic crystallization paths commensurate with their Hy-normative bulk-rock compositions. Sample 14-23, however, follows an alkalic path in accordance with its Ne-normative character. Arrows indicate respective crystallization paths. Squares = 14-15; circles = 14-19; triangles = 14-23.

increase in FeO from phenocryst core to rim to groundmass is typical of tholeiitic pyroxene differentiation.

Sample 14-23, however, follows a very different fractionation path and contains noticeably different elemental abundances. Both TiO_2 and Al_2O_3 are more abundant in 14-23 than in the other two samples and both elements increase with crystallization. SiO_2 abundances are generally similar, but MgO and FeO are lower in 14-23 and CaO increases with crystallization. On the quadrilateral (Figure 17), the 14-23 pyroxene follows an alkalic crystallization trend.

1.3 DISCUSSION

Taviuni and Field Banks are both elongated ridges (Brocher in preparation). As previously noted the Samoan post-erosional zone extends the length of Upolu and Savai'i and is characterized by voluminous basanitic to nephelinic volcanism over virtually its entire length (Natland, 1980). This flexure-induced rift zone is apparently broad as evidenced by the wide belt of Samoan volcanism (Figure 2) and may control the morphology of the linear islands which trend parallel to Pacific Plate motion. Taviuni-Field Bank is strikingly elongate in the same general orientation as Savai'i and Upolu and may have been formed by similar processes. The recovery of undersaturated melilitite or basanitoid lavas on Taviuni-Field Bank, coupled with its geomorphology, is consistent with the hypothesis that the same volcanic processes that produced Recent Samoan volcanism also formed Taviuni-Field Bank. Furthermore, sediments surrounding Taviuni and Field Banks are faulted

through the entire sediment column indicating a young age for the seamount-forming volcanism (Brocher, in preparation). These data are consistent with the age (5.4 ± 0.2 m.y., Duncan, in preparation) and geochemical character of Taviuni-Field lavas and support the hypothesis that this bank is related to recent Samoan post-erosional volcanism.

Figure 18 shows reconstructed positions of the three studied seamounts assuming average plate velocities of 9.5-10.5 cm/yr (Minster and Jordan, 1978) and the determined ages (Duncan, in preparation). Distances are calculated with respect to Combe Bank. It is apparent that the present data indicates that the sampled lavas from Taviuni-Field Bank were formed at a more westerly location than those from Lalla Rookh and Combe Banks. The reconstructed location for Taviuni-Field Bank falls between Upolu and Tutuila consistent with the Recent post-erosional volcanism along the length of the Samoan chain (345 km, Stearns, 1944). Using this rotation rate, Lalla Rookh and Combe Banks would have formed 40 to 250 km east of Rose Atoll. The age and volcanic affinity of Rose Atoll is unknown. However, its morphology is consistent with a young age. The overlap between Lalla Rookh and Combe zero-age reconstructions suggests that they could have formed close to the same location in a fixed frame of reference. It seems unlikely that flexure at the tip of the Tonga Trench would affect the lithosphere this far to the east of the trench axis.

Moreover, ten million years ago the North Fiji and Lau Basins had not begun to open (Weissel, 1977; Malahoff et al., 1982) and the Tonga-Vityaz Trench probably lay at least 200 kilometers to the west of its

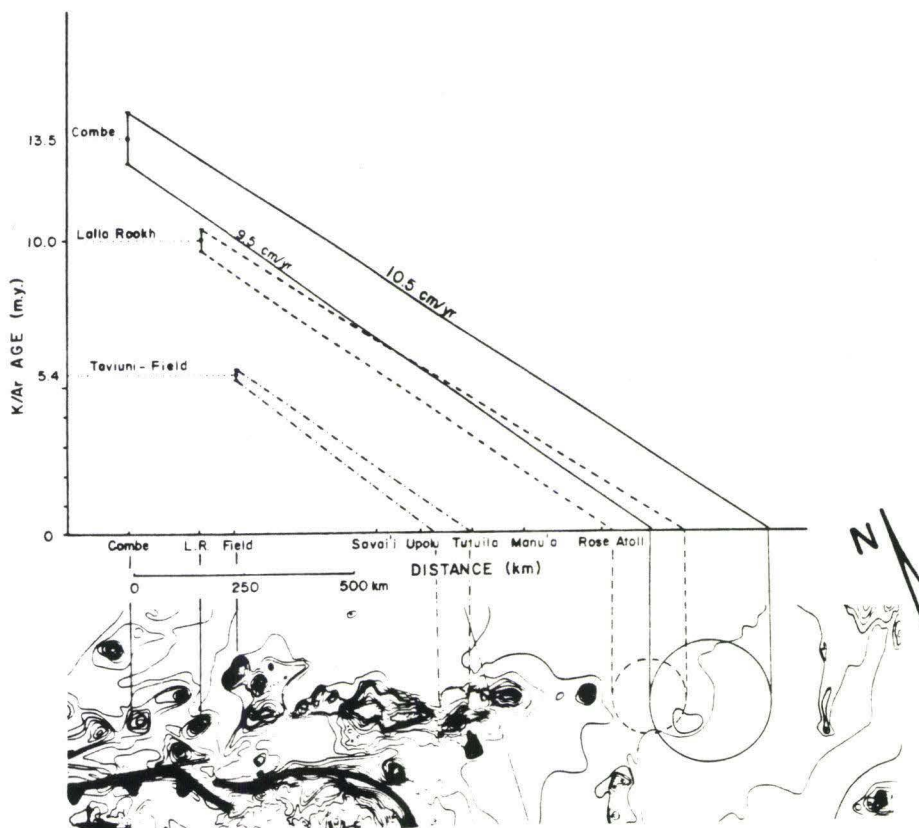


Figure 18. K/Ar age vs. distance along the Samoan seamount lineament. Circles projected onto the map represent the range in possible zero-age positions of the seamounts and banks assuming plate rotation rates of 9.5-10.5 cm/yr and K/Ar ages as shown with their assigned uncertainties (Duncan, in preparation). The upper line in each projection is the upper limit of plate velocity (10.5 cm/yr) used in the calculation, the lower line, the lower limit (9.5 cm/yr) (Minster and Jordan, 1978). The overlap of the circles for Lalla Rookh and Combe Banks indicates the possible location of a hot-spot responsible for Samoan shield and perhaps some "post-erosional" type volcanism.

present location. Given the Pacific-Australia plate convergence rate in the last 10 m.y. the distance between the bend in the Tonga-Vityaz Trench and the indicated point of formation of Lalla Rookh and Combe was probably over 1000 km. The volcanism on Combe Bank resembles Samoan shield volcanism (Macdonald, 1944; Natland, 1980) and is consistent with formation at a hot spot. Lalla Rookh volcanism is, however, nearly identical to Samoan post-erosional volcanism. Therefore, the sampled Lalla Rookh volcanics may relate to undersaturated Samoan post-erosional volcanism although the relationship of this activity to hotspot processes is unclear.

Lalla Rookh's zero age position is 80 to 300 km west of Combe's. While this difference could be within the error of the age determinations (potassium addition and argon diffusion during alteration), it could also reflect different volcanic sources. The lavas from Lalla Rookh resemble Samoan post-erosional lavas (Table 1) and it is expected that they would be erupted after the shield lavas which the Combe lavas closely resemble.

TABLE 1. Chemical Analyses of Volcanic Rocks from
Samoa Seamount Lineament

	1	2	3	4	5
SiO ₂	40.3	46.8	47.4	42.7	46.5
TiO ₂	3.8	3.8	2.7	3.6	3.7
Al ₂ O ₃	10.1	13.1	14.3	11.7	12.8
FeO* ³	12.9	10.8	10.9	12.5	12.2
MnO	0.2	0.2	0.2	0.2	0.2
MgO	12.8	7.8	6.8	12.5	8.6
CaO	11.7	10.2	9.8	10.2	9.7
Na ₂ O	2.6	2.8	3.0	3.0	2.9
K ₂ O	1.5	1.2	0.5	1.5	1.0
P ₂ O ₅	0.7	0.5	0.3	0.5	0.5
H ₂ O ⁺	2.1	1.4	1.6		
CO ₂	0.4	0.1	0.4		
TOTAL	100.2	100.1	100.2	98.5	98.1

* - Total iron as FeO

1. Average of four basanitoid ankaramites, Lalla Rookh Bank.
2. Average of seven alkali basalts, Combe Bank.
3. Average of three tholeiitic to transitional basalts, Alexa Bank.
4. Average of fourteen Samoan post-erosional basanites (Natland, 1975).
5. Average of sixteen Samoan alkalic "shield" basalts (Ibid.).

Evidence for different sources along the Samoan chain comes from trace element abundances. Hedge et al. (1972) noted an increase in Sr^{87}/Sr^{86} in post-erosional lavas westward along the Samoan chain and invoked lateral mantle heterogeneity to explain this variation. Though the data from Lalla Rookh are scattered, a trend of increasing Rb/Sr appears to continue westward through Lalla Rookh Bank. At Combe Bank, however, the low ratio is similar to those for Samoan shield lavas. The depletion of Rb/Sr to the east supports a model (Hedge et al., 1972) of

lateral heterogeneity of the source for Samoan post-erosional lavas. Assuming a positive correlation between $\text{Sr}^{87}/\text{Sr}^{86}$ and Rb/Sr (Natland, 1975) then it appears that sampled volcanism on Lalla Rookh is consanguinous with Samoan post-erosional volcanism. However, the points at which Samoa's post-erosional volcanism and Lalla Rookh's volcanism occurred are spatially removed by nearly 750 km. Hence, post-erosional volcanism is not confined to the vicinity of the Tonga Trench bend. More work needs to be done on $\text{Sr}^{87}/\text{Sr}^{86}$ differences between Samoan shield lavas and post-erosional lavas to better understand source differences.

It is possible Rb is concentrated in rejuvenation stage lavas relative to shield lavas by lesser degrees of partial melting (Rb being concentrated in the initial melts). Undersaturated lavas similar to those at Lalla Rookh make up shield-building lavas at other locations and are thought to be produced by small degrees of partial melting of peridotite (McBirney and Aoki, 1968; Natland, 1980). Therefore, Lalla Rookh may represent a small degree of partial melting of a Samoan shield source.

Given the present data, it is not possible to state unequivocally which stage of Samoan volcanism Lalla Rookh represents. The age of Lalla Rookh is consistent with Samoan shield volcanism, but its lavas resemble Samoan post-erosional lavas. If Lalla Rookh lavas are related to Samoan post-erosional lavas, then Natland's (1980) model for eruption of post-erosional lavas in Samoa, i.e. plate tearing, is not applicable over the entire length of the Samoan chain. In fact, his model only pertains to the most recent stage of volcanism in historic times; it

appears that Samoan "post-erosional" volcanism was caused by some other process 10 m.y.b.p. at Lalla Rookh.

It is unlikely that Alexa Bank is geochronologically related to any stage of Samoan volcanism. A K/Ar age of 27.7 m.y. and an $^{40}\text{Ar}/^{39}\text{Ar}$ age of 36.9 m.y. has been determined by Duncan (in prep.) which is inconsistent with the reconstructions for Combe, Lalla Rookh, and Taviuni-Field Banks. Furthermore, the magnesium, iron, titanium, and phosphorous contents of Alexa lavas are significantly lower than Samoan lavas (Table 1; Figure 16).

The deformation of the Vityaz Trench adjacent to Alexa Bank indicates that Alexa Bank collided with the trench prior to the reversal of subduction (Brocher, in preparation). However, the provenance of Alexa Bank ocean island tholeiites is not clear from the existing age and geochemical data. On the basis of lithospheric flexure modeling by Watts et al. (1980), Alexa Bank could not have formed on young, thin crust as would exist at a spreading center (Robbie Ridge, Figure 1) (Winterer et al., 1974) and any relationship between Robbie Ridge and Alexa Bank is argued against.

Another possible explanation is that dredged lavas represent fragments of the inner trench wall, but in other dredges from trench walls recovered igneous rocks have been arc-related or ultramafic intrusives (Fryer, personal communication, 1983). The recovery of transitional and tholeiitic ocean floor basalt has not been documented, but Bloomer (1983) has described alkalic lavas dredged from the inner trench wall of the Mariana Trench and argues that they represent portions of seamounts that collided with the trench and were "scraped"

off. Dredge 14 lavas may represent a similar tectonic situation as this and the deformed morphology of the Alexa Trough and Alexa Bank (Figure C-6) support this interpretation.

CHAPTER 2

VITYAZ TRENCH LINEAMENT

This chapter outlines the geologic evolution of the Vityaz Arc and Trench system by discussing the geochemical data collected on leg KK820316-2 and its bearing on current models for the recent history of the Vityaz Trench.

2.1 GEOLOGIC SETTING OF VITYAZ ARC-TRENCH

It has been suggested that the Vityaz Trench is a failed subduction zone that, until the late Miocene, actively subducted the Pacific Plate to the south-southwest (Chase, 1971; Gill and Gorton, 1973; Coleman and Packham, 1976). Much of the evidence for the subduction polarity of the paleo-Vityaz Trench comes from studies of volcanism in Vanuatu. In Vanuatu, three distinct phases of volcanism have been recognized (Mallick, 1973; Barsdell et al., 1982). These are: 1) Oligocene to early Miocene calc-alkalic volcanism of the western belt (Santo and Malekula islands), 2) Miocene to early Pliocene basalts and basaltic andesites of the eastern belt (Pentecost and Maewo islands), and 3) Pliocene to Recent basalts and basaltic andesites of the central chain of islands (Banks Islands).

The western belt represents a segment of the paleo-volcanic arc of the Vityaz Arc- Trench system when subduction was from the northeast.

It exhibits a trend of increasing K_2O across the arc to the southwest, a trend consistent with subduction from the northeast (Dickinson and Hatherton, 1967; Dickinson, 1968, 1970).

Based on seismic reflection studies, sediment cores, and magnetic lineations, Kroenke (1972) has argued that the Ontong Java Plateau impinged on the Solomon Islands in the early Miocene causing subduction along the north-facing arc to cease. Late Miocene to early Pliocene tholeiitic lavas were erupted along the eastern belt as the Vityaz Arc rifted apart. This rifting is roughly contemporaneous with initiation of subduction from the south as a result of the collision of the Ontong Java Plateau (Coleman and Packham, 1976; Kroenke, 1972). The collision of Robbie Ridge with the eastern Vityaz Trench may have contributed to the termination of subduction near Fiji.

Although the time of subduction reversal is not certain, by using the empirical correlation of increasing alkalinity of lavas with progression across the island arc (Kuno, 1965; Dickinson and Hatherton, 1967) an arc polarity may be defined. The minimum ages of rocks possessing this polarity constrains the timing of subduction reversal. In the Northern Lau Islands, the abundance of K, Rb, Ba, U, La/Yb, and Rb/Sr increase from east to west while Na/K and K/Rb decrease (Gill et al., 1983). Rocks from Vanua Levu and Viti Levu also exhibit gradational changes becoming more potassic to the southwest from Vanua Levu to Kandavu. These late-Miocene rocks indicate that the subduction zone faced to the northeast prior to this time (Gill, 1976a). The K_2O compositional gradient in Vanuatu's western belt, from low to high K_2O

values across the arc towards the trench (Mallick, 1973; Barsdell et al., 1982), is consistent with the interpretation of an earlier southwestward dipping subduction zone. It also implies that the current northeast dipping Vanuatu subduction zone has not yet produced the pattern of K_2O variation across the arc defined by Dickinson and Hatherton (1967).

Dates of Vityaz Arc fragmentation are reflected by changes of volcanic affinity in the Borderland region. The changes in Fiji record the change in subduction direction, arc fragmentation, and back-arc basin opening. It is possible, indeed likely, that arc fragmentation is still occurring as the Tonga Trench migrates eastward accompanied by the opening of the North Fiji and Lau Basins. This idea will be developed below to explain the formation of the Horne Islands, Manatu seamount, and Wallis Islands.

As the North Fiji Basin (NFB), the Lau Basin, and the NMB developed, Fiji was literally caught in the middle. Consequently, the volcanic events that took place in Fiji through this period are overprinted one atop the other providing a record of the events. The subject of Fijian volcanism has been treated at length by other authors (Chase, 1971; Gill and Gorton, 1973; Hawkins, 1976; Coleman and Packham, 1976; Gill et al, 1983) and will not be dealt with here.

Based on paleomagnetic data, magnetic lineations on the NFB, and the 65 degrees of clockwise rotation in Vanuatu, Falvey (1975,1979) argued that opening of the NFB commenced by about 6 m.y.b.p. The identification of magnetic anomaly 4 lineations on the NFB (Malahoff et

al., 1982) indicates that spreading may have commenced in the NFB by 8 m.y.b.p. A series of transform faults may have formed to accommodate the radial opening of the newly formed North Fiji Basin, migrating to the east-southeast as the NFB opened (Chase, 1971). The Hazel Holme Fracture zone may be a reactivated transform fault of this sequence (Sinton et al., 1983). The active expression is the seismically active lineation north of Fiji trending ENE-WSW along which left lateral transform motion is occurring (Johnson and Molnar, 1972).

The Hunter Fracture Zone forms the other margin of a zone of a left-lateral transform system of which a portion may be actively subducting. Recent eruptions of arc volcanics in Kandavu testify to the active subduction occurring at the Hunter Fracture Zone (Gill, 1976b). Brocher (in preparation) has also identified morphological features in this area which are distinctively arc-trench associated, specifically the presence of a trench, structural high, forearc basin, and volcanic arc in sequence from east to west.

The NMB and the eastern extension of the Vityaz trench is generally aseismic except for an area having deep-focus earthquakes. In this latter region, on the central NFB 300 km southwest of the Vityaz Trench, deep earthquake hypocenters (~ 600 km) have been recorded (Barazangi and Dorman, 1969) trending southeast to northwest subparallel to the Vityaz Trench (Figure 19, after Barazangi and Dorman, 1969 and Sykes et al., 1969). The absence of medium depth seismic events beneath Vanuatu and the presence of deep earthquakes in the NFB was interpreted to reflect segmentation of the once actively subducting slab beneath the Vityaz

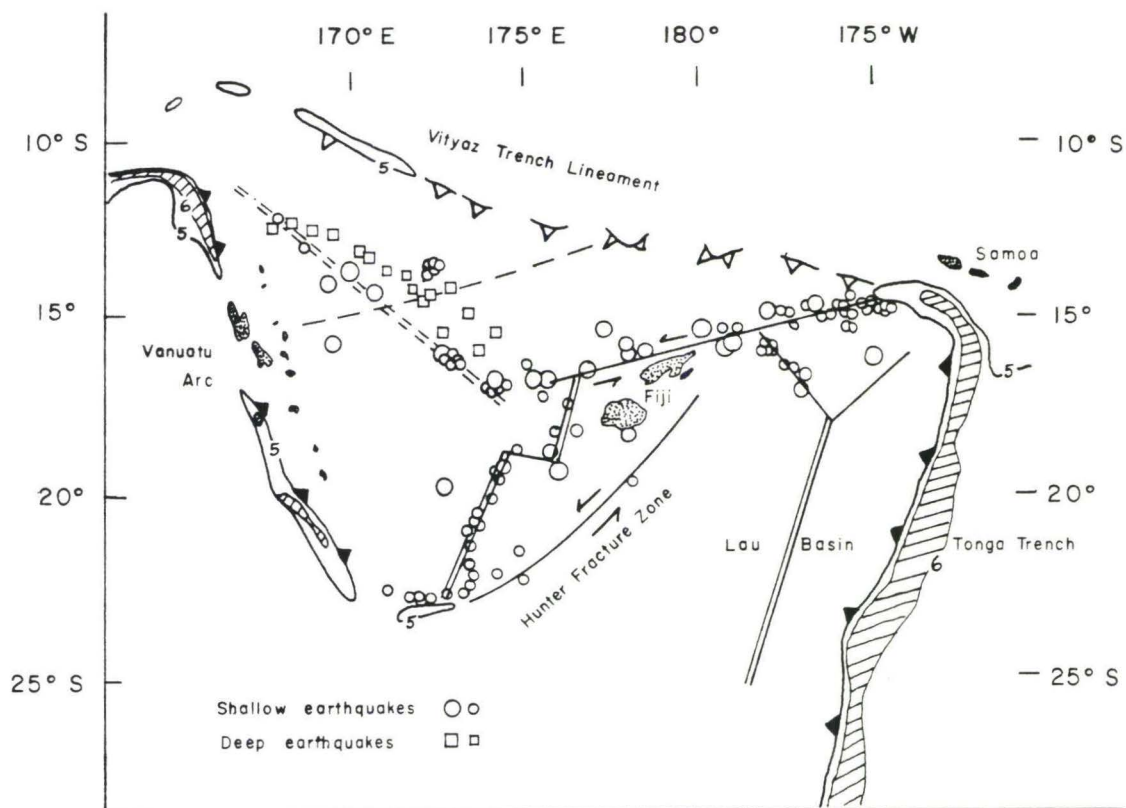


Figure 19. Seismicity of the N.M.B. using data from Barazangi and Dorman (1969), Sykes et al. (1969), Johnson and Molnar (1972), and Barazangi et al. (1973). Schematic representation shows spreading ridges as double lines, dashed where no longer active; transforms as solid lines; shallow earthquakes, circles, deep (> 500 km) earthquakes, squares. Relative size of symbols indicates relative measured magnitude. Depths are in kilometers.

Trench (Barazangi et al, 1973). The cessation of subduction from the north followed by initiation of subduction from the south provides a mechanism for sundering the descending slab.

Petrological evidence for a once-active Vityaz Arc-Trench system is furnished by work on rocks from Tikopea, the Anuda Islands, and the Vityaz Trench (Fryer, 1974) and from Mitre (Fatutaka) Island (Jezek et al., 1977)(Figure 1). Fryer (1974) found that rocks from Tikopea contain higher amounts of silica, alkalis, and phosphate and less iron, calcium, magnesium, and titanium than the rocks from Anuda or the Vityaz Trench. Anuda basalts are enriched in silica, alumina, alkalis, phosphate and titania and depleted in iron, calcium, and magnesium relative to Vityaz Trench basalts. No ages of Anuda rocks are reported, but the island is believed to be a product of Vityaz Trench related volcanism (Fryer, 1974) based on its petrology and its location (see Figure 1). Although enriched slightly in silica and alkalis relative to Vanuatu rocks, Tikopea rocks are calc-alkalic and are genetically similar to Vanuatu andesites (Mallick, 1973; Fryer, 1974).

Jezek et al. (1977) described Pliocene island-arc basaltic andesites with tholeiitic tendencies from Mitre (Fatutaka) Island (Figure 1) located south of the Vityaz Trench on the NFB. They assumed Fatutaka Island to be a remnant of the once active Vityaz Arc which was rendered inactive by its inability to subduct the Robbie Ridge system (Jezek et al., 1977).

Alofi of the Horne Islands and a seamount (named Manatu seamount in this study after the Polynesian word meaning "a thought") southeast of

the Rotuma Trough are discussed together because of their similar geotectonic framework. Both are young and their locations define a lineament parallel to the trend of the remnants of the Vityaz Trench and to the west-northwest trending limb of the Tonga Trench lineament (Figure 20). A discriminant diagram, based on the relative abundances of Ti in lavas from arc versus oceanic island settings, is used. Arc-type lavas are expected to be low in TiO_2 relative to most other tectonic settings and this is reflected in the plot of FeO^*/MgO vs. TiO_2 (Figure 21). It is evident from this plot that Wallis Islands and Alexa Bank plot off the arc trend. The Wallis Islands are discussed later in this section because of their relationship to Vityaz Arc fragmentation, but not to subduction related volcanism.

2.2 GEOCHEMISTRY AND PETROGRAPHY OF DREDGED SAMPLES

2.2.1 Alofi, Horne Islands - RD 6

A rock dredge of Alofi (RD6) yielded altered plagioclase-phyric basalts and very fresh, glassy pillow lavas consistent with the presence of hot springs on the islands (P. Kirch, personal communication to J. M. Sinton, 1982). Ceramic sherds from pottery in Futuna and Alofi have arc rock compositions of andesite, dacite, and rhyodacite (Dickenson, 1976).

Chemical analyses from RD 6 are presented in Appendix A. The data include two distinct parental groups as well as distinct stages of differentiation expressed within the general suite of arc tholeiites to basaltic andesites (Figure 22). All contain extremely low abundances of

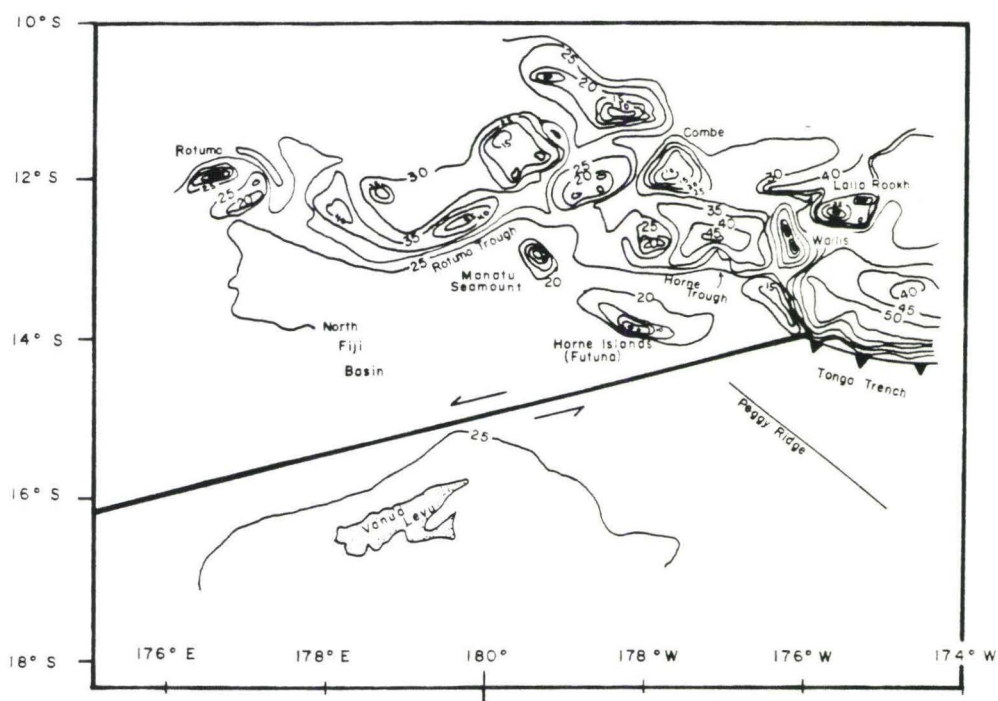


Figure 20. Location map for Manatu seamount and Horne (Futuna) Islands. Depths are in hundreds of meters.

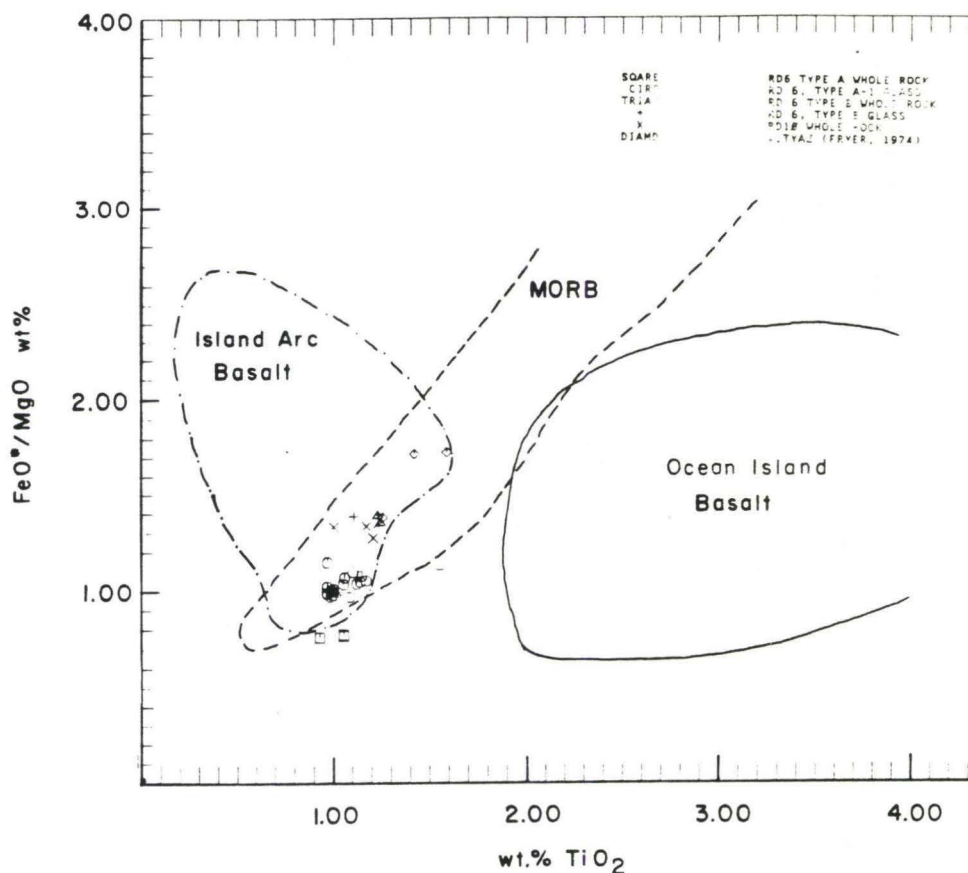


Figure 21. Discriminant plot of wt% FeO^*/MgO vs. TiO_2 to distinguish basalts from various settings. Significant overlap of MORB and island arc basalt fields in the primitive compositional range prevents unequivocal application of this diagram, but at more evolved stages the paths diverge reflecting differences in Fe-Ti oxide fractionation.

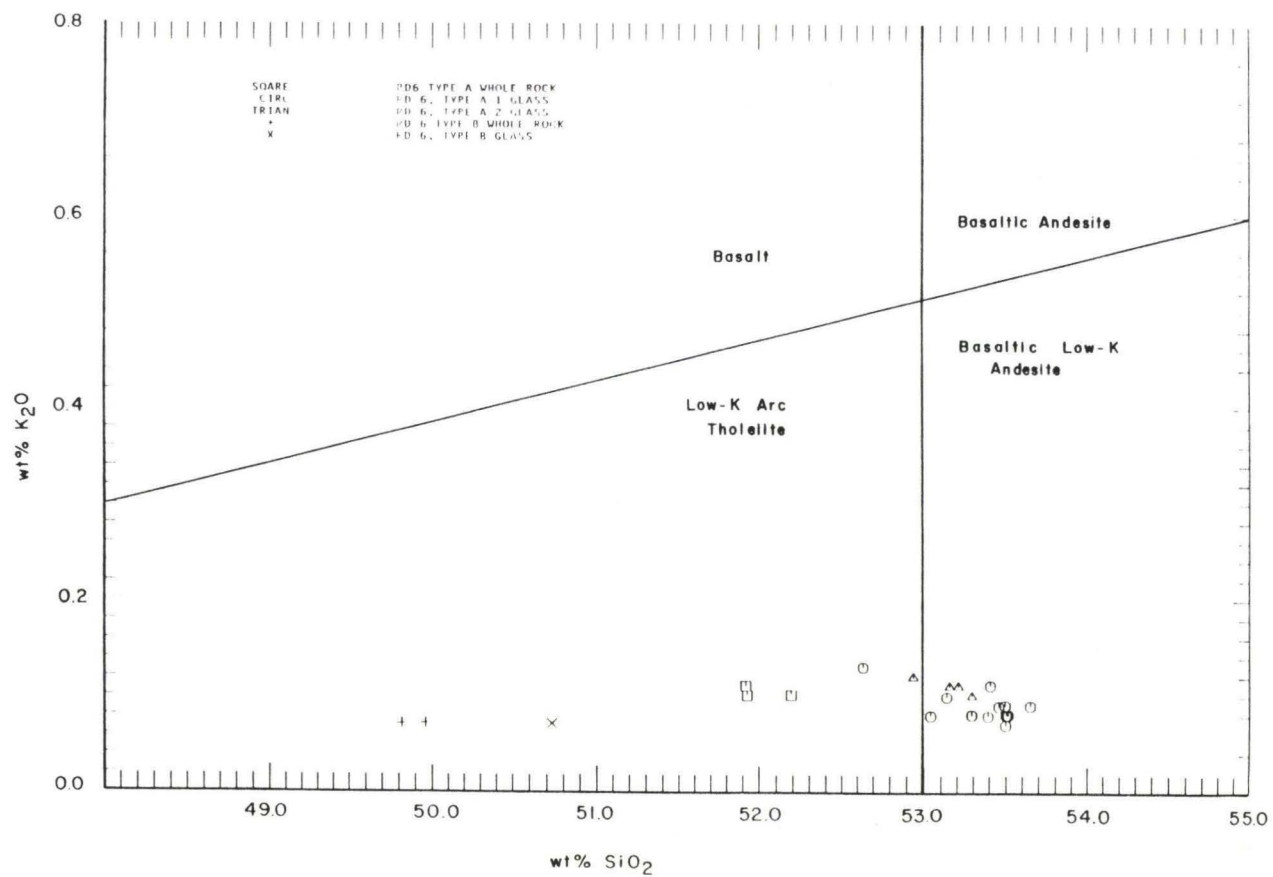


Figure 22. Wt% K₂O vs. SiO₂ classification diagram for arc tholeiites and basaltic andesites (after Gill, 1980). Note the extremely low abundances of K₂O in all of the Horne (dredge 6) lavas.

potash (Figure 22), phosphorous, and TiO_2 (Figure 21) typical of arc tholeiites. Silica contents are 49.0%-53.5% and the samples fall within the tholeiitic field on an alkalis-silica diagram (Figure 23).

Two distinct mineral assemblages characterize the samples from Horne and their chemical compositions reflect these differences. One type is characterized by quench textures with skeletal grains of olivine and plagioclase in a vesicular, glassy groundmass and Mg numbers of 72 to 73 (Type A). The other type (Type B) contains glomerocrysts of plagioclase and clinopyroxene as well as discrete microphenocrysts of clinopyroxene and plagioclase in a groundmass of Fe-Ti oxides and glass. Its Mg numbers are 59 to 60. One glass analysis of a Type B sample (6-14) shows an Mg# equivalent to that of analyzed type B rocks, but with substantially lower Al_2O_3 contents and is assumed to be related to type B by fractionation of plagioclase. Type B rocks contain relict grains of olivine which have been highly altered but which retain their crystal outline. The higher H_2O^- and Fe_2O_3 contents of type B lavas testify to their more altered character. Type B is also more crystal-rich with larger, better formed grains. In hand specimen type B rocks appear to be older, more altered (chloritized) medium-grained dolerites.

The trends defined in Figure 24 suggest that type B cannot be related to type A by any amount of fractional crystallization. The decrease in Mg# from type A to type B with a 2-3% decrease in SiO_2 requires an implausibly large amount of cpx + olivine to crystallize from type A to produce type B. Moreover, there are no silica-rich

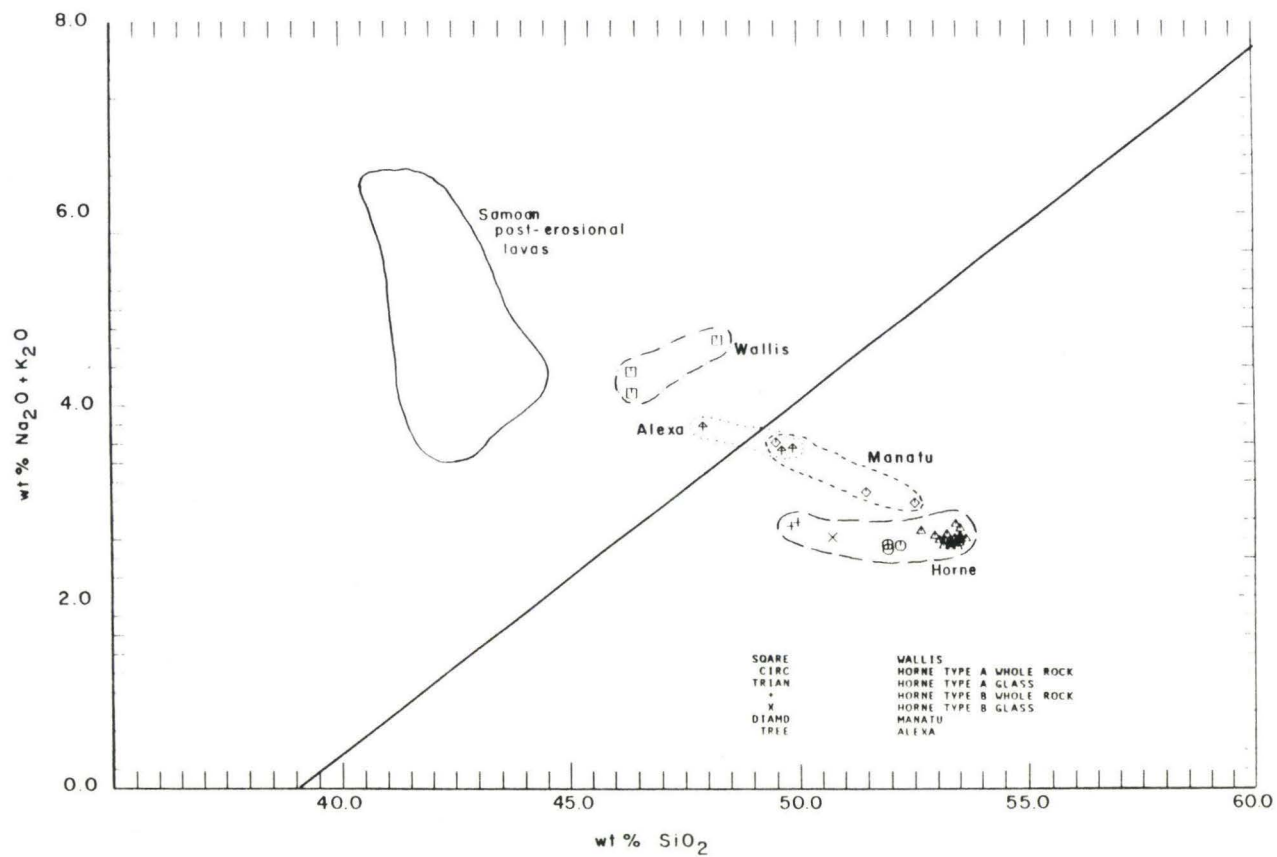


Figure 23. Alkali-silica diagram for lavas from the study area. Also shown for comparison is the field occupied by Samoan post-erosional lavas. Manatu seamount and Horne Islands lavas are distinctly tholeiitic and Wallis is typically alkalic.

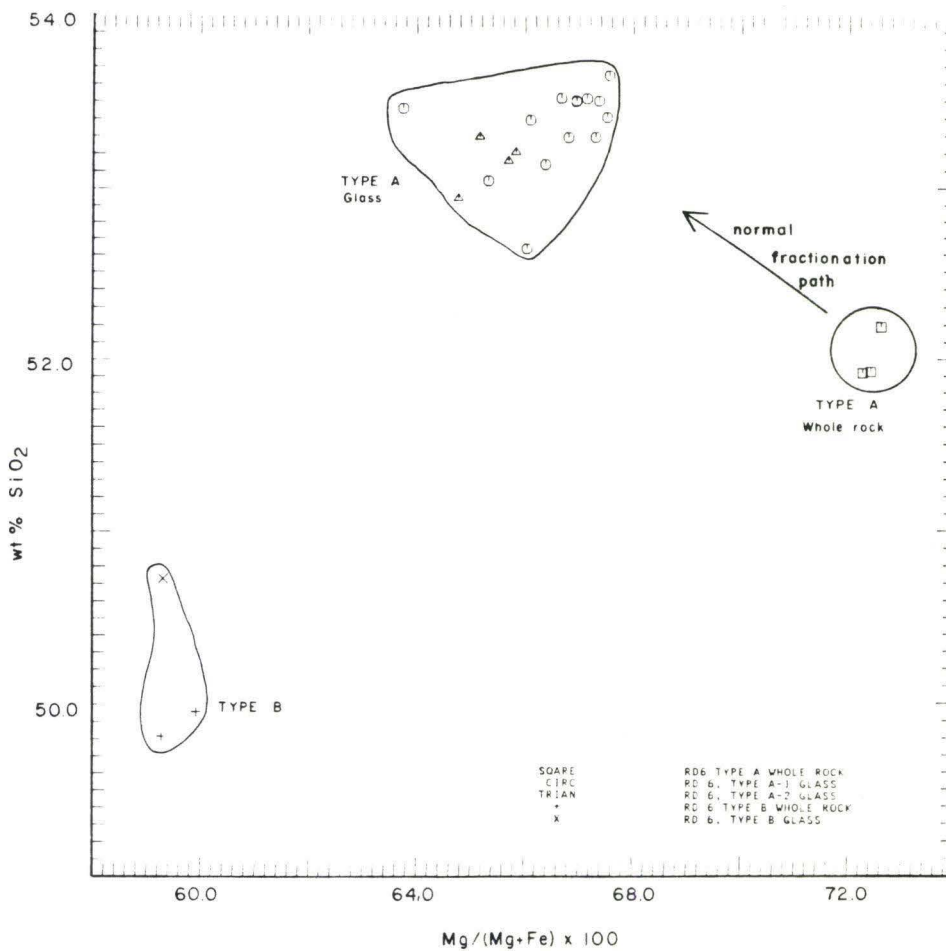


Figure 24. Wt% SiO₂ vs. Mg# for Horne (dredge 6) lavas. The diagram demonstrates the presence of two distinct lava types recovered in dredge 6: arc tholeiitic and ocean-floor-like. These lavas cannot be related by crystal fractionation.

phases present in these rocks to enable a decrease in SiO_2 with fractional crystallization. Therefore, Types A and B appear to be products of different stocks of magma altogether. Both types, however, contain extremely low abundances of Rb, Sr, and high-field-strength elements. Nickel is more abundant in Type A by a factor of eight and is poorer in Yttrium by a factor of two relative to type B. Type B is also higher in K/Rb than Type A (Type A - 450, Type B - 800). This, coupled with substantially higher Mg# (68-72 for Type A, 59 for Type B) and lower TiO_2 contents, implies a higher degree of partial melting, lesser degree of fractionation for type A, or derivation from different source material for the two.

Type A rocks, by far the most abundant in the dredge haul, may be further split into two sub-categories based on differences in Mg#. The general trend in A_1 and A_2 is decreasing MgO with increasing CaO. Furthermore, the compositional difference between Type A whole rock and glass is best explained by olivine fractionation. This is supported by the observed phenocryst assemblage of olivine crystallization followed by plagioclase on the liquidus and incipient cpx joining as a groundmass phase with possible late-stage Fe-Ti oxides.

One may therefore interpret data from dredge 6 to mean that there are two different rock suites represented. Type A possesses higher Mg#, K_2O , Rb, Sr, Ni, SiO_2 , and is quartz normative. It is richer in MgO and incompatible trace elements than type B, but resembles other arc tholeiites, such as those described from New Britain (Basaltic Volcanism Study Project, 1981). Type B lavas contain higher Al_2O_3 , FeO^* , CaO,

total alkalis, K/Rb, TiO_2 , and yttrium. Their chemical compositions border on high-Al basalt (Kuno, 1960) and are similar to basalts from the Vityaz Trench (Fryer, 1974). Based on their vastly different K/Rb (the two types differ by a factor of up to two) and their reversely correlated SiO_2 -Mg# variations, the two are almost certainly derived from different sources, but both possess similarities to subduction related volcanism elsewhere indicating a complex arc-tectonic setting for the Horne Islands with possible influence by back-arc basin magmatic sources.

2.2.2 Manatu Seamount - RD 10

The rocks dredged from the Manatu seamount (dredge 10) ESE of Rotuma Trough (Figure 20) are fine to medium grained plagioclase-, augite-, and hypersthene-phyric tholeiitic basalts. In some of the rocks, equant, euhedral hexagonal crystals of quartz are present (Figure 25). These crystals are probably primary because they occur as discrete grains, not as fracture or vesicle-filling secondary products. Hypersthene as a phenocryst phase is characteristic of arc-type tholeiites to andesites and sets them apart from ocean floor basalts. Plagioclase in these tholeiites is normally zoned with cores of bytownite-labradorite and rims of andesine. Groundmass plagioclase is andesine. One of the samples (10-7) is nepheline normative when Fe_2O_3 is reduced to 1.5% FeO. These samples are altered by seawater interaction and it is probable that they gained alkalis during the course of this alteration (Staudigel et al., 1981). Petrographically

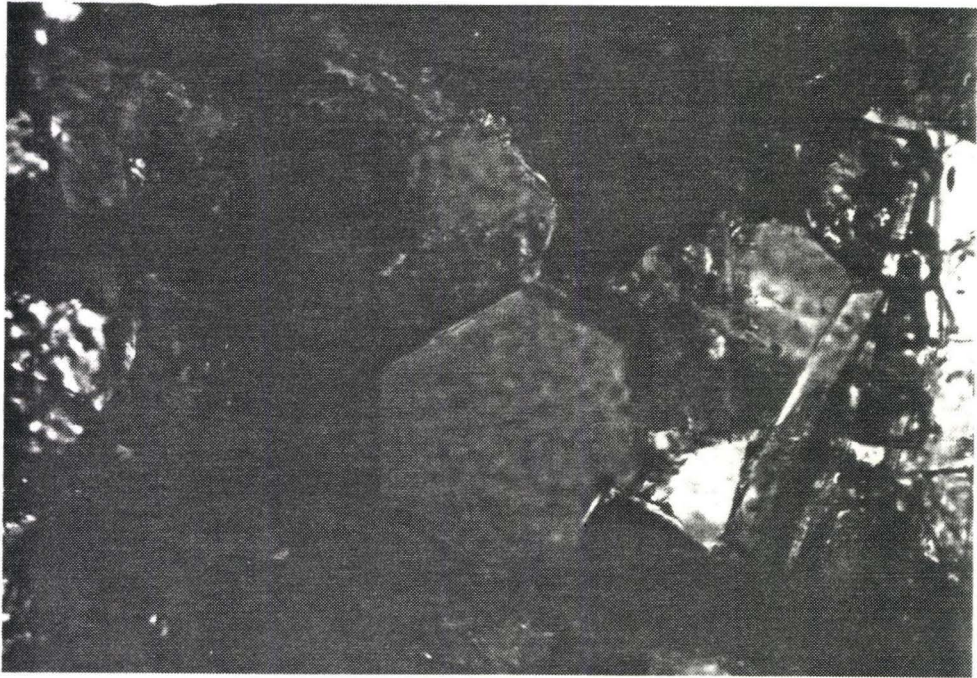


Figure 25. Photomicrograph of euhedral, hexagonal prism of quartz in sample 10-1, Manatu seamount. Texture and habit of the quartz in these samples suggests primary origin and not vein- or cavity-filling phase. Plane-polarized light, 200x.

all the rocks from dredge 10 are similar and differ mainly in the degree of alteration and grain size, some being doleritic.

Classification of the three samples recovered from Manatu seamount as arc tholeiites is based on: 1) a plot of TiO_2 - MnO - P_2O_5 (Mullen, 1983) (Figure 11) in which the samples mainly fall in the arc tholeiite field and 2) petrographic study. The samples are extremely low in P_2O_5 and K_2O with the exception of sample 10-7 which is a highly oxidized and altered, glassy (devitrified) to fine-grained basalt. It has probably absorbed H_2O and K_2O at the expense of SiO_2 in accordance with the processes outlined by Staudigel and Hart (1983).

2.2.3 Wallis Islands - RD 4

The Wallis Islands are a young, alkalic seamount group located astride the Vityaz Trench lineament separating the northwest limb of the Tonga Trench from the first basin segment, Horne Trough, to the west-northwest (Figure 20). The young volcanism (820,000 years old, Duncan, in preparation) on the Wallis Islands is characterized by critically undersaturated olivine basalts which resemble alkalic basalts from other midplate seamounts. Consistent with the Pleistocene volcanism, sediment cover on the submarine flanks of the Wallis Islands is extremely thin (100-200 meters) and interrupts the thicker sediment cover to the east and west. It is not possible to determine recent faulting patterns from existing seismic reflection records in this area so the state of stress near Wallis is unknown.

The Pleistocene age of the rocks from Wallis Island is consistent with their fresh, glassy appearance. They were quenched from a liquid-rich magma since olivine is the only phenocryst phase. The groundmass is composed of quench crystals of olivine and clinopyroxene. In an alkalis-silica plot they lie in the alkalic field distinct from Samoan post-erosional lavas (Figure 23).

None of the lavas from the Wallis Islands, for which Macdonald (1945) described the petrography, resemble the dredged lavas. Most subaerial lavas contain phenocrysts of resorbed olivine + colorless or titaniferous augite + plagioclase. It is possible that the subaerial lavas are simply more crystalline versions of the lavas dredged on the submarine flank of the islands because the glassy groundmass of the dredged lavas contain quench crystals of clinopyroxene suggesting that they could have developed into the olivine basalts described by Macdonald. The olivine in the submarine samples was not in reaction relation with the melt at the time of quenching.

The TiO_2 contents of the Wallis rocks are significantly lower (Figure 26) and the Al_2O_3 contents are significantly higher than the Samoan shield and post-erosional lavas and Lalla Rookh lavas reflecting either different depths of formation, source composition, or degree of melting. Rb/Sr ratios of Wallis lavas are 0.08 and K/Rb ratios are approximately 320. These values are similar to those in Samoan post-erosional lavas. Overall, however, their significantly lower TiO_2 contents suggest a shallower depth of melting and/or different source composition than either type of Samoan volcanism.

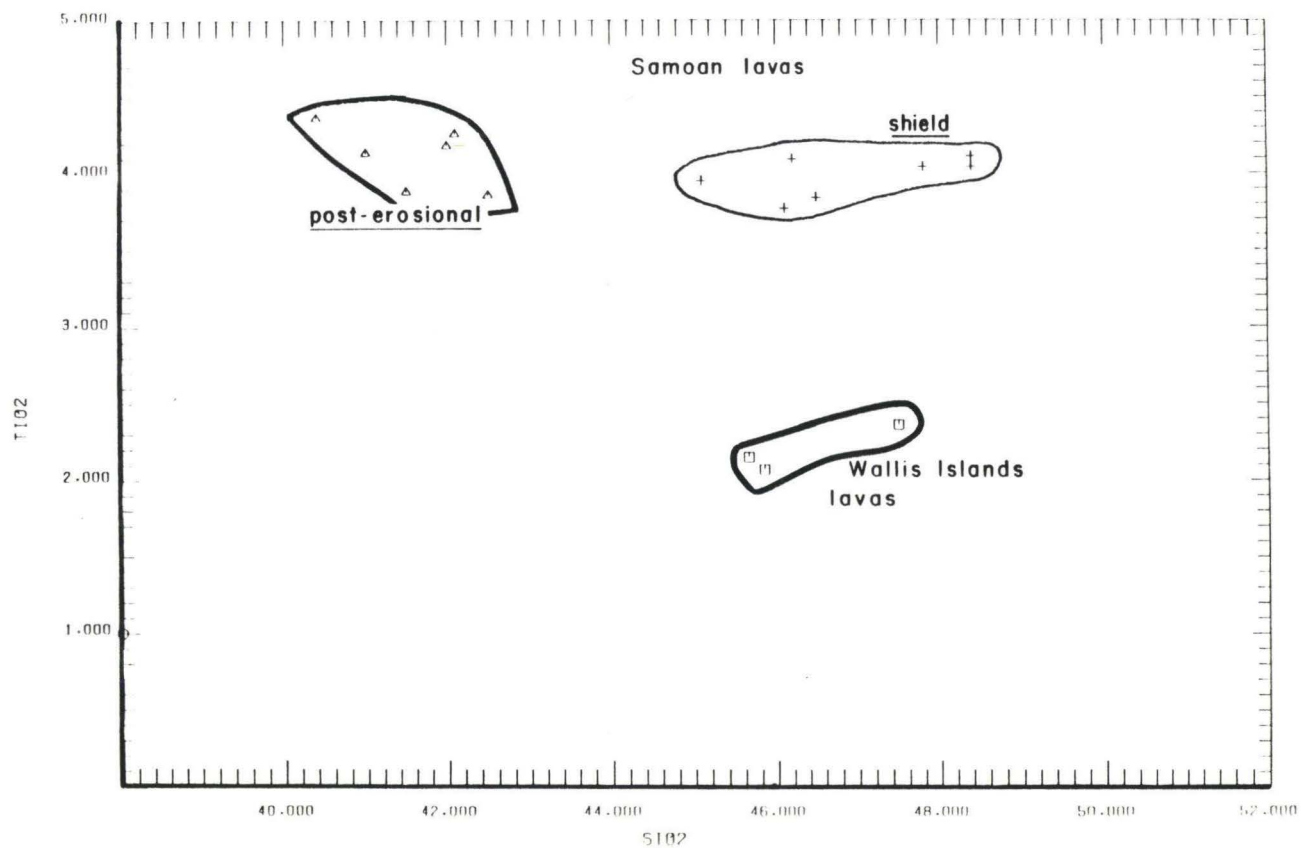


Figure 26. $Wt\% TiO_2$ vs. SiO_2 for Wallis Islands and Samoan Islands lavas to illustrate the chemical differences between the two types of lavas. Samoan volcanic rocks are characterized by their high TiO_2 contents, often twice as high as those of Wallis samples. Samoan data from Natland (1980).

Compositions of the dredged lavas from Wallis Islands are somewhat more primitive than those from Rotuma (Jezek et al., 1977 after Hindle, 1970) (Table 2), but both are alkalic and may be formed by similar processes, at least in their Quaternary eruptive phases. Both lie on or near major fracture zones in the NFB: Rotuma on the Hazel Holme Fracture Zone and Wallis may have once lay on the intersection of the fracture zone north of Fiji and the Tonga-Vityaz Trench. Quaternary spreading and adjustment in the NFB may have resulted in rejuvenation volcanism at their pre-existing edifices.

2.3 DISCUSSION

2.3.1 Arc Volcanism: Horne and Manatu

The absence of olivine in lavas from Manatu seamount sets them apart from Horne Islands lavas. The important point is, however, that both appear to be arc-related lavas dredged at a location where subduction related volcanism is expected from either the Vityaz or Tonga Trench (Table 2).

TABLE 2. Chemical Analyses of Volcanic Rocks from
the Vityaz Trench Lineament

	1	2	3	4	5	6	7	8
SiO ₂	51.7	53.0	52.9	49.0	50.1	49.9	46.3	48.0
TiO ₂	1.0	1.0	1.1	1.2	1.1	1.1	2.2	2.1
Al ₂ O ₃	14.9	15.9	16.1	16.4	14.3	15.2	14.4	17.0
Fe ₂ O ₃	1.0			2.6		4.6		
FeO	7.5	8.2*	8.5*	6.8	10.5*	5.2	11.0*	8.5*
MnO	0.1	0.1	0.2	0.2	0.2	0.2	0.2	0.2
MgO	11.0	8.0	7.9	6.7	7.5	7.2	9.8	7.5
CaO	9.5	10.4	10.2	12.6	12.4	10.9	9.8	9.5
Na ₂ O	2.4	2.5	2.5	2.6	2.5	2.8	3.1	3.7
K ₂ O	0.1	0.1	0.1	0.1	0.1	0.3	1.2	1.8
P ₂ O ₅	0.1	0.1	0.1	0.1	0.1	0.1	0.4	0.5
H ₂ O ⁺	0.5			0.6		1.5	0.8	0.4
TOTAL	99.8	99.4	99.6	98.9	98.7	97.5	99.7	99.5
Mg#	72.2	63.7	62.4	63.6	56.2	71.0	69.0	

* - Total iron as FeO

1. Average of 3 Type A whole-rock analyses, Horne Islands.
2. Average of 14 Type A-1 glass analyses, Horne Islands.
3. Average of 4 Type A-2 glass analyses, Horne Islands.
4. Average of 2 Type B whole-rock analyses, Horne Islands.
5. Type B glass analysis, Horne Islands.
6. Average of 3 whole-rock analyses, Manatu Seamount.
7. Average of three alkalic basalts, Wallis.
8. Ne-normative basalt from Rotuma Island (Hindle, 1970 in Jezek et al., 1977).

The Pliocene to Quaternary (4.9 to 1.8 million years, Duncan, in preparation) arc tholeiitic volcanism of the Horne Islands and Manatu may be evidence of the persistence of subduction at the Vityaz Trench. It is generally believed that subduction along the Vityaz Trench had ceased by the late Miocene, but the persistence of arc volcanism on the

NFB into the Pleistocene is explainable by several mechanisms which are discussed below.

First, the arc volcanism could be related to the ongoing sinking of formerly subducted lithosphere at the Vityaz Trench. The lack of known shallow seismicity parallel to the Vityaz Trench lineament suggests that subduction activity along the Vityaz Trench has ceased. The sinking slab hypothesis to explain volcanism at Horne and Manatu is not well supported by the existing data for several reasons. First, there are no recorded deep earthquakes in the area beneath the edifices (Sykes et al., 1969), no arc-type volcanoes are reported over the deep earthquakes in the NFB, and lastly, the rocks from Horne and Manatu are basaltic and low in potassium and are therefore not apt to form from deep subduction processes.

Another explanation for the volcanism found at these two seamounts is that they are related to the oblique subduction of the Pacific Plate at the northern end of the Tonga Trench. Ongoing arc volcanism as the result of oblique subduction at the Vanuatu Trench in the southern NFB at Matthew and Hunter Islands of the Vanuatu Arc in an analagous position provides support for this model. Given the opening of the Lau Basin since the Pliocene and the eastward motion of the Tonga Trench at 90 mm/yr it is possible that subduction of the Pacific Plate at the Tonga Trench is responsible for arc tholeiitic volcanism observed at the Horne Islands. The dated sample from the Horne Islands (Type B sample) is more altered than the Type A samples. It may, therefore, represent an older phase of volcanism in the edifice-building stage. Its age (4.9

+ 0.4 m.y., Duncan, in preparation) and more ocean-floor basaltic character may also reflect an earlier phase of volcanism through presumably young NFB crust. Closing the Lau Basin according to the 90 mm/yr rate of Pacific-Tonga convergence brings the Tonga Trench within 100 km or so of Horne, a distance compatible with Tonga Trench related volcanism.

Ages of the younger looking Type A lavas from Horne are not known, but may be younger than the dated Manatu lavas ($1.8 + 0.3$ m.y., Duncan, in preparation) judging from their glassy, fresher appearance. If this is the case, then they represent a later stage of subduction volcanism at the Horne Islands. This late-stage volcanism may have progressively ceased from west to east as the subduction along the Vityaz Trench was progressively choked by seamounts of the Samoan seamount lineament (Brocher, in preparation). This progressive shutdown of subduction is supported by increasing sediment and turbidite thicknesses from east to west in the Vityaz Trench segments (Brocher, in preparation). As the subduction ceased, arc-related volcanism may have also ceased sequentially from west to east. Brocher's (in preparation) model (Figure 27) predicts that there should be a younging of volcanism to the east as a result of the migration of the fracture zone through the NFB, but in fact an age progression in the opposite sense is found. This may be explained by the rejuvenation volcanism model described above. It is perhaps sufficient to say that the lavas from Manatu and Horne are arc tholeiites probably related to volcanism at the Vityaz-Tonga Trench, but that their age progression does not clearly support the hypothesis that

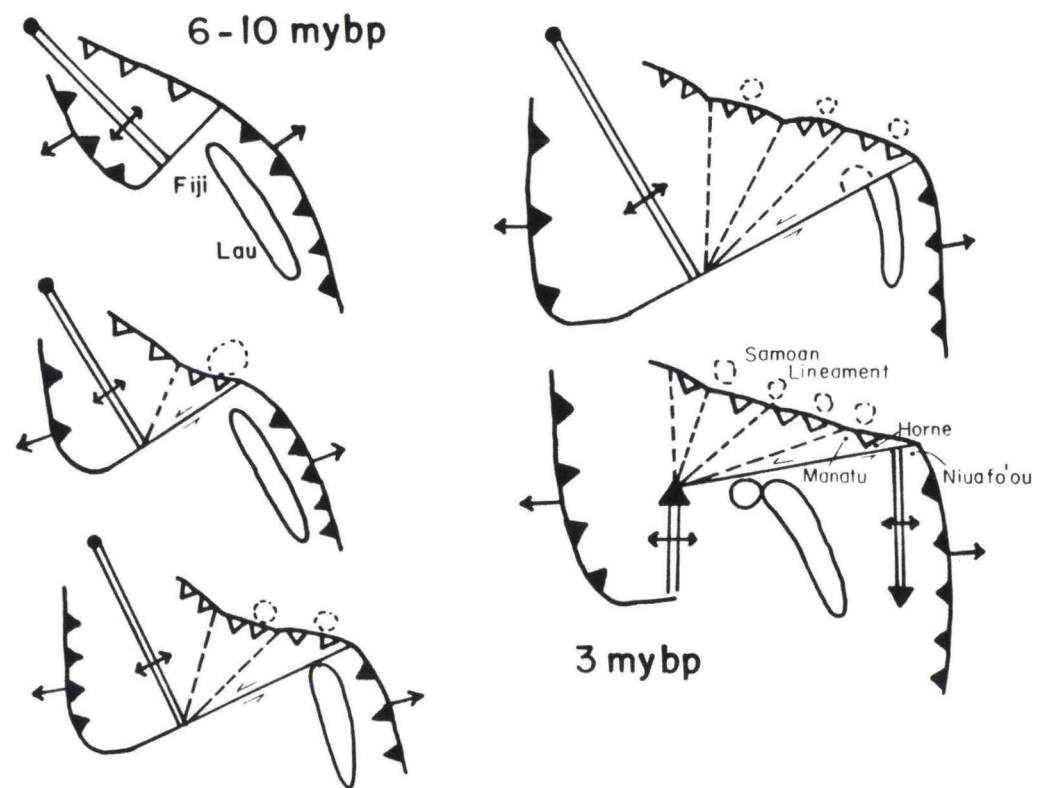


Figure 27. Reconstruction of the N.M.B. from 10 m.y.b.p. to the present (after Brocher, in preparation). Double lines = spreading centers; single lines = fracture zones/transform faults dashed where no longer active; barbed lines = subduction zones, filled-active, unfilled-inactive. Samoan seamount lineament edifices, Manatu seamount, and Horne Islands are discussed in the text and are shown in the figure.

a fracture zone, migrating from northwest to southeast, produced the volcanism at these two edifices. Hence, the mechanism for the development of the NFB is still subject to considerable interpretation and cannot be resolved from these data.

2.3.2 Wallis Islands

Stearns (1945) estimated a mid-Pleistocene to Holocene age of volcanism for the exposed lavas described by Macdonald (1945) and a possible Tertiary age for the substructure of the Wallis Islands based on the presence of a wide barrier reef completely encircling the islands. Because of the age of the dredged lavas from Wallis, the volcanism that produced them is clearly related to the Pleistocene volcanism described by Stearns (1945) and probably represents the quenched version of Macdonald's (1945) Ti-augite bearing olivine basalt. This volcanism probably represents a rejuvenation stage of volcanism on a Tertiary volcanic edifice.

Wallis may represent an old volcanic edifice associated with the Tuvalu chain. A barrier reef at Wallis, used as evidence by Stearns (1945) that the island edifice is of Tertiary age, completely encircles the islands and suggests an advanced stage of volcanic island maturity. The morphology of the Wallis Islands edifice is distinctly N-S trending in contrast to the NW-SE trend of the Samoan Islands chain of edifices (see Chapter 1). The southernmost island of Tuvalu, Nukulaelae, which was also surveyed during our cruise, is an atoll possessing a barrier reef and is elongated N-S similar to the Wallis Islands edifice. The

Wallis Islands are colinear with the Tuvalu Island chain farther to the north along an azimuth similar to that of the Emperor seamounts. Hence, it is possible that the Wallis Island shield is part of a linear island chain consisting of the Kiribasi-Tuvalu Groups and continuing on the Pacific Plate east of the Tonga Trench.

Although the location of the Wallis Islands shield edifice relative to the Vityaz Trench may be fortuitous, the Pleistocene volcanism of the islands probably results from the extension and fragmentation of the arc. As previously discussed, rotation in the NFB was presumably taken up by transform fault zones. The fracture zones in the area, both north and south of Fiji, are necessary to accommodate this rotation. Brocher (in preparation) has argued, based on seismic and geomorphologic study, that as the Vityaz Trench is episodically "shut down" from west to east, extension occurs along the dying Vityaz Trench as the Tonga Trench advances over the Pacific Plate. Collision of a seamount with a trench segment under tension may result in rupturing of the crust at this zone of pre-existing weakness with concomitant volcanism ensuing. Furthermore, the fracture zone north of Fiji provides another zone of weakness at which reactivation of volcanism may take place. Reactivation along other fracture zones may have also resulted in renewed Quaternary volcanism in the NFB (e.g. Rotuma Island at the Hazel Holme Fracture Zone, Sinton et al., 1983) (see Table 1). It is therefore possible that the Pleistocene volcanism in the Wallis Islands was produced by extension along the Vityaz Trench resulting from progressive subduction cessation at the terminus of the fracture zone

north of Fiji. The petrology of the volcanic rocks there is consistent with an extensional origin for the lavas. Undersaturated alkalic volcanism is well known from other extensional provinces, e.g. E. African Rift and the Rio Grande Rift.

High quality seismic surveys across the flanks of the islands and into the flanking basins are necessary to detect predicted extensional faulting in the area. Dredging of the submarine flanks in order to recover portions of the original shield is also essential.

CHAPTER 3

SUMMARY AND CONCLUSIONS

The conclusions reached in this study are divided into two sections corresponding to the format of the thesis.

3.1 SAMOAN SEAMOUNT LINEAMENT

Based on petrologic, tectonic, and geochronologic data, three seamounts west of the Samoan Islands are interpreted as Samoan-related volcanoes.

Lavas from Taviuni-Field Bank contain abundant high-titanium pyroxenes and possibly pseudomorphs after melilite and are analagous to Samoan post-erosional lavas (Macdonald, 1944; Stice, 1968; Natland, 1980). The K/Ar age of the lavas, 5.4 ± 0.2 million years (Duncan, in preparation), is consistent with formation by rifting of the Pacific Plate at the northern tip of the Tonga Trench (Natland, 1980). The linear morphology of Taviuni-Field Bank (Brocher, in preparation) is also analagous to the morphology of Savai'i and Upolu Islands which have been shaped by Recent volcanism along a central rift zone (Stearns, 1944; Kear and Wood, 1959; Natland, 1980).

Lalla Rookh and Combe Banks are older than Taviuni-Field Bank (10.0 ± 0.3 and 13.5 ± 0.9 m.y. respectively, Duncan, in preparation) and were formed near the same position east of Rose Atoll assuming a hot-spot reference frame. Lavas from Lalla Rookh are compositionally similar to

Samoan post-erosional lavas containing high Rb, TiO_2 , MgO and low SiO_2 and Al_2O_3 . Rb/Sr ratios of Lalla Rookh lavas span the range of ratios in Samoan shield and post-erosional lavas. It may be possible to generate the Rb enriched Lalla Rookh lavas from the source for Samoan shield lavas by lesser degrees of partial melting. However, no firm conclusion as to the origin of Lalla Rookh lavas can be made at this time: if Lalla Rookh is related to a post-erosional source then the mechanism for eruption was different than that thought to be responsible for eruption of Samoan post-erosional lavas; if Lalla Rookh is related to a shield source then the difference between Samoan shield and post-erosional volcanism is not a difference in source, but a difference in degree of partial melting.

Due to their great distance from the northern bend of the Tonga Trench at their time of eruption, it is implausible to attribute volcanism at Lalla Rookh or Combe to flexure-induced rifting at the bend. The morphology of Lalla Rookh is also linear, similar to Savai'i and Taviuni-Field (Figure C-2; Brocher, in preparation), and this may point to a rift origin for the volcanic edifice, but the rifting mechanism is not known.

Combe Bank possesses characteristics similar to "normal" Samoan shield lavas, i.e. transitional-alkalic chemistry, low, but variable Rb/Sr, high K/Rb, and a fairly broad range of lava compositions in the transitional zone of an alkali-silica diagram. Its age is consistent with Lalla Rookh's as having been formed 40-200 km east of Rose Atoll. Combe is therefore believed to be an ancestral Samoan-related shield volcano.

Sampling of Rose Atoll and the flanks of the Samoan Islands is required to further constrain the model for the formation of the Samoan shields and for determining the relationship, if any, between the shield lavas and the post-erosional lavas.

Volcanic rocks dredged from Alexa Bank (dredge 14) are Ne-normative to tholeiitic in character and are probably not related to Samoan volcanism based on their age (36.9 m.y., Duncan, in preparation) and on their low abundances of TiO_2 , P_2O_5 , and MgO . However, it should be emphasized that submarine portions of the Samoan shield volcanoes have not been sampled and their compositions are not known.

Dredge 14 lavas may represent several volcanic provinces including oceanic island and ocean floor volcanism. It is not currently possible to evaluate these hypotheses rigorously because of uncertainties as to where the samples actually came from. All of the hypotheses, however, are consistent with tectonic interpretations of this area: 1) alkalic and transitional lavas recovered in dredge 14 could be from an oceanic island source (Alexa Bank); 2) the lavas could be fragments of oceanic crust broken during subduction, and 3) the lavas may have been dislodged from the inner trench wall when Robbie Ridge collided with the Vityaz Trench. However, compositions of the recovered lavas indicate that they probably represent portions of the Alexa Bank edifice emplaced in a process similar to that described by Bloomer (1983) at the Mariana Trench. The deformed morphology of the adjacent Vityaz Trench support the hypothesis that Alexa collided with the Vityaz Trench prior to cessation of subduction from the north. The age of the lavas are inconsistent with a Samoan seamount lineament provenance for Alexa Bank

assuming current rates of rotation. Sampling and surveying of Robbie Ridge may permit a more refined interpretation of the rocks dredged from Alexa Bank.

3.2 VITYAZ TRENCH LINEAMENT

Data from the Horne Islands and Manatu seamount are consistent with Vityaz Trench reversal models for the tectonic evolution of the NMB (Chase, 1971; Brocher, in preparation). The young volcanism at these locations has produced low-K arc tholeiites which are inconsistent with a deep magmatic source (Dickinson and Hatherton, 1967) beneath the North Fiji Basin. Rather, Horne and Manatu are arc volcanoes probably related to subduction at the Vityaz Trench prior to cessation of subduction as the trench shuts down and welds to the Pacific Plate sequentially from west to east. The volcanoes of Manatu and Horne Islands may have been left-laterally transformed along the E-W fracture zone north of Fiji. In this model, the island of Niuafu'ou on the northern Lau Basin will eventually be transformed in the same fashion. The models of Chase (1971) and Brocher (in preparation), call for decreasing ages of volcanism to the east if the volcanism is a result of this migrating fracture zone. The sampled lavas from Horne and Manatu appear to define an age progression opposite to this trend and this may reflect several stages of volcanic activity, analytical uncertainty in the age determinations due to low argon abundances (Duncan, in preparation), or inaccuracy of the tectonic models for the NFB in this area.

This model does provide a mechanism for Pleistocene (presumably rejuvenation) volcanism in the Wallis Islands. The fracture zone intersecting the dying Vityaz Trench marks the eastern limit of Vityaz Trench subduction. To the east of this fracture zone, subduction (locally oblique) is still active. Back-arc spreading in the Lau Basin may cause tension along the pre-existing Vityaz Trench lineament and arc fragmentation where volcanism could take place. The point of intersection of the fracture zone and the trench is also a point of weakness at which lavas may erupt. While the position of the original Wallis edifice astride the Tonga-Vityaz Trench may be fortuitous, the Recent eruptive history is most likely a product of renewed volcanism at a zone of pre-existing weakness (the old Tuvalu related eruptive edifice) and a transient zone of weakness (the migrating fracture). Testing of the model in which Wallis is related to the Tuvalu chain must await geochemical data from the Tuvalu Islands as well as the Wallis edifice.

CHEMICAL ANALYSES - WHOLE-ROCK AND GLASS,
NORTHERN MELANESIAN BORDERLAND

	Lalla Rookh Bank - RD 3				Wallis Island - RD 4			
	3-2WR	3-11WR	3-21WR	3-39WR	4-1WR	4-2WR	4-1GL	6-52WR
SiO ₂	39.12	39.04	42.80	40.04	45.84	45.65	47.48	51.72
TiO ₂	4.28	3.56	3.48	3.80	2.07	2.15	2.36	1.05
Al ₂ O ₃	9.17	9.02	11.60	10.49	13.66	13.54	15.96	14.87
Fe ₂ O ₃	5.62	5.79	3.94	5.42	2.23	2.58	1.38	1.22
FeO	8.24	8.01	8.62	8.18	9.45	8.95	9.22	7.50
MnO	0.18	0.20	0.17	0.21	0.18	0.18	0.12	0.14
MgO	11.39	15.31	11.86	12.65	11.69	11.74	5.95	11.07
CaO	14.28	11.96	9.79	10.88	9.29	9.01	11.02	9.42
Na ₂ O	2.33	2.12	2.84	3.15	2.96	2.97	3.33	2.42
K ₂ O	1.46	0.69	1.35	2.66	1.11	1.30	1.26	0.11
P ₂ O ₅	0.60	0.73	0.68	0.68	0.35	0.37	0.34	0.10
H ₂ O ⁺	1.28	3.08	2.32	1.69	1.08	1.45	0.00	0.46
H ₂ O ⁻	0.87	0.60	0.58	0.34	0.10	0.21	0.00	0.16
CO ₂	0.90	0.34	0.13	0.14	0.16	0.05	0.00	0.10
SO ₃	0.05	0.03	0.04	0.13	0.11	0.09	0.00	0.70
SumOx	99.77	100.48	100.20	100.46	100.28	100.24	98.42	101.04
Trace elements in ppm								
Ni	340	533	363	289	354	354		348
Cu	188	106	91	73	108	98		97
Zn	119	132	127	141	109	114		78
Rb	43.4	15.5	32.8	85.1	30.1	32.4		1.9
Sr	700	748	720	685	374	409		175
Y	27	23	28	26	20	21		14
Pb	6.2	5.2	1.6	7.2	1.6	3.8		2.0
Th	16.1	8.5	6.5	6.6	2.3	1.6		0
U	4.0	3.9	2.7	2.7	0	2.0		0
CIPW Norms from Dry Analyses								
Or	0.0	4.2	8.2	0.0	6.6	7.8	7.6	0.7
Ab	0.0	1.7	12.8	0.0	17.4	17.3	20.7	20.6
An	10.6	13.5	15.4	6.8	21.0	20.1	25.3	29.5
Lc	7.0	0.0	0.0	12.6	0.0	0.0	0.0	0.0
Ne	11.0	9.2	6.4	14.7	4.3	4.5	4.3	0.0
Pl	10.6	15.2	28.2	6.8	38.3	37.4	45.9	50.1
DiCa	21.9	18.0	12.6	18.0	9.8	9.6	11.7	7.0
DiMg	17.2	14.3	9.2	14.0	6.4	6.4	6.2	4.6
DiFe	2.3	1.7	2.2	2.1	2.7	2.4	5.1	1.9
Di	41.4	34.0	24.0	34.1	18.9	18.4	23.1	13.5
HyMg	0.0	0.0	0.0	0.0	0.0	0.0	0.0	21.2
HyFe	0.0	0.0	0.0	0.0	0.0	0.0	0.0	8.7
Hy	0.0	0.0	0.0	0.0	0.0	0.0	0.0	29.9
OlMg	8.5	17.7	14.9	12.7	16.2	16.3	6.2	1.3
OlFe	1.2	2.3	4.0	2.1	7.6	6.8	5.6	0.6
Ol	9.7	19.9	18.8	14.7	23.8	23.1	11.7	1.9
Cs	1.9	0.0	0.0	0.2	0.0	0.0	0.0	0.0
Mt	8.4	8.7	5.9	8.0	3.3	3.8	2.0	1.8
Il	8.4	7.0	6.8	7.4	4.0	4.1	4.6	2.0
Ap	1.4	1.7	1.6	1.6	0.8	0.9	0.8	0.2
SumNorm	99.98	99.97	99.98	99.98	99.99	99.99	99.99	99.99
Mg No	71.1	77.3	71.0	73.4	68.8	70.0	53.5	72.5
Trace element ratios:								
K/Rb	279.25	369.53	341.66	259.47	306.12	333.06	0.00	480.58

Horne Islands - RD 6

	6-22WR A	6-13WR A	6-9GL A1	6-50GL A1	6-54GL A1	6-10GL A1	6-13GL A1	6-0GL A1
SiO ₂	51.67	51.60	52.64	52.65	53.28	53.08	53.31	52.76
TiO ₂	1.05	0.92	1.07	1.12	0.97	0.99	1.05	1.00
Al ₂ O ₃	14.80	15.00	15.49	16.12	16.11	15.88	15.92	16.13
Fe ₂ O ₃	0.85	1.06	0.00	0.00	0.00	0.00	0.00	0.00
FeO	7.84	7.20	8.05	8.55	8.30	7.92	8.36	7.91
MnO	0.13	0.13	0.11	0.08	0.17	0.13	0.12	0.13
MgO	11.16	10.68	8.27	8.22	8.10	8.08	8.06	8.05
CaO	9.43	9.69	10.10	10.46	10.67	10.45	10.28	10.34
Na ₂ O	2.38	2.40	2.60	2.55	2.43	2.49	2.52	2.48
K ₂ O	0.10	0.10	0.11	0.13	0.10	0.07	0.08	0.08
P ₂ O ₅	0.10	0.09	0.13	0.15	0.14	0.13	0.15	0.13
H ₂ O ⁺	0.40	0.58	0.00	0.00	0.00	0.00	0.00	0.00
H ₂ O ⁻	0.16	0.18	0.00	0.00	0.00	0.00	0.00	0.00
CO ₂	0.08	0.04	0.00	0.00	0.00	0.00	0.00	0.00
SO ₃	0.80	0.70	0.00	0.00	0.00	0.00	0.00	0.00
SumOx	100.95	100.37	98.57	100.03	100.27	99.22	99.85	99.01

Trace elements in ppm

Ni	382	308
Cu	104	85
Zn	78	71
Rb	1.9	1.5
Sr	174	172
Y	14	12

CIPW Norms from Dry Analyses

Q	0.0	0.0	1.6	0.8	2.0	2.4	2.3	2.1
Or	0.6	0.6	0.7	0.8	0.6	0.4	0.5	0.5
Ab	20.2	20.5	22.3	21.6	20.5	21.2	21.4	21.2
An	29.5	30.2	30.7	32.1	32.7	32.2	31.9	33.0
Pl	49.8	50.7	53.0	53.7	53.2	53.4	53.3	54.2
DiCa	7.0	7.4	8.0	7.8	8.0	8.0	7.6	7.5
DiMg	4.5	4.9	4.7	4.5	4.5	4.6	4.3	4.3
DiFe	2.0	2.0	3.0	3.0	3.1	3.0	3.0	2.8
Di	13.6	14.4	15.7	15.3	15.7	15.7	14.8	14.7
HyMg	20.7	21.0	16.2	16.0	15.6	15.7	15.8	15.9
HyFe	9.1	8.7	10.4	11.0	10.8	10.2	10.9	10.4
Hy	29.8	29.7	26.6	27.0	26.3	25.9	26.7	26.3
OlMg	1.9	0.7	0.0	0.0	0.0	0.0	0.0	0.0
OlFe	0.9	0.3	0.0	0.0	0.0	0.0	0.0	0.0
Ol	2.8	1.1	0.0	0.0	0.0	0.0	0.0	0.0
Mt	1.2	1.6	0.0	0.0	0.0	0.0	0.0	0.0
Il	2.0	1.8	2.1	2.1	1.8	1.9	2.0	1.9
Ap	0.2	0.2	0.3	0.3	0.3	0.3	0.3	0.3
SumNorm	99.99	99.99	99.99	99.99	99.99	99.99	99.99	99.99

Mg No 71.7 72.6 64.7 63.1 63.5 64.5 63.2 64.5

Trace element ratios:

K/Rb 436.89 553.40

Horne Islands - RD 6

	6-11GL A1	6-15GL A1	6-7GL A1	6-3GL A1	6-8GL A1	6-33GL A1	6-32GL A1	6-12GL A1
SiO2	53.27	53.05	52.82	52.73	53.00	53.60	53.11	52.96
TiO2	0.98	0.96	0.99	0.98	0.99	0.97	1.06	1.01
Al2O3	15.89	15.87	15.73	16.17	15.86	15.40	16.04	16.01
FeO	7.81	7.94	8.00	8.01	8.02	9.10	8.48	7.86
MnO	0.11	0.10	0.12	0.13	0.11	0.10	0.10	0.09
MgO	8.04	8.02	8.01	7.97	7.93	7.91	7.90	7.87
CaO	10.51	10.40	10.36	10.35	10.41	10.51	10.72	10.54
Na2O	2.49	2.60	2.50	2.41	2.52	2.43	2.51	2.44
K2O	0.09	0.08	0.08	0.08	0.08	0.09	0.08	0.09
P2O5	0.11	0.12	0.12	0.12	0.12	0.16	0.13	0.13
SumOx	99.30	99.14	98.73	98.95	99.04	100.27	100.13	99.00
CIPW Norms from Dry Analyses								
Q	2.6	1.9	2.3	2.4	2.3	2.7	1.8	2.7
Or	0.5	0.5	0.5	0.5	0.5	0.5	0.5	0.5
Ab	21.2	22.2	21.4	20.6	21.5	20.5	21.2	20.9
An	32.1	31.7	31.9	33.4	32.0	30.8	32.2	32.8
Pl	53.4	53.9	53.3	54.0	53.6	51.3	53.4	53.6
DiCa	8.2	8.2	8.1	7.4	8.1	8.4	8.4	8.0
DiMg	4.8	4.7	4.6	4.2	4.6	4.6	4.7	4.6
DiFe	3.1	3.1	3.1	2.8	3.1	3.6	3.3	3.0
Di	16.0	16.0	15.8	14.4	15.8	16.6	16.4	15.6
HyMg	15.4	15.4	15.6	15.8	15.3	15.1	15.0	15.2
HyFe	9.9	10.2	10.4	10.6	10.3	11.7	10.6	10.0
Hy	25.4	25.6	25.9	26.5	25.6	26.8	25.6	25.2
Il	1.9	1.8	1.9	1.9	1.9	1.8	2.0	1.9
Ap	0.3	0.3	0.3	0.3	0.3	0.4	0.3	0.3
SumNorm	99.99	99.99	99.99	99.99	99.99	99.99	99.99	99.99
Mg No	64.7	64.3	64.1	63.9	63.8	60.8	62.4	64.1

Horne Islands - RD 6

Combe

	6-28GL A2	6-53GL A2	6-52GL A2	6-51GL A2	6-20WR B	6-30WR B	6-14GL B	7-7WR
SiO2	52.96	53.10	52.83	52.87	49.06	49.03	50.09	47.34
TiO2	1.10	1.14	1.16	1.13	1.21	1.22	1.09	4.17
Al2O3	16.14	16.00	16.16	16.02	16.38	16.43	14.29	14.28
Fe2O3	0.00	0.00	0.00	0.00	2.49	2.70	0.00	6.20
FeO	8.77	8.53	8.29	8.24	7.08	6.58	10.45	4.10
MnO	0.16	0.16	0.09	0.18	0.16	0.15	0.18	0.12
MgO	7.97	7.89	7.85	7.85	6.71	6.66	7.53	5.26
CaO	10.17	10.17	10.29	10.28	12.58	12.53	12.40	10.16
Na2O	2.51	2.43	2.46	2.52	2.62	2.65	2.51	3.11
K2O	0.12	0.10	0.11	0.11	0.07	0.07	0.07	1.76
P2O5	0.14	0.12	0.15	0.17	0.12	0.12	0.13	0.61
H2O+	0.00	0.00	0.00	0.00	0.55	0.69	0.00	1.55
H2O-	0.00	0.00	0.00	0.00	1.09	1.09	0.00	1.56
CO2	0.00	0.00	0.00	0.00	0.09	0.08	0.00	0.00
SO3	0.00	0.00	0.00	0.00	1.40	1.40	0.00	0.03
SumOx	100.04	99.64	99.39	99.37	101.61	101.40	98.74	100.25

Trace elements in ppm

Ni					48	54		88
Cu					118	123		67
Zn					76	77		130
Rb					0.8	0.7		31.4
Sr					143	148		658
Y					28	27		32
Pb					0	0		5.0
Tl					0	0		4.5
U					0	0		2.5

CIPW Norms from Dry Analyses

Q	1.7	2.7	2.4	2.2	0.0	0.0	0.0	0.4
Or	0.7	0.6	0.7	0.7	0.4	0.4	0.4	10.7
Ab	21.2	20.6	20.9	21.5	22.5	22.8	21.5	27.1
An	32.4	32.6	32.9	32.3	33.2	33.3	27.9	20.4
Pl	53.6	53.2	53.9	53.7	55.7	56.2	49.4	47.5
DiCa	7.1	7.2	7.3	7.5	12.3	12.2	14.0	11.5
DiMg	4.0	4.0	4.1	4.2	7.5	7.7	7.0	9.9
DiFe	2.9	2.9	2.8	2.9	4.1	3.8	6.7	0.0
Di	14.0	14.1	14.3	14.7	23.8	23.6	27.7	21.4
HyMg	15.9	15.7	15.5	15.4	7.0	7.7	5.8	3.6
HyFe	11.7	11.2	10.7	10.7	3.9	3.8	5.5	0.0
Hy	27.5	26.9	26.2	26.2	10.9	11.5	11.3	3.6
OlMg	0.0	0.0	0.0	0.0	1.7	1.0	4.3	0.0
OlFe	0.0	0.0	0.0	0.0	1.1	0.6	4.5	0.0
Ol	0.0	0.0	0.0	0.0	2.8	1.6	8.8	0.0
Mt	0.0	0.0	0.0	0.0	3.7	4.0	0.0	1.6
Il	2.1	2.2	2.2	2.2	2.3	2.4	2.1	8.2
Hm	0.0	0.0	0.0	0.0	0.0	0.0	0.0	5.3
Ap	0.3	0.3	0.3	0.4	0.3	0.3	0.3	1.4
SumNorm	99.99	99.99	99.99	99.99	99.99	99.99	99.99	99.98

Mg No	61.8	62.2	62.8	62.9	62.8	64.3	56.2	69.6
-------	------	------	------	------	------	------	------	------

Trace element ratios:

K/Rb					726.34	830.10		465.28
------	--	--	--	--	--------	--------	--	--------

Combe Bank - RD 7

Manatu Smt

	7-9WR	7-11WR	7-12WR	7-20WR	7-14GL	7-14GL	10-1WR	10-4WR
SiO ₂	47.66	46.80	43.98	43.64	48.96	48.88	50.20	51.39
TiO ₂	3.91	2.36	3.33	3.70	4.43	4.59	1.14	0.98
Al ₂ O ₃	13.62	10.05	11.39	13.43	14.25	14.31	15.15	14.94
Fe ₂ O ₃	5.01	3.79	7.81	9.56	1.37	1.37	5.52	4.54
FeO	5.42	8.25	3.75	4.26	9.12	9.15	4.44	5.19
MnO	0.16	0.18	0.15	0.20	0.11	0.10	0.15	0.15
MgO	6.64	15.63	9.05	5.94	5.92	5.84	7.04	6.96
CaO	11.26	8.38	8.26	11.75	10.76	10.85	10.76	10.69
Na ₂ O	2.91	1.95	3.06	2.67	3.01	3.01	2.77	2.69
K ₂ O	0.91	0.33	1.89	0.74	1.22	1.24	0.24	0.22
P ₂ O ₅	0.50	0.28	0.42	1.04	0.43	0.40	0.13	0.13
H ₂ O ⁺	1.23	1.28	4.17	1.52	0.00	0.00	1.12	1.33
H ₂ O ⁻	0.73	0.81	3.05	1.47	0.00	0.00	1.61	1.05
CO ₂	0.18	0.14	0.11	0.08	0.00	0.00	0.00	0.00
SO ₃	0.02	0.02	0.02	0.04	0.00	0.00	0.03	0.02
SumOx	100.16	100.25	100.44	100.04	99.58	99.74	100.30	100.28

Trace elements in ppm

Ni	128	676	275	174	0	0	73	52
Cu	113	101	94	152	0	0	149	135
Zn	127	111	109	125	0	0	75	78
Rb	12.5	11.1	22.9	6.3	0	0	11.1	16.8
Sr	474	263	385	472	0	0	112	106
Y	33	22	27	33	0	0	28	26
Pb	0	0	1.8	2.3	0	0	0	0
Th	1.7	0	2.8	1.5	0	0	0	0
U	1.6	0	0	2.6	0	0	0	0

CIPW Norms from Dry Analyses

Q	1.4	0.0	0.0	0.4	0.0	0.0	4.4	5.3
Or	5.5	2.0	12.0	4.5	7.2	7.3	1.5	1.3
Ab	25.1	16.8	24.3	23.3	25.6	25.5	24.0	23.3
An	21.9	18.1	12.6	23.2	21.9	21.9	28.9	28.6
Ne	0.0	0.0	1.9	0.0	0.0	0.0	0.0	0.0
Pl	47.0	34.9	36.9	46.5	47.4	47.5	52.9	51.9
DiCa	13.3	9.4	12.0	12.6	12.1	12.3	10.4	10.3
DiMg	11.5	7.0	10.3	10.9	7.3	7.4	8.3	7.5
DiFe	0.0	1.5	0.0	0.0	4.2	4.2	0.9	1.9
Di	24.8	17.9	22.3	23.5	23.5	23.9	19.7	19.7
HyMg	5.4	17.0	0.0	4.4	4.0	3.3	9.7	10.3
HyFe	0.0	3.7	0.0	0.0	2.3	1.9	1.1	2.6
Hy	5.4	20.7	0.0	4.4	6.2	5.3	10.8	12.9
OlMg	0.0	11.0	9.7	0.0	2.5	2.7	0.0	0.0
OlFe	0.0	2.6	0.0	0.0	1.6	1.7	0.0	0.0
Ol	0.0	13.6	9.7	0.0	4.1	4.4	0.0	0.0
Mt	6.8	5.6	3.1	3.8	2.0	2.0	8.2	6.7
Il	7.6	4.6	6.8	7.2	8.4	8.7	2.2	1.9
Hm	0.4	0.0	6.2	7.3	0.0	0.0	0.0	0.0
Ap	1.2	0.6	1.0	2.4	1.0	0.9	0.3	0.3
SumNorm	99.98	99.99	99.96	99.96	99.99	99.99	99.99	99.99

Mg No 68.6 77.1 81.1 71.3 53.6 53.2 73.9 70.5

Trace element ratios:

K/Rb 604.31 246.79 685.10 975.04 179.48 108.70

RD 10 Alexa Bank - RD 14

	10-7WR	14-15	14-19	14-23
SiO2	48.07	48.49	47.37	46.28
TiO2	1.17	2.64	2.77	2.55
Al2O3	15.61	14.03	13.85	14.95
Fe2O3	3.84	7.71	5.81	6.87
FeO	6.03	3.58	6.71	4.13
MnO	0.18	0.15	0.17	0.22
MgO	7.44	6.73	6.31	7.38
CaO	11.13	10.17	8.82	10.27
Na2O	2.94	2.83	2.86	3.32
K2O	0.56	0.62	0.50	0.32
P2O5	0.12	0.32	0.31	0.31
H2O+	2.15	1.31	1.57	1.78
H2O-	1.24	1.47	2.17	1.49
CO2	0.00	0.06	0.74	0.39
SO3	0.02	0.02	0.19	0.02
SumOx	100.55	100.13	100.15	100.28

Trace elements in ppm

Ni	66	78	50	134
Cu	132	177	88	108
Zn	80	88	198	85
Rb	5.9	19.1	8.5	4.3
Sr	288	329	301	349
Y	26	29	33	28
Pb	0	2.1	2.2	0
Th	0	0	0	1.9
U	0	1.5	0	1.5

CIPW Norms from Dry Analyses

Q	0.0	4.2	4.0	0.0
Or	3.4	3.8	3.1	2.0
Ab	25.6	24.6	25.3	29.1
An	28.6	24.4	24.6	25.8
Pl	54.2	49.0	49.9	54.9
DiCa	11.6	10.6	8.0	10.4
DiMg	8.0	9.2	6.0	9.0
DiFe	2.7	0.0	1.2	0.0
Di	22.2	19.7	15.3	19.4
HyMg	3.1	8.1	10.5	5.8
HyFe	1.0	0.0	2.2	0.0
Hy	4.1	8.1	12.6	5.8
OlMg	5.6	0.0	0.0	3.0
OlFe	2.1	0.0	0.0	0.0
Ol	7.7	0.0	0.0	3.0
Mt	5.7	4.5	8.8	6.9
Il	2.3	5.2	5.5	5.0
Hm	0.0	4.8	0.0	2.4
Ap	0.3	0.7	0.7	0.7
SumNorm	99.99	99.99	99.98	99.98

Mg No 68.7 77.0 62.6 76.1

Trace element ratios:

K/Rb 787.89 269.46 488.29 617.75

APPENDIX B

Pyroxene Analyses - Northern Melanesian Borderland

Taviuni-Field Ti-Salites

	1-2Ti	1-2Ti	1-2Ti	1-2Ti	1-2Ti	1-2Ti	1-2Ti	1-2Ti
SiO ₂	37.73	37.88	33.15	36.54	34.59	36.57	36.67	35.70
TiO ₂	5.79	5.40	9.72	6.21	9.48	7.15	6.64	8.07
Al ₂ O ₃	12.11	12.05	12.67	13.33	13.06	13.15	13.69	12.81
Cr ₂ O ₃	0.00	0.00	0.00	0.00	0.00	0.04	0.01	0.00
FeO	10.49	8.85	10.97	10.41	10.79	10.51	10.68	10.23
MnO	0.17	0.14	0.26	0.07	0.22	0.10	0.19	0.11
MgO	9.13	10.04	8.08	7.10	9.14	9.42	7.81	9.77
CaO	23.77	23.69	22.70	19.98	22.92	22.20	20.99	22.87
Na ₂ O	0.79	0.48	0.78	3.55	0.73	1.22	1.83	0.47
K ₂ O	0.02	0.03	0.05	0.86	0.01	0.23	0.53	0.02
SUM	100.00	98.56	98.18	98.05	100.94	100.59	99.04	100.05

CATIONS ON THE BASIS OF 6 OXYGENS

Si	1.467	1.480	1.329	1.455	1.342	1.414	1.439	1.388
Al ₂	0.533	0.520	0.599	0.545	0.597	0.536	0.561	0.587
Al ₃	0.021	0.035	0.000	0.080	0.000	0.013	0.072	0.000
Ti	0.169	0.159	0.293	0.186	0.277	0.208	0.196	0.236
Cr	0.000	0.000	0.000	0.000	0.000	0.001	0.000	0.000
Fe ₂	0.341	0.269	0.368	0.347	0.350	0.340	0.351	0.333
Mn	0.006	0.005	0.002	0.002	0.007	0.003	0.006	0.004
Mg	0.529	0.585	0.483	0.421	0.529	0.543	0.457	0.566
Ca	0.990	0.992	0.975	0.852	0.953	0.919	0.883	0.952
Na	0.060	0.036	0.061	0.274	0.055	0.091	0.139	0.035
K	0.001	0.001	0.003	0.044	0.000	0.011	0.027	0.001
Z	2.000	2.000	1.927	2.000	1.939	2.000	2.000	1.974
Y	1.066	1.073	1.145	1.036	1.163	1.108	1.082	1.138
X	1.051	1.030	1.038	1.170	1.008	1.022	1.048	0.989
Sum	4.117	4.102	4.111	4.206	4.110	4.130	4.131	4.101
M/M+F	60.8	66.9	56.8	54.9	60.2	61.5	56.6	63.0
Ca	0.531	0.530	0.533	0.525	0.518	0.509	0.520	0.514
Mg	0.284	0.313	0.264	0.260	0.287	0.301	0.269	0.305
Fe	0.186	0.157	0.202	0.215	0.194	0.190	0.210	0.181

	Taviuni-Field Ti-Salites				Taviuni-Field Cpx phenocryst			
	1-2Ti	1-2Ti	1-2Ti	1-2Ti	1-2C	1-2C	1-2C	1-2C
SiO2	35.46	35.68	36.09	37.23	50.12	50.19	49.59	50.32
TiO2	7.96	7.27	8.08	7.33	1.33	1.54	1.40	1.39
Al2O3	12.07	12.60	12.69	15.20	4.04	4.07	5.92	3.89
Cr2O3	0.00	0.05	0.06	0.00	1.11	1.04	1.08	0.93
FeO	10.51	11.37	10.67	9.74	4.10	4.46	4.35	4.31
MnO	0.04	0.12	0.18	0.09	0.00	0.00	0.00	0.00
MgO	10.19	7.98	9.69	6.86	16.26	14.95	14.91	15.61
CaO	22.94	22.26	22.80	18.55	23.26	23.33	23.07	23.46
Na2O	0.71	0.92	0.09	1.72	0.34	0.26	0.29	0.31
K2O	0.11	0.16	0.60	2.56	0.00	0.00	0.00	0.02
SUM	99.99	98.41	100.95	99.28	100.56	99.84	100.61	100.24

CATIONS ON THE BASIS OF 6 OXYGENS

Si	1.385	1.418	1.395	1.451	1.838	1.854	1.815	1.852
Alz	0.556	0.582	0.578	0.549	0.162	0.146	0.185	0.148
Al _y	0.000	0.000	0.000	0.149	0.013	0.032	0.071	0.021
Ti	0.234	0.217	0.235	0.215	0.037	0.043	0.039	0.038
Cr	0.000	0.002	0.002	0.000	0.032	0.030	0.031	0.027
Fe2	0.343	0.378	0.345	0.317	0.126	0.138	0.133	0.133
Mn	0.001	0.004	0.006	0.003	0.000	0.000	0.000	0.000
Mg	0.593	0.473	0.558	0.398	0.889	0.823	0.814	0.856
Ca	0.960	0.948	0.944	0.774	0.914	0.924	0.905	0.925
Na	0.054	0.071	0.007	0.130	0.024	0.019	0.021	0.022
K	0.005	0.008	0.030	0.127	0.000	0.000	0.000	0.001
Z	1.941	2.000	1.973	2.000	2.000	2.000	2.000	2.000
Y	1.172	1.082	1.146	1.082	1.096	1.066	1.087	1.075
X	1.019	1.027	0.980	1.032	0.938	0.942	0.925	0.948
Sum	4.133	4.108	4.099	4.114	4.034	4.008	4.013	4.023
M/M+F	63.3	55.6	61.8	55.7	87.6	85.7	85.9	86.6
Ca	0.506	0.526	0.509	0.519	0.474	0.490	0.489	0.483
Mg	0.313	0.262	0.301	0.257	0.461	0.437	0.439	0.447
Fe	0.182	0.212	0.189	0.215	0.065	0.073	0.072	0.069

	Taviuni-Field Cpx phenocryst				Lalla Rookh			
	1-2C	1-2R	1-2R	1-2R	1-2R	1-2R	3-16G	3-16G
SiO2	50.94	50.96	50.83	48.32	50.45	51.23	47.92	45.09
TiO2	1.51	1.41	1.42	1.01	1.25	1.08	2.56	3.26
Al2O3	4.03	3.22	2.86	11.69	3.86	3.34	10.25	12.96
Cr2O3	1.01	0.83	0.68	0.80	1.06	0.87	0.00	0.00
FeO	4.39	4.23	4.24	3.95	4.36	4.08	6.98	7.84
MnO	0.00	0.00	0.02	0.03	0.00	0.01	0.14	0.24
MgO	16.37	15.62	15.42	15.72	15.47	15.69	10.39	10.00
CaO	23.19	23.77	23.72	21.18	23.43	23.47	17.92	16.59
Na2O	0.26	0.23	0.21	0.24	0.40	0.33	3.42	3.30
K2O	0.00	0.01	0.00	0.01	0.03	0.00	0.06	0.65
SUM	101.70	100.28	99.40	102.95	100.31	100.10	99.64	99.93

CATIONS ON THE BASIS OF 6 OXYGENS

Si	1.845	1.873	1.885	1.711	1.856	1.882	1.777	1.680
Alz	0.155	0.127	0.115	0.289	0.144	0.118	0.223	0.320
Al _y	0.017	0.013	0.010	0.199	0.024	0.027	0.225	0.249
Ti	0.041	0.039	0.040	0.027	0.035	0.030	0.071	0.091
Cr	0.029	0.024	0.020	0.022	0.031	0.025	0.000	0.000
Fe2	0.133	0.130	0.131	0.117	0.134	0.125	0.216	0.244
Mn	0.000	0.000	0.001	0.001	0.000	0.000	0.004	0.008
Mg	0.884	0.856	0.852	0.830	0.848	0.859	0.574	0.555
Ca	0.900	0.936	0.942	0.803	0.924	0.924	0.712	0.662
Na	0.018	0.016	0.015	0.016	0.029	0.024	0.246	0.238
K	0.000	0.000	0.000	0.000	0.001	0.000	0.003	0.031
Z	2.000	2.000	2.000	2.000	2.000	2.000	2.000	2.000
Y	1.104	1.062	1.053	1.195	1.072	1.067	1.091	1.147
X	0.918	0.953	0.957	0.820	0.954	0.947	0.961	0.931
Sum	4.022	4.015	4.011	4.016	4.025	4.015	4.052	4.079
M/M+F	86.9	86.8	86.6	87.6	86.3	87.3	72.6	69.5
Ca	0.470	0.487	0.489	0.459	0.485	0.484	0.472	0.451
Mg	0.461	0.445	0.442	0.474	0.445	0.450	0.381	0.378
Fe	0.069	0.068	0.069	0.067	0.070	0.066	0.147	0.171

Lalla Rookh Cpx phenocrysts-Cores (C), Rims (R), Groundmass (G)

	3-16G	3-16G	3-16G	3-16P	3-36PC	3-36PC	3-36PC	3-36PC
SiO2	43.02	44.54	46.63	49.15	48.98	47.75	49.12	48.97
TiO2	4.35	3.83	3.14	2.47	2.44	1.97	1.50	1.55
Al2O3	10.07	10.88	8.13	5.09	4.80	6.49	5.16	5.94
Cr2O3	0.00	0.00	0.00	0.00	0.00	0.24	0.00	0.00
FeO	8.00	8.90	7.28	7.22	6.71	6.71	9.04	7.18
MnO	0.05	0.13	0.13	0.08	0.10	0.00	0.22	0.05
MgO	10.62	12.48	11.98	14.60	14.05	15.12	12.19	14.37
CaO	22.10	18.21	21.34	23.00	23.13	22.02	21.54	21.69
Na2O	0.71	1.83	0.67	0.36	0.59	0.64	1.57	0.85
K2O	0.04	0.59	0.56	0.01	0.01	0.00	0.04	0.00
SUM	98.96	101.39	99.86	101.98	100.81	100.94	100.38	100.60

CATIONS ON THE BASIS OF 6 OXYGENS

Si	1.641	1.651	1.746	1.799	1.813	1.762	1.840	1.810
Alz	0.359	0.349	0.254	0.201	0.187	0.238	0.160	0.190
Alv	0.093	0.126	0.104	0.019	0.022	0.044	0.068	0.069
Ti	0.125	0.107	0.088	0.068	0.068	0.055	0.042	0.043
Cr	0.000	0.000	0.000	0.000	0.000	0.007	0.000	0.000
Fe2	0.255	0.276	0.226	0.221	0.208	0.207	0.293	0.222
Mn	0.002	0.004	0.004	0.002	0.003	0.000	0.007	0.002
Mg	0.604	0.689	0.668	0.797	0.775	0.832	0.681	0.792
Ca	0.903	0.723	0.856	0.902	0.917	0.871	0.865	0.859
Na	0.052	0.132	0.049	0.026	0.042	0.046	0.114	0.061
K	0.002	0.028	0.027	0.000	0.000	0.000	0.002	0.000
Z	2.000	2.000	2.000	2.000	2.000	2.000	2.000	2.000
Y	1.078	1.202	1.093	1.107	1.075	1.145	1.081	1.128
X	0.957	0.863	0.931	0.928	0.960	0.916	0.981	0.920
Sum	4.036	4.085	4.024	4.036	4.036	4.061	4.062	4.048
M/M+F	70.3	71.4	74.6	78.3	78.9	80.1	70.6	78.1
Ca	0.512	0.427	0.487	0.469	0.482	0.456	0.471	0.458
Mg	0.342	0.407	0.361	0.414	0.407	0.435	0.371	0.422
Fe	0.146	0.165	0.132	0.116	0.111	0.108	0.158	0.119

Lalla Rookh Cpx Cores (C), Rims (R), Groundmass (G)

	3-36PC	3-36PR	3-36PR	3-36PR	3-36PR	3-36PR	3-36PR	3-36G
SiO2	49.32	42.64	47.61	43.54	41.81	45.74	43.93	42.11
TiO2	1.24	5.37	2.18	4.62	5.07	3.11	4.79	4.75
Al2O3	5.16	9.82	7.09	9.38	9.75	6.86	5.80	9.47
Cr2O3	0.00	0.00	0.00	0.00	0.00	0.24	0.00	0.04
FeO	5.98	7.93	7.17	8.29	8.47	6.99	12.86	8.13
MnO	0.04	0.13	0.01	0.08	0.07	0.01	0.12	0.13
MgO	15.55	11.27	13.84	11.82	12.70	14.22	14.36	11.32
CaO	22.27	22.76	19.57	22.53	23.16	23.10	20.92	22.52
Na2O	0.82	0.52	1.32	0.61	0.43	0.43	0.32	0.67
K2O	0.00	0.00	0.78	0.01	0.00	0.02	0.02	0.05
SUM	100.38	100.44	99.57	100.96	101.46	100.72	103.12	99.19

CATIONS ON THE BASIS OF 6 OXYGENS

Si	1.821	1.600	1.781	1.632	1.570	1.707	1.644	1.612
Alz	0.179	0.392	0.219	0.368	0.430	0.293	0.256	0.388
Alv	0.046	0.044	0.093	0.047	0.001	0.008	0.000	0.039
Ti	0.034	0.152	0.061	0.130	0.143	0.087	0.135	0.137
Cr	0.000	0.000	0.000	0.002	0.000	0.007	0.000	0.001
Fe2	0.185	0.250	0.224	0.260	0.266	0.218	0.403	0.260
Mn	0.001	0.004	0.000	0.003	0.002	0.000	0.004	0.004
Mg	0.856	0.633	0.772	0.660	0.711	0.791	0.801	0.646
Ca	0.681	0.919	0.784	0.905	0.932	0.924	0.639	0.924
Na	0.059	0.038	0.096	0.044	0.031	0.031	0.023	0.050
K	0.000	0.000	0.037	0.000	0.000	0.001	0.001	0.002
Z	2.000	2.000	2.000	2.000	2.000	2.000	1.900	2.000
Y	1.122	1.084	1.151	1.102	1.124	1.112	1.342	1.087
X	0.940	0.957	0.917	0.950	0.963	0.956	0.863	0.976
Sum	4.062	4.041	4.068	4.052	4.087	4.068	4.105	4.063
M/M+F	82.3	71.7	77.5	71.8	72.8	78.4	66.6	71.3
Ca	0.458	0.509	0.440	0.495	0.488	0.478	0.410	0.504
Mg	0.445	0.351	0.433	0.361	0.372	0.409	0.391	0.352
Fe	0.097	0.141	0.126	0.144	0.140	0.113	0.199	0.144

	Combe Bank - Glomerocrysts (GL), Cores (C), Rims (R) Phenocrysts (P)							
	3-36GM	7-9GLC	7-9GLC	7-9GLC	7-9GLR	7-9GLR	7-9GLR	7-9PC
SiO2	47.10	51.49	51.04	51.53	50.43	49.65	49.86	50.04
TiO2	3.12	1.23	1.36	1.12	1.53	1.79	1.85	1.55
Al2O3	5.92	2.62	3.72	2.65	4.03	4.10	4.47	4.11
Cr2O3	0.00	0.70	1.16	0.74	0.88	0.44	0.81	0.77
FeO	7.67	6.68	6.63	6.73	6.94	7.40	7.17	6.69
MnO	0.16	0.07	0.12	0.05	0.15	0.10	0.12	0.12
MgO	14.86	16.44	16.61	17.93	15.76	15.46	16.37	16.44
CaO	22.33	20.92	20.66	20.35	20.85	20.62	21.01	20.52
Na2O	0.41	0.29	0.36	0.31	0.34	0.44	0.44	0.38
K2O	0.12	0.00	0.00	0.00	0.00	0.00	0.03	0.00
NiO	0.00	0.01	0.00	0.00	0.07	0.00	0.00	0.00
SUM	101.69	100.45	101.66	101.41	100.95	100.00	102.13	100.62

CATIONS ON THE BASIS OF 6 OXYGENS

Si	1.740	1.894	1.856	1.876	1.851	1.843	1.815	1.840
Alz	0.258	0.106	0.144	0.114	0.149	0.157	0.185	0.160
Alv	0.000	0.007	0.016	0.000	0.025	0.023	0.007	0.018
Ti	0.007	0.034	0.037	0.031	0.042	0.050	0.051	0.043
Cr	0.000	0.020	0.033	0.021	0.026	0.013	0.023	0.022
Fe2	0.237	0.205	0.202	0.205	0.213	0.230	0.218	0.206
Mn	0.005	0.002	0.004	0.002	0.005	0.003	0.004	0.004
Mg	0.818	0.901	0.900	0.973	0.862	0.856	0.888	0.901
Ca	0.884	0.824	0.805	0.794	0.820	0.820	0.819	0.809
Na	0.029	0.021	0.025	0.022	0.024	0.032	0.031	0.027
K	0.006	0.000	0.000	0.000	0.000	0.000	0.001	0.000
Z	1.997	2.000	2.000	1.990	2.000	2.000	2.000	2.000
Y	1.147	1.170	1.192	1.231	1.173	1.174	1.191	1.194
X	0.919	0.845	0.830	0.816	0.844	0.852	0.852	0.836
Sum	4.062	4.016	4.023	4.037	4.019	4.026	4.043	4.030
M/M+F	77.5	81.4	81.7	82.6	80.2	78.8	80.3	81.4
Ca	0.455	0.426	0.421	0.402	0.432	0.430	0.425	0.421
Mg	0.421	0.466	0.471	0.493	0.454	0.448	0.460	0.470
Fe	0.124	0.107	0.107	0.105	0.115	0.122	0.115	0.109

Combe Bank Cpx - Phenocrysts (P), Cores (C), Rims (R)

	7-9PC	7-9PC	7-9PC	7-9PR	7-9PR	7-9PR	7-9PR	7-9P
SiO2	50.22	51.16	50.14	49.43	51.43	49.83	51.35	50.00
TiO2	1.39	1.25	1.55	2.21	1.20	1.69	1.18	1.48
Al2O3	3.75	3.62	4.09	4.94	2.71	4.05	2.90	3.89
Cr2O3	0.66	0.83	0.97	0.78	0.48	1.06	0.79	1.12
FeO	6.44	6.32	6.94	7.61	6.58	6.86	6.87	6.50
MnO	0.13	0.06	0.00	0.09	0.06	0.04	0.07	0.09
MgO	16.71	16.85	16.68	15.93	17.41	16.35	17.48	16.56
CaO	20.68	20.44	20.66	20.10	20.70	20.79	20.01	20.76
Na2O	0.38	0.35	0.41	0.42	0.37	0.35	0.28	0.38
K2O	0.00	0.03	0.01	0.03	0.02	0.02	0.00	0.00
F	0.00	0.00	0.00	0.00	0.48	1.06	0.00	1.12
SUM	100.56	100.91	102.20	101.54	101.33	101.86	100.93	101.65

CATIONS ON THE BASIS OF 6 OXYGENS

Si	1.847	1.868	1.815	1.809	1.872	1.811	1.877	1.818
Alz	0.153	0.132	0.175	0.191	0.116	0.174	0.123	0.167
Alv	0.000	0.024	0.000	0.022	0.000	0.000	0.002	0.000
Ti	0.030	0.034	0.042	0.061	0.033	0.046	0.032	0.040
Cr	0.025	0.024	0.028	0.023	0.014	0.030	0.023	0.032
Fe2	0.198	0.193	0.210	0.233	0.200	0.209	0.210	0.198
Mn	0.004	0.002	0.000	0.003	0.002	0.001	0.002	0.003
Mg	0.916	0.917	0.900	0.869	0.945	0.886	0.953	0.898
Ca	0.815	0.800	0.801	0.788	0.807	0.810	0.784	0.809
Na	0.027	0.025	0.029	0.030	0.026	0.025	0.020	0.027
K	0.000	0.001	0.000	0.001	0.001	0.001	0.000	0.000
Z	2.000	2.000	1.990	2.000	1.988	1.985	2.000	1.985
Y	1.192	1.195	1.180	1.209	1.193	1.172	1.222	1.171
X	0.842	0.826	0.831	0.819	0.834	0.835	0.804	0.836
Sum	4.034	4.021	4.112	4.028	4.071	4.114	4.026	4.120
M/M+F	82.2	82.6	81.1	78.9	82.5	80.9	81.9	82.0
Ca	0.422	0.418	0.419	0.416	0.413	0.425	0.402	0.424
Mg	0.474	0.480	0.471	0.459	0.483	0.465	0.489	0.471
Fe	0.105	0.102	0.110	0.125	0.103	0.110	0.109	0.105

Combe Bank Megacrysts (MGX), Groundmass (G)

	7-9MGX	7-9MGX	7-9MGX	7-9MGX	7-9G	7-9G	7-9G
SiO2	51.61	50.58	50.58	52.12	48.27	50.60	49.88
TiO2	1.11	1.32	1.38	1.13	2.39	1.63	1.81
Al2O3	2.53	3.76	3.73	2.86	4.51	2.94	8.89
Cr2O3	0.71	0.87	0.96	0.63	0.30	0.11	0.63
FeO	6.58	6.61	6.44	6.66	8.71	9.72	6.57
MnO	0.13	0.09	0.11	0.05	0.18	0.25	0.16
MgO	17.76	16.50	16.86	17.38	15.54	16.86	13.52
CaO	20.50	21.16	21.33	20.27	20.55	18.95	19.10
Na2O	0.41	0.36	0.37	0.38	0.44	0.41	1.25
K2O	0.01	0.00	0.00	0.02	0.02	0.01	0.04
F	0.71	0.87	0.96	0.63	0.30	0.11	0.63
SUM	101.90	101.92	102.50	101.99	101.14	101.57	102.34

CATIONS ON THE BASIS OF 6 OXYGENS

Si	1.868	1.835	1.825	1.880	1.788	1.859	1.788
Alz	0.108	0.161	0.159	0.120	0.197	0.127	0.212
AlY	0.000	0.000	0.000	0.001	0.000	0.000	0.163
Ti	0.030	0.036	0.037	0.031	0.067	0.045	0.049
Cr	0.020	0.025	0.027	0.018	0.009	0.003	0.018
Fe2	0.199	0.201	0.194	0.201	0.270	0.299	0.197
Mn	0.004	0.003	0.003	0.002	0.006	0.008	0.005
Mg	0.958	0.892	0.907	0.934	0.856	0.923	0.722
Ca	0.795	0.822	0.825	0.783	0.816	0.746	0.733
Na	0.029	0.025	0.026	0.027	0.032	0.029	0.087
K	0.000	0.000	0.000	0.001	0.001	0.000	0.002
Z	1.976	1.995	1.983	2.000	1.985	1.986	2.000
Y	1.212	1.156	1.169	1.187	1.209	1.278	1.154
X	0.824	0.848	0.850	0.811	0.848	0.776	0.822
Sum	4.093	4.099	4.112	4.069	4.077	4.052	4.047
M/M+F	82.8	81.6	82.4	82.3	76.1	75.6	78.6
Ca	0.406	0.429	0.427	0.408	0.418	0.378	0.443
Mg	0.490	0.465	0.470	0.487	0.440	0.467	0.436
Fe	0.104	0.106	0.102	0.105	0.141	0.155	0.122

Manatu Seamount - Cpx

	10-1	10-1	10-1	10-1	10-1	10-1	10-1	10-1
SiO2	52.35	52.74	51.41	51.72	51.94	52.09	52.08	52.20
TiO2	0.51	0.28	0.28	0.31	0.40	0.46	0.41	0.43
Al2O3	2.96	2.31	2.85	2.89	3.20	3.10	2.61	3.29
Cr2O3	0.03	0.31	0.48	0.50	0.18	0.22	0.22	0.41
FeO	8.20	5.62	5.39	6.07	7.77	6.61	6.65	5.90
MnO	0.34	0.10	0.11	0.15	0.31	0.09	0.15	0.14
MgO	16.94	17.69	17.29	17.69	18.25	16.84	18.77	17.29
CaO	18.57	19.70	20.05	19.50	17.81	20.76	19.55	20.00
Na2O	0.31	0.30	0.22	0.24	0.24	0.31	0.23	0.28
K2O	0.00	0.00	0.00	0.01	0.03	0.00	0.02	0.02
SUM	100.21	99.05	98.00	98.08	100.13	100.46	100.69	99.96

CATIONS ON THE BASIS OF 6 OXYGENS

Si	1.923	1.943	1.917	1.912	1.904	1.907	1.900	1.911
Alz	0.077	0.057	0.083	0.088	0.096	0.093	0.100	0.089
AlY	0.051	0.043	0.042	0.038	0.043	0.041	0.012	0.053
Ti	0.014	0.008	0.008	0.009	0.011	0.013	0.011	0.012
Cr	0.001	0.009	0.014	0.015	0.005	0.006	0.006	0.012
Fe2	0.252	0.173	0.168	0.188	0.238	0.202	0.203	0.181
Mn	0.011	0.003	0.003	0.005	0.010	0.003	0.005	0.004
Mg	0.928	0.971	0.961	0.975	0.997	0.919	1.020	0.944
Ca	0.731	0.777	0.801	0.772	0.700	0.814	0.764	0.785
Na	0.022	0.021	0.016	0.017	0.017	0.022	0.016	0.020
K	0.000	0.000	0.000	0.000	0.001	0.000	0.001	0.001
Z	2.000	2.000	2.000	2.000	2.000	2.000	2.000	2.000
Y	1.256	1.207	1.197	1.228	1.304	1.184	1.257	1.205
X	0.753	0.799	0.817	0.790	0.718	0.836	0.781	0.805
Sum	4.009	4.006	4.014	4.018	4.022	4.021	4.039	4.011
M/M+F	78.6	84.9	85.1	83.9	80.7	82.0	83.4	83.9
Ca	0.380	0.404	0.414	0.398	0.360	0.420	0.384	0.410
Mg	0.483	0.505	0.497	0.503	0.513	0.474	0.512	0.493
Fe	0.137	0.092	0.089	0.099	0.127	0.106	0.104	0.097

Manatu Seamount - Cpx, Opx

	10-1 Cpx	10-13 Opx	10-13 Opx	10-13 Opx	10-13 Opx	10-13 Opx	10-13 Cpx	10-13 Cpx
SiO ₂	51.86	52.92	52.83	52.97	52.63	53.70	52.46	52.25
TiO ₂	0.41	0.40	0.38	0.33	0.42	0.42	0.33	0.49
Al ₂ O ₃	2.73	1.49	1.83	1.93	1.88	1.58	2.36	2.36
Cr ₂ O ₃	0.08	0.00	0.00	0.00	0.00	0.00	0.10	0.15
FeO	7.64	20.38	19.12	19.18	19.25	19.39	6.88	7.62
MnO	0.27	0.68	0.43	0.57	0.43	0.44	0.27	0.19
MgO	17.92	24.38	23.65	24.73	25.35	24.24	17.54	17.75
CaO	18.31	1.93	1.88	1.91	1.89	2.05	19.74	19.65
Na ₂ O	0.18	0.05	0.09	0.08	0.07	0.02	0.18	0.23
K ₂ O	0.00	0.00	0.02	0.00	0.00	0.01	0.00	0.00
SUM	99.40	102.23	100.23	101.70	101.92	101.85	99.86	100.69

CATIONS ON THE BASIS OF 6 OXYGENS

Si	1.916	1.923	1.942	1.922	1.907	1.944	1.929	1.913
Al _z	0.084	0.064	0.058	0.078	0.080	0.056	0.071	0.087
Al _y	0.035	0.000	0.022	0.005	0.000	0.011	0.031	0.015
Ti	0.011	0.011	0.011	0.009	0.011	0.011	0.009	0.013
Cr	0.002	0.000	0.000	0.000	0.000	0.000	0.003	0.004
Fe ₂	0.236	0.619	0.588	0.582	0.583	0.587	0.212	0.233
Mn	0.008	0.021	0.013	0.018	0.013	0.013	0.008	0.006
Mg	0.987	1.320	1.296	1.338	1.369	1.308	0.961	0.969
Ca	0.725	0.075	0.074	0.074	0.073	0.080	0.778	0.771
Na	0.013	0.004	0.006	0.006	0.005	0.001	0.013	0.016
K	0.000	0.000	0.001	0.000	0.000	0.000	0.000	0.000
Z	2.000	1.986	2.000	2.000	1.988	2.000	2.000	2.000
Y	1.280	1.971	1.930	1.951	1.977	1.931	1.225	1.241
X	0.738	0.079	0.081	0.080	0.078	0.081	0.791	0.787
Sum	4.018	4.036	4.011	4.031	4.043	4.012	4.016	4.028
M/M+F	80.7	68.1	68.8	69.7	70.1	69.0	82.0	80.6
Ca	0.371	0.037	0.038	0.037	0.036	0.040	0.397	0.390
Mg	0.504	0.649	0.657	0.665	0.671	0.658	0.491	0.490
Fe	0.125	0.314	0.305	0.298	0.293	0.302	0.112	0.121

	Manatu, Cores (C), Rims (R)				Alexa, Cores (C), Rims (R)			
	10-13	10-13C	10-13R	10-13C	14-15C	14-15R	14-15G	14-19C
SiO2	52.12	51.50	50.99	51.49	51.96	51.88	49.52	51.60
TiO2	0.62	0.40	0.61	0.49	0.80	0.84	1.40	0.74
Al2O3	2.53	4.13	2.57	2.87	2.98	2.34	4.86	3.14
Cr2O3	0.00	0.28	0.00	0.00	0.27	0.00	0.25	0.18
FeO	9.76	6.84	10.90	7.81	6.29	7.72	8.21	7.54
MnO	0.23	0.23	0.30	0.20	0.28	0.15	0.25	0.26
MgO	17.36	16.58	15.15	17.92	16.81	17.22	15.55	16.93
CaO	19.29	19.50	18.79	19.25	21.37	18.81	18.75	20.09
Na2O	0.32	0.21	0.38	0.25	0.35	0.19	0.35	0.27
K2O	0.00	0.00	0.04	0.00	0.00	0.00	0.06	0.00
SUM	102.23	99.67	99.73	100.28	101.11	99.15	99.20	100.75

CATIONS ON THE BASIS OF 6 OXYGENS

Si	1.897	1.896	1.913	1.895	1.895	1.924	1.848	1.892
Alz	0.103	0.104	0.087	0.105	0.105	0.076	0.152	0.108
Alx	0.005	0.075	0.027	0.019	0.023	0.027	0.062	0.028
Ti	0.017	0.011	0.017	0.014	0.022	0.023	0.039	0.020
Cr	0.000	0.003	0.000	0.000	0.008	0.000	0.007	0.005
Fe2	0.297	0.211	0.342	0.240	0.192	0.239	0.256	0.231
Mn	0.007	0.007	0.010	0.006	0.009	0.005	0.008	0.008
Mg	0.942	0.910	0.847	0.983	0.914	0.952	0.865	0.925
Ca	0.752	0.769	0.755	0.759	0.835	0.748	0.750	0.789
Na	0.023	0.015	0.028	0.018	0.025	0.014	0.025	0.019
K	0.000	0.000	0.002	0.000	0.000	0.000	0.003	0.000
Z	2.000	2.000	2.000	2.000	2.000	2.000	2.000	2.000
Y	1.268	1.222	1.243	1.262	1.167	1.247	1.238	1.218
X	0.775	0.784	0.785	0.777	0.860	0.761	0.778	0.809
Sum	4.043	4.007	4.028	4.039	4.027	4.008	4.016	4.027
M/M+F	76.0	81.2	71.2	80.4	82.6	79.9	77.1	80.0
Ca	0.376	0.406	0.387	0.382	0.428	0.385	0.399	0.404
Mg	0.471	0.480	0.434	0.494	0.469	0.490	0.460	0.474
Fe	0.152	0.115	0.183	0.124	0.103	0.126	0.141	0.122

Alexa Bank Cpx - Cores (C), Rims (R), Groundmass (G)

	14-19C	14-19R	14-19R	14-19G	14-23C	14-23C	14-23C	14-23R
SiO2	50.62	50.19	51.34	49.04	51.10	50.02	50.16	48.32
TiO2	0.74	0.68	0.71	1.35	1.33	1.24	1.07	1.73
Al2O3	3.09	3.49	3.26	3.67	3.69	4.09	3.37	5.32
Cr2O3	0.07	0.05	0.06	0.00	0.06	0.30	0.12	0.05
FeO	7.83	7.47	7.78	10.75	8.74	8.14	8.02	8.36
MnO	0.32	0.12	0.12	0.37	0.28	0.09	0.22	0.23
MgO	17.25	17.05	17.52	15.16	16.85	17.32	15.58	15.02
CaO	19.85	19.61	20.22	18.44	19.37	18.88	19.63	20.40
Na2O	0.24	0.34	0.24	0.26	0.39	0.20	0.28	0.52
K2O	0.02	0.02	0.00	0.00	0.00	0.06	0.04	0.01
SUM	100.03	99.02	101.25	99.04	101.81	100.34	98.49	99.96

CATIONS ON THE BASIS OF 6 OXYGENS

Si	1.875	1.873	1.876	1.856	1.863	1.845	1.887	1.805
Alz	0.125	0.127	0.124	0.144	0.137	0.155	0.113	0.195
Alx	0.010	0.027	0.016	0.020	0.021	0.023	0.037	0.039
Ti	0.021	0.019	0.020	0.038	0.036	0.034	0.030	0.049
Cr	0.002	0.001	0.002	0.000	0.002	0.009	0.004	0.001
Fe2	0.243	0.233	0.238	0.340	0.266	0.251	0.252	0.261
Mn	0.010	0.004	0.004	0.012	0.009	0.003	0.007	0.007
Mg	0.953	0.949	0.954	0.855	0.916	0.952	0.874	0.836
Ca	0.788	0.784	0.792	0.748	0.757	0.746	0.791	0.816
Na	0.017	0.025	0.017	0.019	0.028	0.014	0.020	0.038
K	0.001	0.001	0.000	0.000	0.000	0.003	0.002	0.000
Z	2.000	2.000	2.000	2.000	2.000	2.000	2.000	2.000
Y	1.238	1.233	1.233	1.266	1.250	1.272	1.204	1.193
X	0.806	0.810	0.809	0.767	0.784	0.763	0.814	0.854
Sum	4.045	4.043	4.042	4.033	4.034	4.036	4.017	4.048
M/M+F	79.7	80.3	80.1	71.5	77.5	79.1	77.6	76.2
Ca	0.395	0.398	0.398	0.382	0.389	0.382	0.411	0.425
Mg	0.478	0.482	0.480	0.437	0.470	0.488	0.454	0.435
Fe	0.127	0.120	0.122	0.180	0.141	0.130	0.135	0.140

Alexa, Rims (R), Groundmass (G)

	14-23R	14-23R	14-23G	14-23G
SiO ₂	46.82	47.00	48.47	48.32
TiO ₂	2.18	2.51	2.12	2.15
Al ₂ O ₃	6.65	6.41	6.05	6.27
Cr ₂ O ₃	0.42	0.32	0.14	0.07
FeO	8.24	7.76	8.66	8.42
MnO	0.12	0.06	0.16	0.25
MgO	14.01	13.91	14.52	14.25
CaO	19.84	20.97	19.88	20.79
Na ₂ O	0.40	0.43	0.51	0.43
K ₂ O	0.01	0.02	0.03	0.00
SUM	98.69	99.39	100.54	100.95

CATIONS ON THE BASIS OF 6 OXYGENS

Si	1.770	1.766	1.797	1.787
Al _z	0.230	0.234	0.203	0.213
Al _y	0.066	0.050	0.062	0.050
Ti	0.062	0.071	0.059	0.060
Cr	0.013	0.010	0.004	0.002
Fe ₂	0.261	0.244	0.269	0.260
Mn	0.004	0.002	0.005	0.003
Mg	0.790	0.779	0.802	0.786
Ca	0.804	0.844	0.790	0.824
Na	0.029	0.031	0.037	0.031
K	0.000	0.001	0.001	0.000
Z	2.000	2.000	2.000	2.000
Y	1.195	1.156	1.201	1.176
X	0.833	0.877	0.828	0.855
Sum	4.028	4.032	4.029	4.031
M/M+F	75.2	76.2	74.9	75.1
Ca	0.433	0.452	0.423	0.439
Mg	0.425	0.417	0.430	0.418
Fe	0.142	0.131	0.147	0.143

Appendix C. Dredge Locations

Table C-1. ANZUS/SOPAC LEG 2 ROCK DREDGES

DREDGE #	Geographic Area	Latitude	Longitude	Water Depth (m)	Recovery
1	Field Bank	12°12.0'S	174°37.6'W	2000-1400	2 kg altered basalt <1 kg limestone
2	Lalla Rookh Bank	13°02.5'S	175°38.3'W	2800	1 kg altered hyaloclastic breccia
3	Lalla Rookh Bank	12°59.1'S	175°38.1'W	2800-2400	80 kg basalt 350 kg altered hyaloclastic breccia 60 kg limestone and calcareous sandstone
4	Wallis Island	13°05.1'S	176°12.6'W	2250	<1 kg pillow basalt 40 kg calcareous siltstone
5	NE of Peggy Ridge	15°39.5'S	178°29.7'W	2200-1900	650 kg pillow basalt 20 kg pumice 90 kg mudstone
6	Horne Islands	14°24.1'S	177°52.5'W	2000-1500	1900 kg olivine-phyric pillow basalts and plagiophyric dolerites
7	Combe Bank	12°42.1'S	177°41.1'W	2800-2550	100 kg basalt 70 kg hyaloclastic breccia 30 kg limestone and siltstone
8	Robbie Bank	10°55.3'S	177°00.9'W	2125-1700	1300 kg limestone
9	Tuscarora Bank	11°51'S	177°53'W	1800-1400	10 kg altered hyaloclastic breccia
10	Manatu Seamount	13°22.1'S	179°16.5'W	1500-700	450 kg basalt and dolerite 200 kg talus breccia 100 kg limestone and marl
12	NE of Nurakita Bank	10°01.1'S	179°24.7'W	4000-3370	250 kg altered gabbro 200 kg massive basalt 50 kg vesicular pillow basalt 250 kg talus breccia and hyaloclastic breccia <1 kg pumice
13	N. Fiji Basin	14°28.8'S	177°41.2'W	2600-2250	1400 kg pillow basalt 150 kg Mn crusts, consolidated ash
14	Alexa Bank	11°41.1'S	175°02.8'E	3900-2400	450 kg massive basalt and dolerite 260 kg amygdaloidal basalt 5 kg altered hyaloclastic breccia 27 kg argillite 70 kg black laminated shale 90 kg siltstone

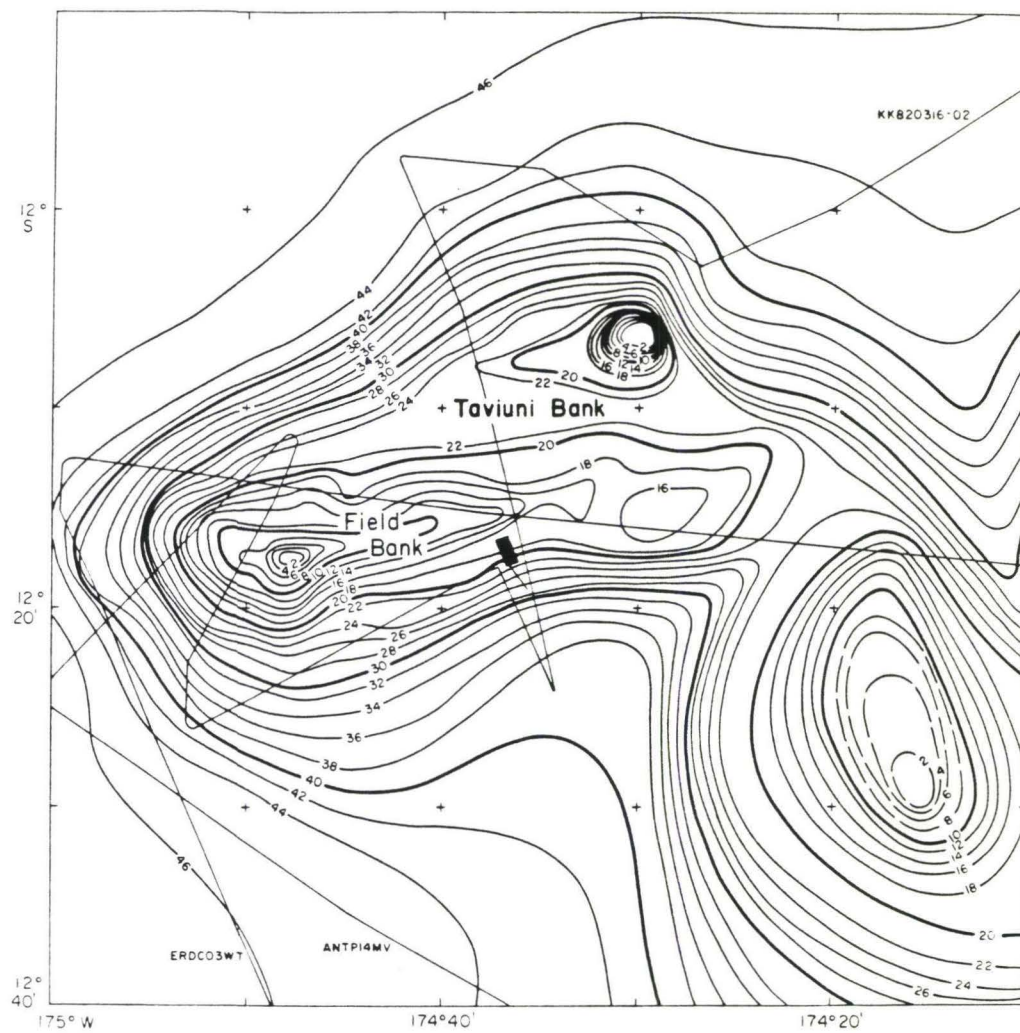


Figure C-1. Dredge location and bathymetry of Taviuni-Field Bank. Thin lines--ship tracks; black rectangle--dredge site. Contours in hundreds of meters. Maps drawn by Brocher (in preparation).

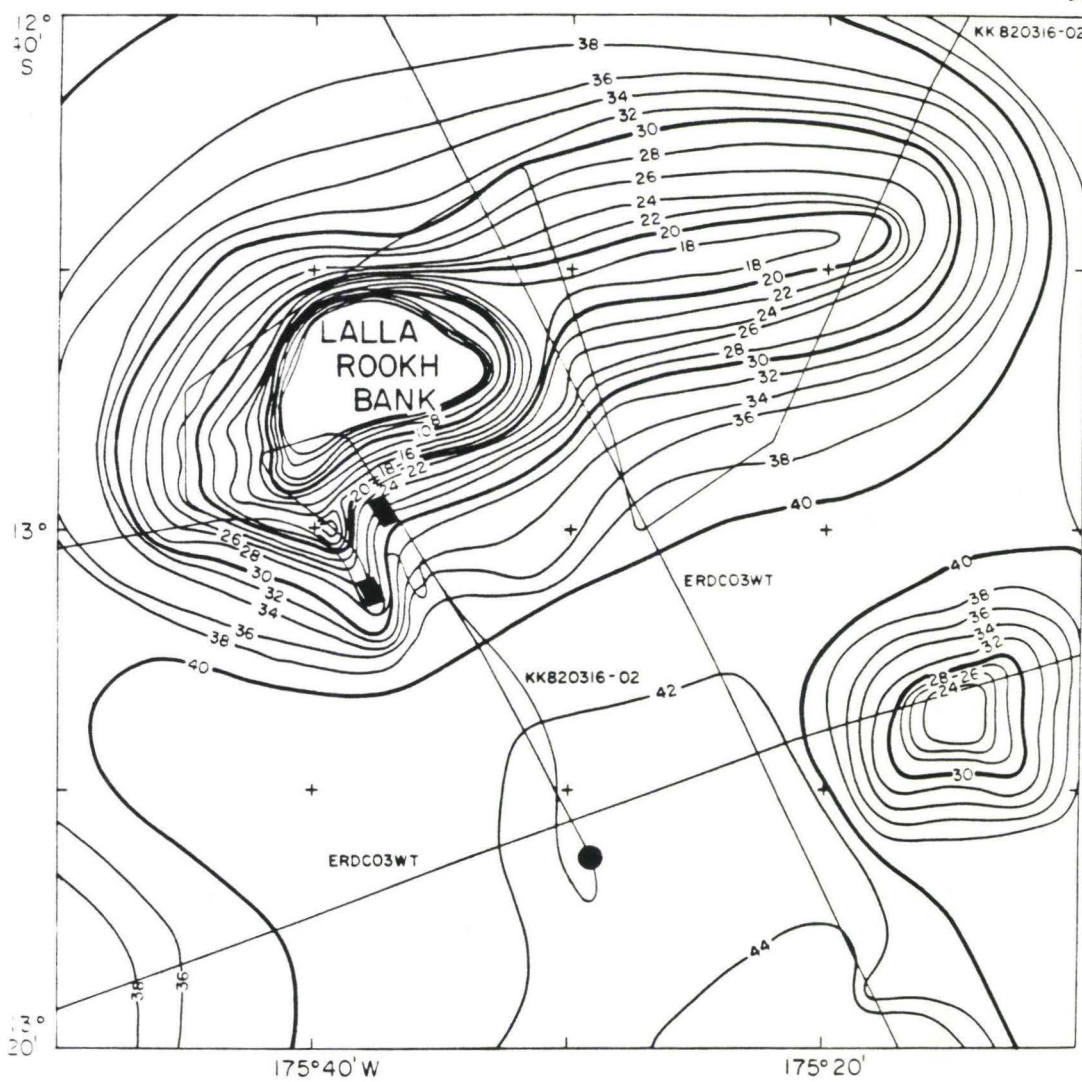


Figure C-2. Dredge locations and bathymetry for Lalla Rookh Bank. Circle indicates site of piston core station. Other symbols as in Figure C-1.

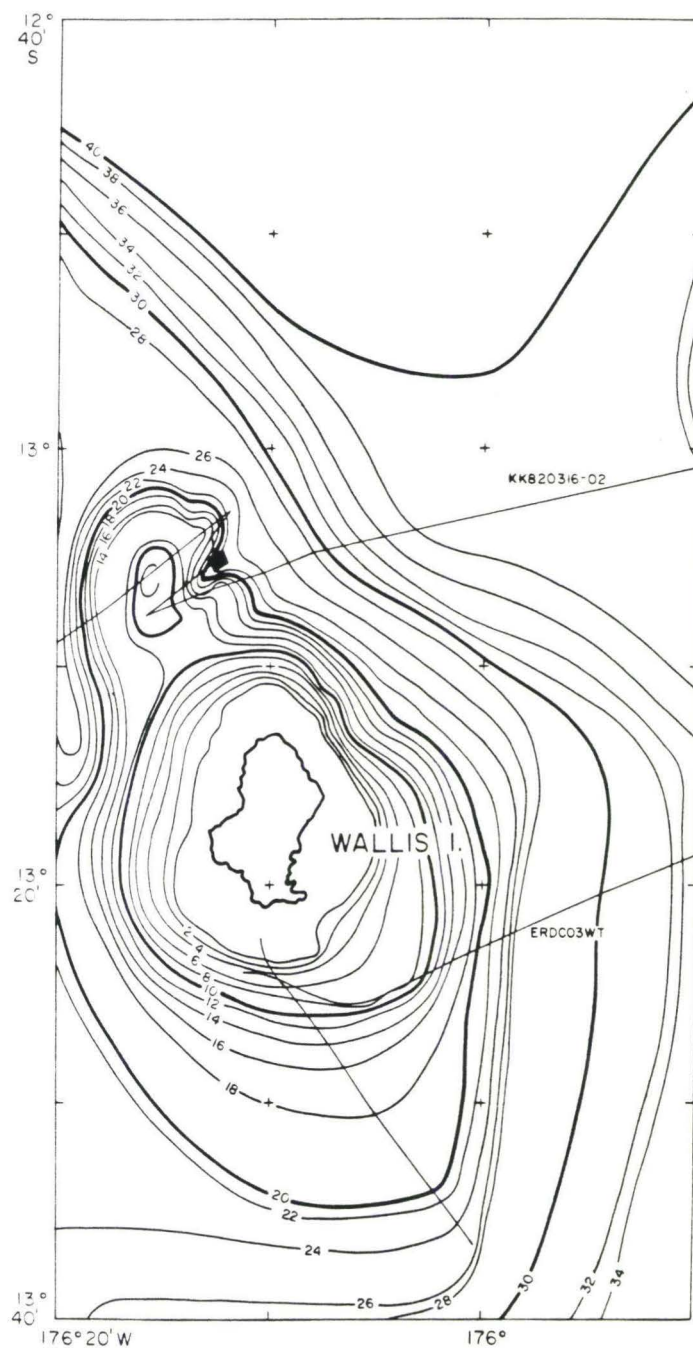


Figure C-3. Dredge location and bathymetry for Wallis Island, RD 4. Symbols as in C-1.

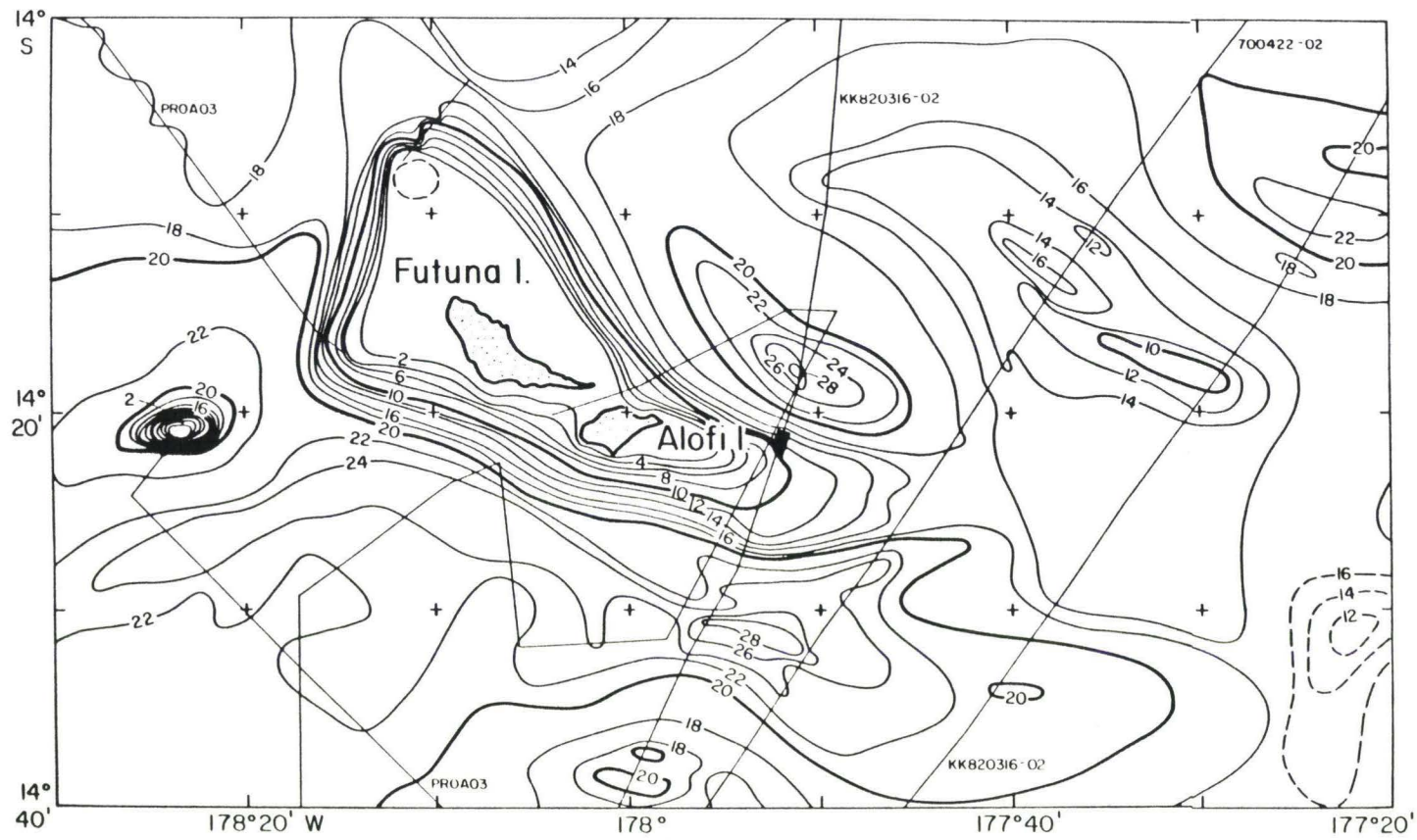


Figure C-4. Dredge location and bathymetry for Horne (Futuna) Islands, RD 6. Symbols as in Figure C-1.

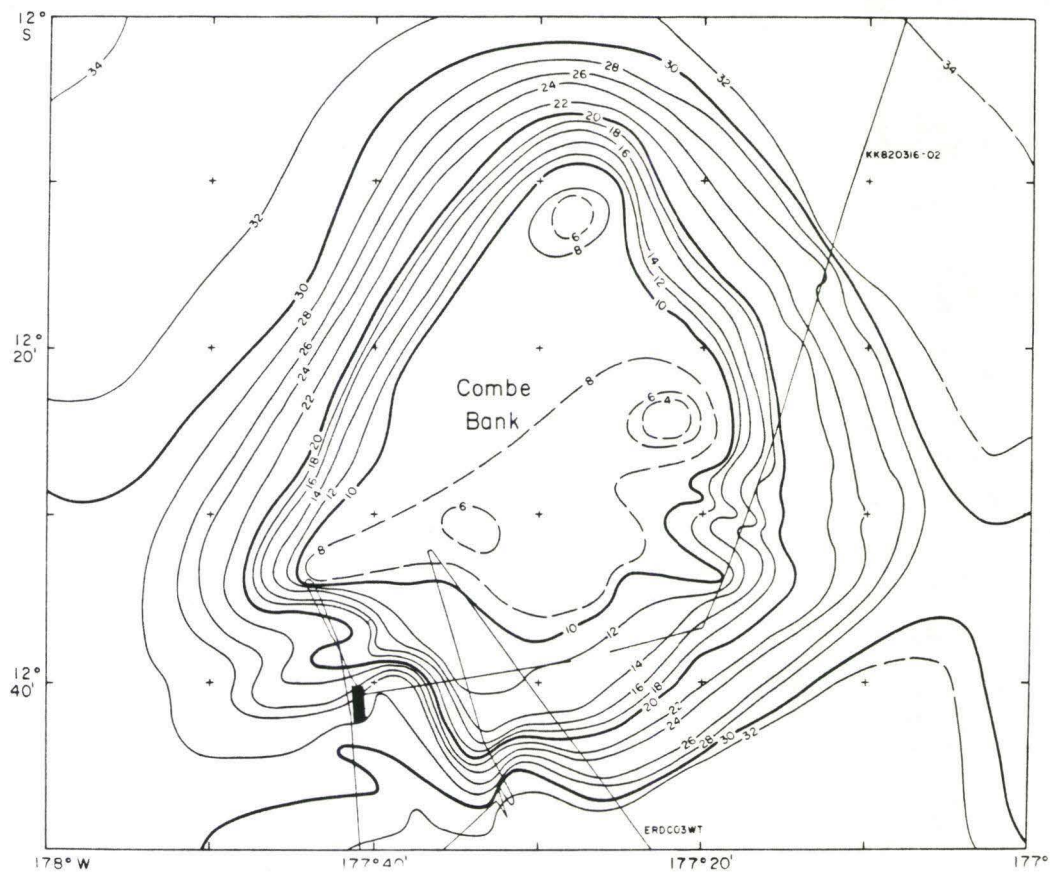


Figure C-5. Dredge location and bathymetry for Combe Bank, RD 7. Symbols as in Figure C-1.

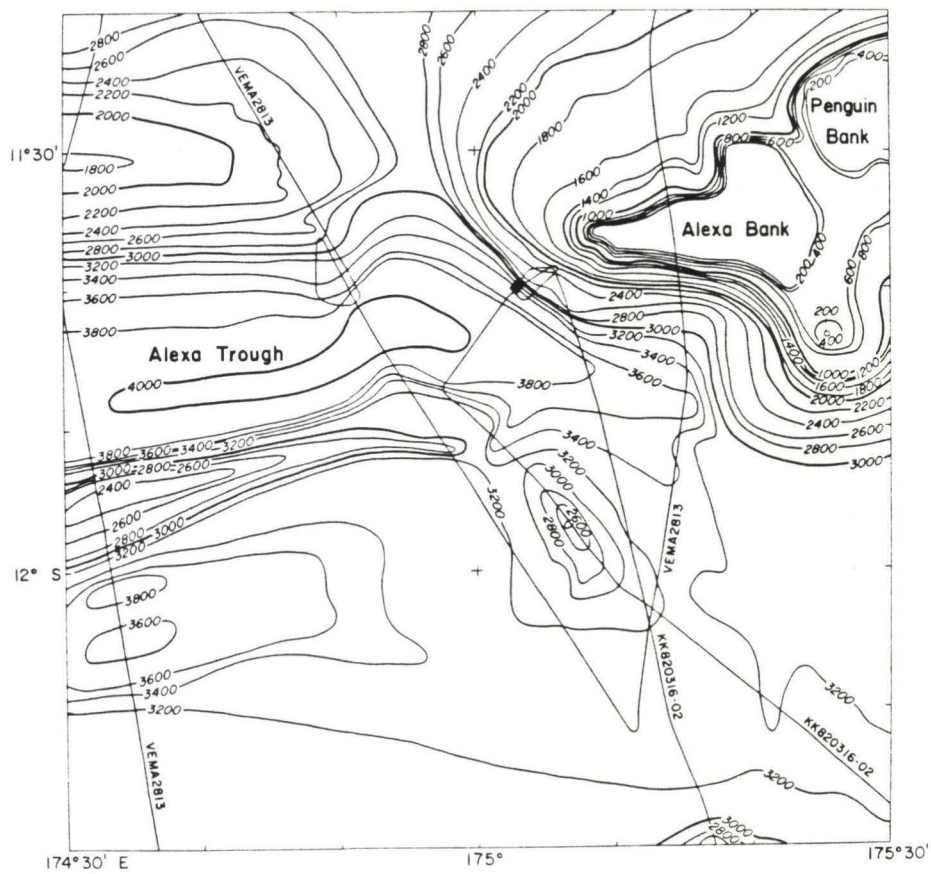


Figure C-6. Dredge location and bathymetry for Alexa Bank, RD 14. Symbols as in Figure C-1, except contours which are in meters.

APPENDIX D

PETROGRAPHY

In this section I will describe the petrographic and petrologic characteristics of each volcanic edifice discussed in this paper. Samples marked by an asterisk were analyzed by either X-ray fluorescence spectroscopy or by electron microprobe, or both.

Field (Taviuni) Bank: RD 1 - sample 1-2

Modal mineralogy:

phenocrysts:	altered melilite	25%-30%
	subhedral olivine	15%
	Ti-augite	- one crystal
microphenocrysts and groundmass:	Ti-salite	10%-15%
	Ti-magnetite	10%
	Chromite	1%-2%
	alteration	25%-30%
	vesicles	15%-20%

Texture: Intergranular to intersertal, vesicular, olivine-phyric melilitite or basanitoid lava. Determination of melilitite is uncertain, but is based on "peg" structure and tetragonal habit. Microprobe analysis of this mineral did not aid in its identification due to the extremely altered nature of the mineral and the rock.

Lalla Rookh Bank - RD 3Type 1: 3-32, 3-43

Modal mineralogy:

phenocrysts:	plagioclase ~An70	20%
	augite	10%-15%
	altered olivine	5%-7%
microphenocrysts:	plagioclase ~An65	20%
	augite	3%-5%
groundmass:	clinopyroxene	5%
	skeletal plag.	5%

glass	15%
vesicles	7%

Texture: Mainly intersertal with plagioclase and clinopyroxene microlites and glass forming the groundmass of this mildly vesicular basaltic rock. Clinopyroxene forms glomeroporphyritic masses 2-4 mm in size which resemble recrystallized megacrysts with 120° angles between crystal faces. Sample 3-43 contains oscillatory zoned augites and a few very large phenocrysts in an otherwise fine-grained to glassy matrix. Evidence of disequilibrium is expressed in the recrystallization texture of some of the clinopyroxenes and may indicate a multi-stage crystallization history for the magma as it ascended.

Type 2: 3-26, 3-39*

Modal mineralogy:

phenocrysts:	olivine	20% (0.1-0.3 mm)
groundmass:	clinopyroxene	35%-40%
	olivine	10%
	glass	10%
	vesicles	20%-30%

Texture: Blades of cpx form the groundmass around large euhedral and skeletal olivines. The cpx often plates the crystal faces of olivine, which forms mainly in glomeroporphyritic clots. The texture reflects the chilling of an alkalic, olivine- and clinopyroxene-rich magma erupted under shallow water conditions. The general absence of plagioclase in the mode reflects the undersaturated nature of this melt. Clinopyroxene is also quite late to join the liquidus. The highly vesicular character of the rock implies shallow eruption or the presence of volatile components in the magma or both.

Type 3: 3-2*, 3-13, 3-36, 3-42; coarse-grained ankaramites

Modal mineralogy:

phenocrysts:	Ti-augite	20%
	olivine	7%-10%
microphenocrysts:	Ti-augite	15%
	Ti-magnetite	10%
groundmass:	cpx	15%-20%
	glass	15%
	Ti-magnetite	10%

Texture: Large Ti-augite (0.5-1.5 mm) and olivine (0.5- 1.2 mm) in a glassy to microcrystalline groundmass. Intersertal to intergranular texture. Evidence of stellate microlites of Ti-augite growing from Ti-magnetites similar in form to #1-2. Magnetite is also often enclosed in normally zoned augite phenocrysts. The augites are strongly pleochroic in pale brown and lavender, are commonly twinned, and sector zoned. Some augites display minor exsolution lamellae and some cores contain abundant glass inclusions. Ilmenite occupies the anhedral cores of many of the Ti-augites and lies along their cleavage planes. However, the ilmenite inclusions are limited in occurrence to the cores of the augites and delineate an earlier stage of growth possibly followed by resorption and subsequent growth of the rims. Sample 3-36 contains many sector zoned augites with $2V=55^\circ$ in the cores and $\sim 60^\circ$ in the rims. This sample also contains a xenocrystal fragment (xenolith?) 1.5mm in diameter containing dark green and colorless phases as well as spinel. Due to the small size of the microcrystals making up the xenocrystal ($\sim 5 \times 10^{-3}$ mm) microprobe analysis of the individual grains was not possible.

Type 4: 3-11*, 3-16, 3-21*; ankaramites

Modal mineralogy:

phenocrysts:	olivine	15%
	Ti-augite	7-10%
microphenocrysts:	cpx	15%
	olivine	5%
groundmass:	cpx	25%
	devitrified glass	
	and alteration	10%
	Fe-Ti oxide	20%
	minor plagioclase	<2%

Texture: Subhedral to skeletal olivines 0.2-0.4 mm in size and augites 0.2-0.5 mm in size in a matrix of intergranular cpx and intersertal glass and alteration products. The augite is generally unzoned, but occasionally shows sector zoning in the groundmass and microphenocryst phases. These rocks are ankaramites, but are finer grained than #3-2, #3-13, #3-36, and #3-42.

Wallis Islands: RD 4 - samples 4-1*, 4-2*.

Modal mineralogy:

phenocrysts:	skeletal olivine	10-15%
groundmass:	quench crystals	
	cpx and olivine	40-50%
	glass	15%
	vesicles	15%
	Fe-Ti oxides	2-4%

Texture: euhedral and skeletal olivine phenocrysts set in a groundmass of glass and quench crystals of cpx and olivine. Microcrystalline ilmenite needles fill in the interstices of cpx plumes in groundmass. Rapidly quenched lava is inferred from this texture.

Horne Islands: RD 6

Type A-1: samples 6-3*, 6-10*, 6-13*

Modal mineralogy:

microphenocrysts and groundmass:	skeletal olivine	10-15%
	skeletal plag.	35%
	glass	35%
	vesicles	10-15%

Texture: Large skeletal olivine phenocrysts in a groundmass of trachytoid textured plagioclase microlites and glass. Plumose quench textures of incipient cpx in glass.

Type B: sample 6-14*

Modal mineralogy:

phenocrysts:	clinopyroxene	10%
	olivine-plag.	
	glomerocrysts	25-30%
groundmass:	plagioclase	15%
	glass	35-45%

Texture: Sample 6-14 contains occasional large, rounded augites as well as large olivines and plagioclase glomerocrysts in a predominantly glassy groundmass. This perhaps represents inclusion of accumulated phases in the erupted magma.

Type B: samples 6-30*, 6-31, 6-36

Modal mineralogy:

phenocrysts:	plag. glomero-	
	crysts	5-8%
groundmass:	cpx glomero-	
	crysts	1%
	plagioclase	25-30%
	cpx	25-30%
	Fe-Ti oxides	15%
	glass	10-15%

Texture: Subophitic with intergranular and intersertal portions. Glass is often brown in color and devitrified. Sample 6-36 possesses uniform grain size cpx=plag.>glass, interstitial opaques, intergranular texture, crystals:glass = 4:1. Plagioclase glomerocrysts 3-5 mm. Large plagioclase grains are oscillatory zoned. Relict grains of highly altered olivine retains its crystal form, but altered to green serpentine.

Combe Bank: RD 7 - samples 7-7*, 7-8, 7-12*

Modal mineralogy:

phenocrysts:	plagioclase	20%
	cpx	20%
groundmass:	ilmenite	10%
	Fe-Ti oxide	5%
	vesicles	40%
	glass	3-5%

Texture: Intergranular plag-augite-ilmenite basalt. Ilmenite is oriented, but not along any obvious crystallographic or cleavage planes. Ilmenite often cross-cuts plagioclase laths. Presence of ilmenite in large proportions is unique in these rocks. Sample 7-8 glassier than other two, less vesicular, more altered. 7-12 contains zeolite vesicle filling.

Sample 7-9*

Modal mineralogy:

phenocrysts:	olivine	5-8%
	cpx	7-10%
groundmass:	plagioclase	30-35%
	plagioclase	10-15%
	cpx	10%

ilmenite	5-8%
alteration	5-10%

Texture: Virtually holocrystalline - crystals:glass = 90:10 or 95:5. Recrystallized cpx glomerocrysts abundant. Ilmenite shows preferred orientation, subparallel and subequal spacing. Cpx and plagioclase often form glomerophyric masses with plagioclase radiating from the core of partially recrystallized cpx mass.

Sample 7-11*

Modal mineralogy:

phenocrysts:	embayed olivine	30-35%
	plagioclase	15-20%
microphenocrysts and groundmass:	plagioclase	10-15%
	cpx	10-15%
	Fe-Ti oxides	3-5%
	glass	5-8%

Texture: Olivine-phyric, plag-cpx subophitic to intersertal groundmass. Olivine phenocrysts are embayed due to resorption. Olivines generally fresh, but serpentinized along fractures. Some contain glass inclusions in cores continuous across grain boundaries. Some contain bubble or fluid trains.

Sample 7-20*

Modal mineralogy:

phenocrysts:	plagioclase	20-25%
	cpx	10-15%
	olivine altered to iddingsite	15%
groundmass:	glass	15-20%
	ilmenite	5%
	Fe-Ti oxides	3%
	vesicles	10-15%

Texture: Intersertal, intergranular plagioclase-, olivine-, clinopyroxene-phyric basalt. Glass in groundmass is mainly devitrified. Oxides fill in interstices. Phenocrysts are fine-grained - 0.1 to 0.2 mm.

Manatu Seamount: RD 10 - samples 10-1*, 10-13*

Modal mineralogy:

phenocrysts:	plagioclase	35-40%
	twinned cpx	10-15%
	hypersthene	3-5%
	quartz	1-2%
groundmass:	Fe-Ti oxide	3-4%
	saussuritization	10-15%

Texture: Holocrystalline, subophitic to intergranular. Quartz appears primary, i.e. not associated with fractures or vesicles and occurs as intergranular growth with cpx. Plagioclase An₅₈. The rocks are fairly weathered mainly cpx and some feldspar. 10-13 coarser grained than 10-1 and more altered mainly in cpx. 10-13 contains more hypersthene which crystallized before plagioclase. Hypersthene in large prismatic grains. Cpx is highly altered.

Samples 10-3, 10-4*, 10-9

Modal mineralogy:	plagioclase	25-30%
	cpx	10-15%
	Fe-Ti oxide	2-3%
	vesicles	15-20%
	devitrified glass	20-30%

Texture: Fine-grained, subophitic to intersertal finely vesicular basalt w/glassy inclusions containing skeletal plagioclase. Magnetite is very fine-grained and lined up along plagioclase crystal boundaries. Crystallization sequence: 1. cpx 2. plagioclase 3. oxides.

Alexa Bank: RD 14 - samples 14-15*, 14-19*

Modal mineralogy:

phenocrysts:	plagioclase	25%
	cpx	20%
	olivine	10%
groundmass:	Fe-Ti oxide	3-5%
	devitrified glass and alter- ation	35-40%

Texture: Fine-grained plagioclase-cpx intergranular basalt. Plagioclase appears to be first crystallized phase. High degree of alteration prevents detailed description of components.

Appendix E

ANALYTICAL METHODS

The techniques and equipment used for analysis in this study were developed and maintained by people other than myself. I am grateful to them for their assistance in the use of the equipment and for the opportunity to use their laboratories, particularly the laboratory of Dr. Richard C. Price at LaTrobe University, Bundoora, Australia.

Sample preparation for whole rock analysis

Least weathered samples were selected and fresh portions were separated using a hydraulic jaw splitter. The samples were then crushed to powder in a tungsten carbide vibrating mill.

Major element Analyses

Whole-rock analyses were carried out using a fully automated Philips X-ray fluorescence spectrometer operated and maintained by Dr. R. C. Price of LaTrobe University. Samples were measured in duplicate and glass buttons prepared using the techniques of Norrish and Hutton (1969). The concentrations reported are averages of duplicate analyses. Accuracy of measurements of major elements is + 1%, minor elements + 5%.

Trace Elements

Trace elements were obtained using pressed powder pellets in the Philips XRF laboratory at LaTrobe, using techniques similar to those of Norrish and Chappell (1977).

Flame Photometry

Potassium and Sodium were measured using the flame photometer at LaTrobe University. An internal lithium standard was used and samples were run in duplicate. Accuracy of measurements is $\pm 1\%$ for both elements.

Other

Fe^{2+} was measured by titration. In subsequent normative calculations, Fe^{3+} was adjusted, assuming alteration effects, to $\text{Fe}^{3+}/\text{Fe}^{2+} = 0.15$.

H_2O^- was measured by heating 0.5 gram of powdered rock sample in platinum boats at 110 degrees Celsius overnight and measuring the weight loss. H_2O^+ and CO_2 were then measured by heating the samples in a furnace for 30 minutes and measuring the weight gain in P_2O_5 and Carbosorb collectors. Tables of chemical compositions are presented for both dry, normalized and uncorrected analyses.

MicroprobeVolcanic glass

Glass samples were chosen from the respective dredge hauls with the object of obtaining a suite representative of the rocks collected. Rocks from dredge hauls 4 (submarine flanks of Wallis Islands), 5 (Peggy Ridge), 6 (Submarine flanks of Horne Islands), 7 (Combe Bank), 12 (Scarp NE of Nurakita Bank), and 13 (N. Fiji Basin) contained volcanic glass either as pillow margins or as fragments in hyaloclastic breccias. The glass was collected, mounted in plastic discs, secured with epoxy, and polished sequentially down to a 0.05 microns grit size. Polished thin sections of the breccias were prepared. The sections, discs and standards were carbon-coated under vacuum to a uniform thickness. Standard discs were coated at the same time as the unknowns to maintain consistency of analyses.

The microprobe unit is a three spectrometer Cameca-MBX, wavelength dispersive electron microprobe with computer controlled spectrometer positioning and counting functions. Natural volcanic glass standards from Juan de Fuca ridge (VG-2) and Makaopuhi (VG-A99) were used to standardize the microprobe for major elements SiO_2 , TiO_2 , Al_2O_3 , FeO , MgO , CaO , Na_2O , K_2O , and minor elements MnO and P_2O_5 . Internal consistency was ensured by analyzing the standards several times and restandardizing if individual element analyses showed significant deviation from reported values (+3-8% for major elements, +15-30% for minor elements) after averaging three analyses. The standards were reanalyzed periodically throughout the course of a day's analyses and

individual elements re-standardized according to the same criteria as above. At the end of the probe session, the standards were re-analyzed and correction factors applied to the sample analyses to normalize the analyses to the standard glasses.

Instrument operating conditions are summarized below:

filament voltage - 15 kv
sample absorbed current - 10-15 namps
beam diameter - 20-30 microns (defocused to
minimize alkali volatilization)

Reported analyses represent averages of 3-5 analyses of different glass chips from an individual sample. Raw data were corrected using ZAF (atomic number, absorption, and fluorescence), dead time, and background corrections. Accuracy of analyses is +0.2-1.5% for major elements and +2-10% for minor elements.

Minerals

Samples were chosen for mineral probes based on petrographic inspection for freshness and crystal condition. Polished thin sections were prepared using alumina powder down to 0.05 microns. Pyroxenes were the primary target for the microprobe analyses and standards were chosen accordingly. It is not clear to what extent element coordination affects analyses and for this reason I used mainly pyroxene standards to minimize any ill effects differences in coordination might have on analyses. For some important elements, e.g. titanium, standardization with clinopyroxene was not practical due to low abundances in the standards and other minerals were used. Most phenocrysts were analyzed two to three times in close proximity and the analyses were averaged if

variations did not reflect crystallization zoning. Zoned minerals were analyzed in the core and rim and by sectors where applicable. Groundmass phases and microphenocrysts were analyzed once. The accuracy of these analyses is $\pm 1\%$ for major elements and $\pm 7.5-10.0\%$ for minor elements based on the standard calibrations.

The following table summarizes the operating conditions and standards used in the mineral analyses:

filament voltage - 15 kv
 absorbed sample current - 14-16 namps
 beam diameter - 6-15 microns

	Element	Standards
Pyroxenes:	Na_2O	Amelia albite
	K_2O	microcline
	SiO_2	Kakanui augite
	Al_2O_3	"
	CaO	"
	MgO	"
	FeO	"
	MnO	Doped diopside glass
	Cr_2O_3	chromite
	TiO_2	ilmenite
Olivine:	SiO_2	San Carlos olivine
	MgO	"
	FeO	"
	NiO	Doped diopside glass

Plagioclase: Na_2O	Amelia albite
K_2O	microcline
SiO_2	Amelia albite
Al_2O_3	Anorthite
CaO	"
MgO	Kakanui augite
FeO	"

REFERENCES

- Barazangi, M. and Dorman, J., World seismicity maps compiled from ESSA, Coast and Geodetic Survey, epicenter data, 1961-1967, Bull. Seismol. Soc. Amer., 59, 369-380, 1969.
- Barazangi, M., Isacks, B. L., Oliver, J., Dubois, J., and Pascal, G., Descent of lithosphere beneath New Hebrides, Tonga-Fiji, and New Zealand: evidence for detached slabs, Nature, 242, 98-101, 1973.
- Barsdell, M., Smith, I. E. M., and Sporli, K. B., The origin of reversed geochemical zoning in the northern New Hebrides volcanic arc, Contrib. Mineral. Petrol., 81, 148-155, 1982.
- Basaltic Volcanism Study Project, Basaltic Volcanism on the Terrestrial Planets, Pergamon Press, Inc., New York, 1981, 1286 pp.
- Bloomer, S. H., Distribution and origin of igneous rocks from landward slopes of the Mariana Trench: implications for its structure and evolution, Journ. Geophys. Res., 88, 7411-7428, 1983.
- Brocher, T. M., Geophysics of the Northern Melanesian Borderland between 174°E and 170°W, AAPG spec. pub. on CCOP/SOPAC tripartite cruises, in preparation.
- Bultitude, R. J. and Green, D. H., Experimental study of crystal-liquid relationships at high pressures in olivine nephelinite and basanite compositions, J. Petrol., 12, 121-148, 1971.
- Chase, C. G., Tectonic history of the Fiji Plateau, Geol. Soc. Amer. Bull., 82, 3087-3110, 1971.
- Coleman, P. J. and Packham, G. H., The Melanesian Borderlands and the India-Pacific Plates' boundary, Earth Sci. Rev., 12, 197-233, 1976.
- Dickinson, W. R., Circum-Pacific andesite types, Journ. Geophys. Res., 73, 2261-2269, 1968.
- Dickinson, W. R., Relations of andesitic volcanic chains and granitic batholith belts to the deep structure of volcanic arcs, Proc. Geol. Soc. London, 1662, 27-30, 1970.
- Dickinson, W. R., Temper sands in sherds from Futuna, Alofi, and Uvea (Horne and Wallis Islands), appendix 2 to P. V. Kirch, Archaeological investigations in Futuna and Uvea (Western Polynesia): a preliminary report, J. Polynesian Soc., 85, 64-67, 1976.

- Dickinson, W. R. and Hatherton, T., Andesitic volcanism and seismicity around the Pacific, Science, 157, 801-803, 1967.
- Duncan, R. A., Radioisotope geochronology of the Northern Melanesian Borderland, AAPG spec. pub. on 1982 CCOP/SOPAC tripartite cruises, in preparation.
- Falvey, D. A., Arc reversals and a tectonic model for the North Fiji Basin, Bull. Austr. Soc. Explor. Geophys., 6, 47-49, 1975.
- Falvey, D. A., Analysis of paleomagnetic data from the New Hebrides, Bull. Austr. Soc. Explor. Geophys., 9, 117-123, 1978.
- Fodor, R. V. and Bunch, T. E., Mineral chemistry of volcanic rocks from Maui, Hawaii: pyroxenes, Geol. Soc. Amer. Abstracts with Programs, p. 158, 1972.
- Fodor, R. V., Keil, K., and Bunch, T. E., Contributions to the mineral chemistry of Hawaiian rocks IV. Pyroxenes in rocks from Haleakala and West Maui volcanoes, Maui, Hawaii, Contrib. Mineral. Petrol., 50, 173-195, 1975.
- Fryer, P., Petrology of some volcanic rocks from the Northern Fiji Plateau, Geol. Soc. Amer. Bull., 85, 1717-1720, 1974.
- Gill, J. B., Composition and ages of Lau Basin and Ridge volcanic rocks: implications for evolution of an interarc basin and remnant arc, Geol. Soc. Amer. Bull., 87, 1384-1395, 1976a.
- Gill, J. B., From island arc to oceanic islands: Fiji southwestern Pacific, Geology, 4, 123-126, 1976b.
- Gill, J. B., Orogenic Andesites and Plate Tectonics, Springer-Verlag, Berlin, 390 p., 1980.
- Gill, J. B. and Gorton, M., A proposed geological and geochemical history of eastern Melanesia, in The Western Pacific: Island Arcs, Marginal Seas, Geochemistry, P. J. Coleman (ed.), W. Australia Univ. Press, Nedlands, 543-566, 1973.
- Gill, J. B., Stork, A. L., and Whelan, P. M., Volcanism accompanying back-arc basin development in the southwest Pacific, in press, 1983.
- Hart, S. R., Brooks, C., Krogh, T. E., Davis, G. L. and Nava, D., Ancient and modern volcanic rocks: a trace element model, Earth Planet. Sci. Lett., 10, 17-28, 1970.
- Hawkins, J. W., Petrology of a differentiated alkalic rock series from a seamount near the Tonga Trench, Geol. Soc. Amer. abstracts with Programs, 6, p.189, 1974.

- Hawkins, J. W., Petrology and geochemistry of basaltic rocks of the Lau Basin, Earth Planet. Sci. Lett., 28, 283-297, 1976.
- Hawkins, J. W. and Natland, J. H., Nephelinites and basanites of the Samoan linear volcanic chain: their possible tectonic significance, Earth Planet. Sci. Lett., 24, 427-439, 1975.
- Hedge, C. E., Peterman, Z. E., and Dickinson, W. R., Petrogenesis of lavas from Western Samoa, Geol. Soc. Amer. Bull., 83, 2709-2714, 1972.
- Hindle, W. H., The geochemistry of volcanism from Vanua Levu and other islands of the Fiji Group and their petrogenetic significance, Masters thesis, Univ. of Leeds, 1970.
- Ito, E. and Anderson, A. T., Jr., Submarine metamorphism of gabbros from the Mid-Cayman Rise: petrographic and mineralogic constraints on hydrothermal processes at slow-spreading ridges, Contrib. Mineral. Petrol., 82, 371-388, 1983.
- Jezek, P. A., Bryan, W. B., Haggerty, S. E., and Johnson, H. P., Petrography, petrology, and tectonic implications of Mitre Island, Northern Fiji Plateau, Marine Geol., 24, 123-148, 1977.
- Johnson, T. and Molnar, P., Focal mechanisms and plate tectonics of the southwest Pacific, Journ. Geophys. Res., 77, 5000-5032, 1972.
- Karig, D. E., Ridges and basins of the Tonga-Kermadec island arc system, J. Geophys. Res., 75, 239-254, 1970.
- Kear, D. and Wood, B. L., The geology and hydrology of Western Samoa, New Zeal. Geol. Surv. Bull., 63, 92 p., 1959.
- Kroenke, L. W., Geology of the Ontong Java Plateau, PhD. thesis, University of Hawaii, 1972.
- Kuno, H., High-Al basalt, Journ. Petrol., 1, 121-145, 1960.
- Kuno, H., Lateral variation of basalt magma across continental margins and island arcs, Bull. Volcan., 29, 195-222, 1966.
- LeBas, M. J., The role of aluminum in igneous clinopyroxenes with relation to their parentage, Am. J. Sci., 260, 267-288, 1962.
- Macdonald, G. A., Petrography of the Samoan Islands, Geol. Soc. Amer. Bull., 55, 1333- , 1944.
- Macdonald, G. A., Petrography of the Wallis Islands, Geol. Soc. Amer. Bull., 56, 861-872, 1945.
- Macdonald, G. A., Composition and origin of Hawaiian lavas, in R. R. Coats, R. L. Hay, and C. A. Anderson (eds.), Studies in

- Volcanology: a Memoir of Howel Williams, Geol. Soc. Amer. Mem. 116, 477-522, 1968.
- Macdonald, G. A. and Katsura, T., Chemical composition of Hawaiian lavas, Journ. Petrol., 5, 82-133, 1964.
- Macdonald, G. A., Abbott, A. T., and Peterson, F. L., Volcanoes in the Sea, The Geology of Hawaii, 2nd edition, Univ. of Hawaii Press, Honolulu, 517 p., 1983.
- Malahoff, A., Feden, R. H., and Fleming, H. S., Magnetic anomalies and tectonic fabric of marginal basins north of New Zealand, Journ. Geophys. Res., 87, 4109-4125, 1982.
- Mallick, D. I. J., Some petrological and structural variations in the New Hebrides, in The Western Pacific: Island Arcs, Marginal Seas, Geochemistry, W. Australia Univ. Press, Nedlands, 193-211, 1973.
- McBirney, A. R. and Aoki, K., Petrology of the island of Tahiti, in R. R. Coats, R. L. Hay and C. A. Anderson (eds.), Studies in Volcanology: a Memoir of Howel Williams, Geol. Soc. Amer. Mem. 116, 523-556, 1968.
- Minster, J. B. and Jordan, T., Present-day plate motions, Journ. Geophys. Res., 83, 5331-5354, 1978.
- Morgan, W. J., Deep mantle convection plumes and plate motions, Amer. Assoc. Petrol. Geol., Bull., 56, 203-213, 1972.
- Mullen, E. D., MnO/TiO₂/P₂O₅: a minor element discriminant for basaltic rocks of oceanic environments and its implications for petrogenesis, Earth Planet. Sci. Lett., 62, 53-62, 1983.
- Natland, J. H., Petrologic studies of linear island chains: Samoan Islands and Line Islands, PhD. thesis, Univ. Cal., San Diego, 1975.
- Natland, J. H., The progression of volcanism in the Samoan linear volcanic chain, Am. J. Sci., 280-A, 709-735, 1980.
- Norrish, K. and Hutton, J. T., An accurate X-ray spectrographic method for the analyses of a wide range of geologic samples, Geochim. Cosmochim. Acta, 33, 431-451, 1969.
- Norrish, K. and Chappell, B. W., X-ray fluorescence spectrometry, in Physical Methods in Determinative Mineralogy, 2nd edition, J. Zussman (ed.), Academic Press, New York, 201-272, 1977.
- Onuma, K. and Yagi, K., The join CaMgSi₂O₆-Ca₂MgSi₂O₆-CaTiAl₂O₆ in the system CaO-MgO-TiO₂-SiO₂ and its bearing on the titanpyroxenes, Min. Mag., 38, 471-480, 1971.

- Reay, A, Rooke, J. M., Wallace, R. C., and Whelan, P., Lavas from Niuafu'ou Island, Tonga resemble ocean-floor basalts, Geology, 2, 605-606, 1974.
- Sinton, J. M., Ultramafic inclusions and high pressure xenocrysts in submarine basanitoid, equatorial Mid-Atlantic Ridge, Contrib. Mineral. Petrol., 70, 49-57, 1979.
- Sinton, J. M., Johnson, K. T. M., and Price, R. C., Submarine arc and back-arc lavas of the N. Melanesian Borderland, Lau and N. Fiji Basins, Trans. Amer. Geophys. Union, in press, 1983.
- Staudigel, H. and Hart, S. R., Alteration of basaltic glass: mechanisms and significance for the oceanic crust-seawater budget, Geochim. Cosmochim. Acta, 47, 337-350, 1983.
- Staudigel, H., Hart, S. R., and Richardson, S. H., Alteration of the oceanic crust: processes and timing, Earth Planet. Sci. Lett., 52, 311-327, 1981.
- Stearns, H. T., Geology of the Samoan Islands, Geol. Soc. Amer. Bull., 55, 1279-1332, 1944.
- Stearns, H. T., Geology of the Wallis Islands, Geol. Soc. Amer. Bull., 56, 849-860, 1945.
- Stice, G. D., Petrography of the Manu'a Islands, Samoa, Contrib. Mineral. Petrol., 19, 343-357, 1968.
- Sykes, L. R., Isacks, B. L., and Oliver, J., Spatial distribution of deep and shallow earthquakes of small magnitude in the Fiji-Tonga region, Bull. Seismol. Soc. Amer., 59, 1093-1113, 1969.
- Thompson, R. N., Some high pressure pyroxenes, Min. Mag., 39, 768-787, 1974.
- Tracy, R. J. and Robinson, P., Zoned titanian augite in alkali olivine basalt from Tahiti and the nature of titanium substitution in augite, Amer. Mineral., 62, 634-645, 1977.
- Watts, A. B., Bodine, J. H., and Ribe, N. M., Observations of flexure and the geologic evolution of the Pacific Ocean basin, Nature, 283, 532-537, 1980.
- Weissel, J. K., Evolution of the Lau Basin by the growth of small plates, in Island Arcs, Deep-Sea Trenches, and Back-Arc Basins, M. Talwani and W. C. Pitman (eds.), Maurice Ewing series I, Amer. Geophys. Union, 429-436, 1977.
- Wilkinson, J. F. G., Ultramafic inclusions and high pressure megacrysts from a nephelinite sill, Nandewar Mountains, northeast New South Wales, and their bearing on the origin of certain ultramafic

- inclusions in volcanic rocks, Contrib. Mineral. Petrol., 51, 235-262, 1975.
- Wilson, J. T., Evidence from islands on the spreading of ocean floors, Nature, 197, 536-538, 1963.
- Winterer, E. L., Lonsdale, P. F., Matthews, J. L., and Rosendahl, B. R., Structure and acoustic stratigraphy of the Manihiki Plateau, Deep-Sea Res., 21, 793-814, 1974.
- Yang, H. Y., Al- and Ti-rich clinopyroxene in the system $\text{CaMgSi}_2\text{O}_6$ - $\text{CaAl}_2\text{SiO}_6$ - $\text{CaTiAl}_2\text{O}_6$, Proc. Geol. Soc. China, 18, 48-57, 1975.
- Yang, H.Y., The join $\text{CaMgSi}_2\text{O}_6$ - $\text{CaAl}_2\text{SiO}_6$ - $\text{CaTiAl}_2\text{O}_6$ and its bearings on the origin of the Ca- and Al- rich inclusions in the meteorites, Proc. Geol. Soc. China, 19, 107-126, 1976.
- Yoder, H. S., Jr. and Tilley, C. E., Origin of basalt magmas: an experimental study of natural and synthetic rock systems, J. Petrol., 3, 342-532, 1962.

THE EAST-WEST CENTER—officially known as the Center for Cultural and Technical Interchange Between East and West—is a national educational institution established in Hawaii by the U.S. Congress in 1960 to promote better relations and understanding between the United States and the nations of Asia and the Pacific through cooperative study, training, and research. The Center is administered by a public, nonprofit corporation whose international Board of Governors consists of distinguished scholars, business leaders, and public servants.

Each year more than 1,500 men and women from many nations and cultures participate in Center programs that seek cooperative solutions to problems of mutual consequence to East and West. Working with the Center's multidisciplinary and multicultural staff, participants include visiting scholars and researchers; leaders and professionals from the academic, government, and business communities; and graduate degree students, most of whom are enrolled at the University of Hawaii. For each Center participant from the United States, two participants are sought from the Asian and Pacific area.

Center programs are conducted by institutes addressing problems of communication, culture learning, environment and policy, population, and resource systems. A limited number of "open" grants are available to degree scholars and research fellows whose academic interests are not encompassed by institute programs.

The U.S. Congress provides basic funding for Center programs and a variety of awards to participants. Because of the cooperative nature of Center programs, financial support and cost-sharing are also provided by Asian and Pacific governments, regional agencies, private enterprise and foundations. The Center is on land adjacent to and provided by the University of Hawaii.

1777 East-West Road
Honolulu, Hawaii, 96848

DATE DUE

~~JUL 24 1987~~

~~SEP 8 1987~~

HIGH SMITH REORDER #45-230